Ozone Initiated Chemistry and Its Impact on Cabin Air Quality

*Qingyan "Yan" Chen, Ph.D and Aakash C. Rai, Ph.D

National Air Transportation Center of Excellence for
Research in the Intermodal Transport Environment (RITE)
Airliner Cabin Environment Research Program
Purdue University

May 29, 2014

Report No. RITE-ACER-CoE-2014-Purdue

NOTICE

This work was funded by the U.S Federal Aviation Administration
Office of Aerospace Medicine under
Cooperative Agreements 07-C-RITE and 10-C-RITE.

Technical Report Documentation Page

1. Report No. RITE-ACER-CoE-2014-Purdue	2. Government Accession No.	3. Recipient's Catalog No.
4. Title and Subtitle Ozone Initiated Chemistry and Its Impact on Cabin Air Quality		5. Report Date May 29, 2014 6. Performing Organization Code
7. Author(s) Qingyan "Yan" Chen and Aakash C. Rai		8. Performing Organization Report No.
9. Performing Organization Name and Address Purdue University West Lafayette, Indiana		10. Work Unit No. (TRAIS) 11. Contract or Grant No. 07-C-RITE and 10-C-RITE
12. Sponsoring Agency name and Address Office of Aerospace Medicine Federal Aviation Administration 800 Independence Ave., S.W. Washington, DC 20591		13. Type of Report and Period Covered Technical Report 2/1/2010 to 8/31/2014 14. Sponsoring Agency Code
15. Supplemental Notes Work was accomplished under Public law 108-76.		

16. Abstract

Ozone is a major indoor air pollutant, and exposure to it is associated with increased morbidity and mortality risks for humans. This study first measured the ozone consumption by, and ozone-initiated VOC emissions from, reactions with a T-shirt soiled with human skin-oils. The results show that the rate of ozone removal by the T-shirt increased with increasing soiling level and ventilation rate, decreased at high ozone concentrations, and was relatively unaffected by the humidity level. The ozone-initiated VOC emissions were generally higher at higher ozone concentrations, humidity level, soiling degree of the T-shirt, and ventilation rate. Our measurements also show that the ozone/T-shirt reactions generated sub-micron particles, and this generation was enhanced by the soiling of the T-shirt with skin-oils. We used computational fluid dynamics (CFD) to study ozone consumption and developed new empirical models for computing the emissions of several major VOCs generated from ozone/clothing reactions. Good agreement was generally observed between the CFD results and the available experimental data. This investigation developed a numerical model to probe particle generation from ozone reactions with human-worn clothing under realistic indoor conditions. The model can predict ultra-fine particles generated.

17. Key Words Ozone, VOC, ultrafine particles, experimental measurements, computational fluid dynamics, models, chambers, mockup cabin, aircraft cabin	18. Distribution Statement		
19. Security Classif. (of this report) Unclassified	20. Security Classif. (of this page) Unclassified	21. No. of Pages 143	22. Price

Form DOT F 1700.7 (8-72) Reproduction of completed page authorized

TABLE OF CONTENTS

Page

LIST OF TABLES

LIST OF FIGURES

Figure Page

Figure Page

Figure Page

Figure Page

Appendix Figures

SUMMARY

Ozone is a major indoor air pollutant, and exposure to it is associated with increased morbidity and mortality risks for humans. Ozone is also a major driver of indoor air chemistry, and it reacts with various indoor materials such as fragrances, cleaners, paints, carpets, etc. to generate a myriad of byproducts. These ozone-initiated byproducts include numerous volatile and semi-volatile organic compounds as well as particles, which can be even more harmful to human health than ozone itself. Therefore, it is imperative to characterize the indoor exposure of humans to ozone and ozone-initiated byproducts.

A large number of investigations have measured ozone reactions with terpene-based consumer products and found these reactions to be sources of volatile organic compounds (VOCs) and particles in buildings. Ozone chemistry in airliner cabins has also received considerable attention because the ozone concentration is typically much higher in aircraft cabins than in buildings, which translates to a high risk of exposure to ozone and its byproducts for passengers and crew. These investigations have shown that the occupants themselves provide significant sites for ozone consumption and VOC emissions through ozone reactions with their skin, hair, and clothing. In contrast to the large number of experimental studies devoted to ozone reaction chemistry, only a few modeling studies can be found in the literature. It is crucial to develop modeling tools because they can provide cheap and quick estimates of human exposure to ozone and the byproducts of its reactive chemistry and can also aid in the development of possible mitigation strategies. Therefore, the aim of this investigation was to develop modeling tools for studying exposure to ozone and its initiated byproducts in indoor environments

with an emphasis on airliner cabins, which have been identified as high-risk environments.

To generate the experimental data needed for developing the models, we first measured the ozone consumption by, and ozone-initiated VOC emissions from, reactions with a T-shirt soiled with human skin-oils. The measurements were conducted in an environmental chamber, and they were designed to identify the impact of various factors on ozone reactions. These factors included ozone concentration, relative humidity, the degree to which the T-shirt was soiled by human skin-oils, and ventilation rate. It was found that ozone reactions with the soiled T-shirt consumed ozone and generated VOCs. The ozone deposition velocity, which was used to quantify the ozone removal rate by the soiled T-shirt, ranged from 0.15 to 0.29 cm/s. The rate of ozone removal by the T-shirt increased with increasing soiling level and ventilation rate, decreased at high ozone concentrations, and was relatively unaffected by the humidity level. The ozone-initiated VOC emissions included C6–C10 straight-chain saturated aldehydes, acetone, and 4-oxopentanal (4-OPA). The VOC emissions were generally higher at higher ozone concentrations, humidity level, soiling degree of the T-shirt, and ventilation rate. The total molar yield was approximately 0.5 in most of the experiments, which means that for every two moles of ozone removed by the T-shirt surface, one mole of VOCs was produced.

In addition to measurements of ozone consumption and ozone-initiated VOC emissions, we explored the possibility of particle generation from ozone reactions with the soiled T-shirt by using the same environmental chamber setup. Our measurements showed that the ozone/T-shirt reactions did indeed generate sub-micron particles, and this generation was enhanced by the soiling of the T-shirt with skin-oils. In these reactions, a burst of ultrafine particles (UFPs) was observed approximately one hour after the injection of ozone into the chamber, and then the particles grew to larger sizes. Particle generation from the ozone/T-shirt reactions was also significantly affected by the various factors that were studied, and these reactions were identified as another potential source of indoor UFPs.

On the basis of the aforementioned measurements, we subsequently developed modeling techniques for studying ozone reactions in realistic indoor settings. We used computational fluid dynamics (CFD) to study ozone consumption by, and ozone-initiated VOC emissions from, different surfaces in an aircraft cabin. The CFD model for ozone was based on existing models in the literature, and we developed new empirical models for computing the emissions of several major VOCs generated from ozone/clothing reactions, such as acetone, 4-OPA, nonanal, and decanal. Good agreement was generally observed between the CFD results and the available experimental data for ozone consumption by different surfaces in the aircraft cabin. For the VOC concentrations, the model predictions showed accurate trends qualitatively, but there were quantitative discrepancies between the predictions and the corresponding measurements, which were mainly due to the small experimental dataset used for model development. Nevertheless, the models are promising and can be improved with the use of additional data. Our CFD analysis also obtained detailed concentration distributions of ozone and its initiated VOCs in the aircraft cabin. The analysis predicted that in the breathing zone of the passengers, the concentration of ozone would typically be 10% lower, and that of ozone-initiated VOCs 10–50% higher, than their respective bulk air concentrations. Therefore, to accurately assess passengers' exposure to ozone and its initiated VOCs, their breathing zone concentrations should be used.

Finally, this investigation developed a numerical model to probe particle generation from ozone reactions with human-worn clothing under realistic indoor conditions. The model was based on the particle generation measured in our environmental chamber as well as physical models of particle nucleation, condensational growth, and deposition. In five out of the six test cases, the model was able to predict particle size distributions reasonably well. The failure in the remaining case demonstrated the fundamental limitations of the nucleation models that were employed. The numerical model that had been developed was then used to predict particle generation under various building and airliner-cabin conditions. These predictions indicate that ozone/clothing reactions could be an important source of UFPs in densely occupied indoor spaces such as classrooms and airliner cabins. Such reactions could account for about 40% of the total UFPs measured on a Boeing 737-

700 flight. However, the model predictions at this stage are indicative and should be improved further.

In summary, this investigation studied ozone reactions with human-worn clothing through chamber measurements and numerical simulations and came to the following conclusions:

- Our measurements showed that the ozone/clothing reactions consumed ozone and generated several VOCs such as C6–C10 straight-chain saturated aldehydes, acetone, and 4-OPA, together with sub-micron particles.
- Ozone consumption and ozone-initiated VOCs and particle generation were generally found to be significantly affected by the different factors that were studied, such as ozone concentration, relative humidity, soiling degree of clothing, and ventilation rate.
- Our CFD simulations showed that the concentration of ozone decreased, and that of ozone-initiated VOCs increased, in the breathing zones of aircraft cabin passengers as compared with the corresponding bulk air concentrations. Thus, it is recommended that the breathing zone concentrations be used for estimating the exposure of passengers to ozone and ozone-initiated VOCs.
- The numerical model for particle generation extended our chamber measurements to realistic indoor environments. The model results showed that ozone/clothing reactions could be an important source of UFPs in densely occupied indoor spaces such as classrooms and airliner cabins.

CHAPTER 1. INTRODUCTION

Ozone is a major air pollutant that poses significant health concerns for humans (EPA, 2006). Ozone exposure has been found to be associated with respiratory problems such as asthma, bronchoconstriction, airway hyperresponsiveness, and inflammation (EPA, 2006). There is also evidence that links ozone to cardiovascular morbidity (EPA, 2006). Several investigations have even associated ozone exposure with premature mortality (Bell et al., 2005, 2004; Ito et al., 2005; Levy et al., 2005). For example, a study based on 40% of the total U.S. population identified an increase of 0.52% in daily mortality per 10 ppb increase in the previous week's ground-level ozone concentration (Bell et al., 2004). Another nationwide study (Bell et al., 2006) showed that increased ground-level ozone was associated with increased mortality even at very low concentrations (10–25 ppb). The severity of ozone effects in relation to the proportion of the population affected is qualitatively presented in Figure 1.1.

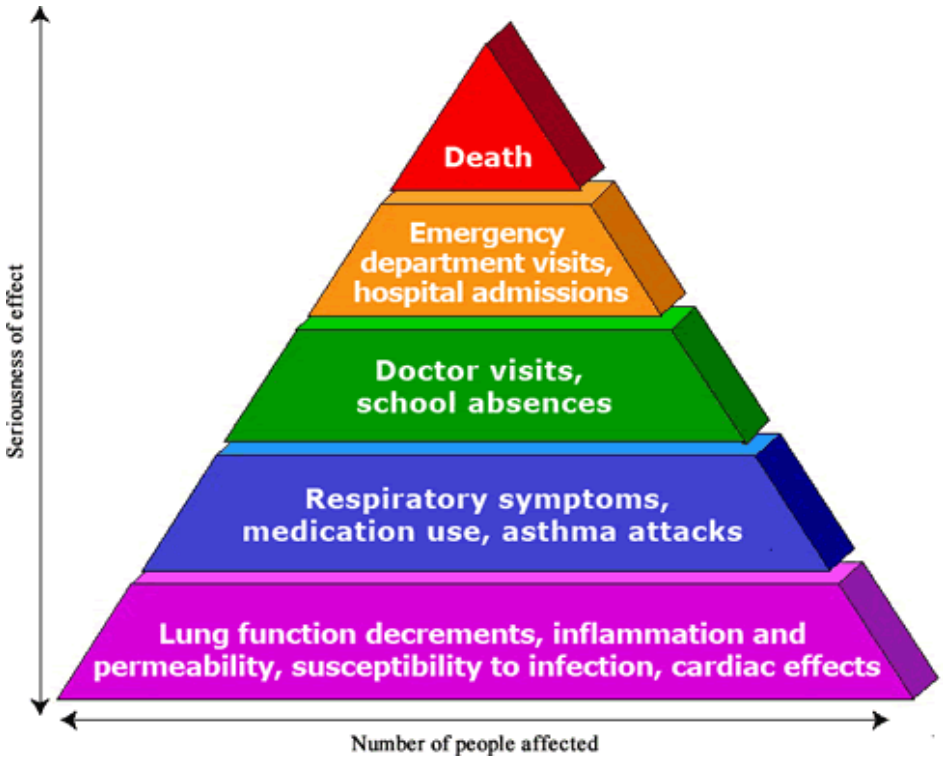

Figure 1.1. Health effects of ozone (www.epa.gov/apti/ozonehealth/population.html).

Thus, to protect public health, a number of regulations have been established that limit the ozone concentration in the atmosphere. For example, in 1997 the US Environmental Protection Agency (EPA) set the ground-level ozone limit to 80 ppb (calculated as the annual fourth-highest daily maximum 8-hr concentration, averaged over 3 years). In spite of this regulation, in the 2000–2002 time period 36–56% of ozone monitors determined that the standard had not been met. The consequences were an estimated 800 premature deaths, 4,500 hospital and emergency department admissions, 900,000 school absences, and over 1 million minor restricted activity days (Hubbell et al., 2005). In 2008, because of the growing scientific evidence of the ill effects of ozone, the EPA further reduced the ground-level ozone concentration limit to 75 ppb. Observance of the new ozone regulation could lead to health-related benefits that are valued between $2 billion and $17 billion annually (EPA, 2008).

The median value of the ground-level ozone (mean daily maximum 8-hour averaged concentration) across the United States is 49 ppb (EPA, 2006). However, the ozone level

can be as high as 500–800 ppb at typical airplane cruising altitudes (NRC, 2002). This ambient ozone is transported to indoor spaces such as homes, offices, and airliner cabins, mainly through their ventilation systems. The indoor ozone level is generally lower than the outdoor level because of ozone removal by indoor surfaces and gas phase reactions in buildings and aircraft, and by the ozone converters used in many modern aircraft to remove ozone from the cabin air supply. Thus, the typical ozone concentration is about 10 ppb in buildings and about 50 ppb in airliners. The high ozone concentrations inside airliner cabins constitute a substantial health risk to occupants.

The issue of ozone exposure in airliners has received considerable attention in the past two decades with the rapid increase in air travel. In 2012, 736.7 million passengers travelled on US flights, and this number is expected to exceed one billion by 2027 (FAA (Federal Aviation Administration), 2013). Furthermore, there has been an increase in the number of young and elderly passengers, including children, infants, and people with medical conditions (NRC, 2002). The health consequences of ozone exposure are particularly significant for individuals with pre-existing cardiopulmonary conditions, frequent fliers, and cabin crew members (Nazaroff and Weschler, 2010). Passengers and cabin crew often complain about issues related to air quality such as fatigue; irritation and dryness of lips, eyes, and skin; headaches; dizziness; sore throat; and sinus irritation. These conditions have been associated with exposure to ozone (Strøm-Tejsen et al., 2008).

The issue of ozone exposure is further exacerbated by the fact that its reaction byproducts in indoor settings (both buildings and airliners) can be even more harm harmful than ozone itself (Weschler, 2004). Volatile organic compounds (VOCs) are one class of such harmful byproducts. They are usually emitted as gases from a variety of indoor materials such as paints, furniture, and building supplies, and these emissions are called primary VOC emissions (Brown et al., 1994; Kostiainen, 1995). However, another important source of indoor VOCs are the gaseous and surface reactions of ozone with various indoor materials, which produce secondary VOC emissions. For example, Reiss et al. (1995) studied the reaction of ozone with interior latex paint in a tube flow reactor and

observed secondary carbonyl emissions. Morrison and Nazaroff (2000, 2002) investigated ozone reactions with carpets in an environmental chamber and found secondary emissions of saturated and unsaturated aldehydes. These ozone-initiated VOC emissions are particularly important in aircraft cabins because of the typically high ozone levels encountered during flights (Bhangar et al., 2008; Spengler et al., 2004; Weisel et al., 2013). Weschler's group (Tamás et al., 2006; Weschler et al., 2007; Wisthaler et al., 2005) studied the ozone-initiated reactive chemistry in an aircraft cabin mockup through a series of experiments. They concluded that humans themselves constitute the primary site for ozone-initiated chemistry, and occupants were found to be responsible for the generation of most of the VOCs identified in the cabin.

The health consequences of ozone-generated VOCs are not well studied (Weisel et al., 2013), and only a few of them are recognized as health hazards. One such VOC is formaldehyde, a known carcinogen to humans (Cogliano et al., 2005) and also a reaction byproduct of ozone with many indoor materials such as carpets (Morrison and Nazaroff, 2002), paints (Reiss et al., 1995), cleaners, and fragrances (Destaillats et al., 2006; Singer et al., 2006). Another such VOC is 4-oxopentanal (4-OPA), which is generated from the ozonolysis of squalene (a major component of human skin oils). Exposure to 4-OPA has recently been identified as a cause of irritant and allergic responses, which are symptoms generally associated with sick building syndrome (Anderson et al., 2012).

Another class of ozone-generated byproducts is particulate matter, which is also a serious health concern for humans. Several studies have associated exposure to outdoor particles with increased morbidity and mortality risks (Dominici et al., 2006; Pope and Dockery, 2006; Pope, 2000). However, outdoor exposure to particles is usually less significant than indoor exposure because people spend the majority of their time indoors. Therefore, it is presumable that many of the adverse health effects that are apparently due to outdoor particles are actually caused by exposure indoors (Jones, 1999), where ozone/terpene reactions are an important source of particles (Sarwar and Corsi, 2007; Singer et al., 2006; Weschler and Shields, 1999). For example, Long et al. (2000) found that ozone/terpene reactions drastically increased (with a peak increase of 7–100 times) the particle number

concentrations in Boston-area homes. They also found that more than 50% of those particles (by volume) were ultrafine in nature. Such ultrafine particles (UFPs) can be deposited deep in the lungs and presumably are responsible for many of the adverse health effects associated with particles (Donaldson et al., 2001, 1998; Seaton et al., 1995; Sioutas et al., 2005). Hence, several researchers focused on measuring UFP generation from ozone/terpene reactions (Coleman et al., 2008b; Destaillats et al., 2006; Ito and Harashima, 2008). They found that such reactions were indeed a major source of indoor UFPs. Thus, ozone-initiated particles are also a potential health risk, but this risk is tentative because the composition and toxicities of these particles are unknown (Carslaw et al., 2009; Weschler, 2006).

Therefore, it is well established that ozone and its reaction byproducts are significant health hazards for humans. Moreover, because people spend 90% of their time indoors (Klepeis et al., 2001) and ozone reaction byproducts are present indoors in much larger concentrations than outdoors (Weschler, 2006), it is crucial to assess the extent of indoor exposure to ozone and its byproducts. Although the ozone concentration is generally lower in the indoor air than outdoors because of its reactions with various indoor materials, indoor ozone inhalation is still estimated to be between 25% and 60% of total ozone intake (Weschler, 2006). Therefore, this study was undertaken in order to evaluate the exposure risk to humans from ozone and ozone-initiated reactive chemistry in the indoor air with an emphasis on airliner cabins, which have been identified as high-risk environments.

CHAPTER 2. LITERATURE REVIEW

This chapter presents an analysis of the available literature on ozone-initiated reactive chemistry in indoor environments. We first review experimental investigations of ozone consumption and ozone-initiated VOC and particle generation. Next, we discuss the available modeling tools for simulating indoor ozone chemistry. Finally, we summarize the state of the art and identify gaps in the existing knowledge, which were used to formulate our research objectives.

2.1 Experimental Studies

This section reviews the available literature on ozone consumption and the generation of ozone-initiated byproducts. This literature consists primarily of experimental investigations conducted in environmental chambers and/or realistic indoor environments. We first describe measurements of ozone consumption and ozone-initiated VOC emissions from reactions with different indoor materials. Next, we discuss measurements of ozone-initiated particle generation from terpene-based consumer products, which have been identified as an important source of indoor particles.

2.1.1 Ozone Consumption and Ozone-initiated VOC Emissions

The indoor environment can be thought of as a large chemical vessel in which reactions take place continuously (Weschler and Shields, 1997). Ozone is a major driver of this indoor chemistry and reacts with various compounds in the gas phase and on indoor surfaces to produce oxidation byproducts (Weschler, 2011). These byproducts are called ozone-derived secondary emissions, and they may be more harmful than the primary emissions from various indoor surfaces (Morrison, 2008; Weschler, 2006, 2000). Therefore, many investigations have studied ozone reactions with commonly used indoor products such as fragrances and cleaning agents. Gas-phase reactions of ozone with

terpene-containing cleaners and air fresheners were found to consume ozone and generate harmful VOCs such as formaldehyde and acetaldehyde (Destaillats et al., 2006 and Singer et al., 2006). Likewise, surface applications of terpene-containing cleaning agents and their subsequent reactions with ozone were also found to produce hazardous VOCs (Destaillats et al., 2006).

In addition to reactions with terpene-based consumer products, ozone reactions on various indoor surfaces also generate secondary VOC emissions. For example, Reiss et al. (1995) studied ozone reactions with interior latex paint in a tube flow reactor and observed secondary carbonyl emissions. Morrison and Nazaroff (2000, 2002) investigated ozone reactions with carpets in an environmental chamber and found secondary emissions of saturated and unsaturated aldehydes. Kagi et al. (2009) showed that ozone reacted with flooring material surfaces and increased the formaldehyde and acetaldehyde emissions from them. Coleman et al. (2008a) studied ozone reactions with various samples of aircraft surfaces and clothing fabrics in an environmental chamber. They concluded that the occupants' clothing was the dominant contributor to ozone removal and VOC emissions in an aircraft cabin environment.

Besides the above studies conducted in environmental chambers, several investigations have measured ozone reactions in buildings. For example, Lee et al. (1999) measured ozone decay rates in 43 residences in southern California and found that the decay rate was correlated with the type of house, number of bedrooms, and surface-area-to-volume ratio. Another investigation by Wang and Morrison (2006, 2010) measured ozone reactions inside homes on walls, floors, carpets, and kitchen counter surfaces. They found that the secondary VOC emissions from indoor surfaces can persist for decades because of the slow destruction rate of surface reactants by ozone and their replenishment by human activities.

The ozone-initiated chemistry in airliner cabins has also received considerable attention because of the typically high ozone levels encountered in flights as compared with those in buildings. Spengler et al. (2004) measured the average ozone concentration in 106 flights. They found that the ozone concentration in 20% of the flights exceeded the 100

ppb limit set by the U.S. Federal Aviation Administration (FAA). Bhangar et al. (2008)(Bhangar et al., 2008) collected real-time ozone data from 76 flights and found that ozone levels varied strongly with the season and the presence or absence of an ozone converter (employed in the air-supply system to reduce the ozone level). Weisel et al. (2013) measured VOCs on 52 U.S. transcontinental or international flights and developed linear regression models that are based on the log transformed mean ozone concentration, percent occupancy, and plane type.

In-flight measurements of ozone and ozone-initiated VOCs provide valuable information about cabin air quality, but they are very expensive and tedious. It is also difficult to identify the various factors affecting ozone removal and byproduct formation through in-flight measurements. To overcome these difficulties, Weschler's group (Tamás et al., 2006; Weschler et al., 2007; Wisthaler et al., 2005) studied the ozone-initiated reactive chemistry through a series of experiments in an aircraft cabin mockup. They concluded that cabin occupants constitute a major site for ozone-initiated chemistry. Occupants and their clothing were found to be responsible for more than 55% of the ozone removal and the generation of most of the VOCs identified in the cabin.

As the above review clearly shows, ozone consumption and ozone-initiated VOC emissions have been extensively studied through measurements in environmental chambers as well as real indoor spaces. However, very few investigations have identified the impact of environmental factors on VOC emissions. A study by Coleman et al. (2008a) demonstrated that environmental factors (such as ozone and humidity) can significantly affect VOC emissions from indoor ozone reactions. For example, they found that ozone-initiated VOC emissions from laundered cotton fabric approximately doubled when the relative humidity increased from 10% to 50%. However, because their experiments used a small-scale chamber and likely had well-mixed conditions, their results might not be suitable for many indoor settings that typically do not have well-mixed conditions (Sørensen and Weschler, 2002). Moreover, they did not study the effects of ventilation rate and the degree of T-shirt soiling by human skin-oils on VOC emissions, which should be explored further.

2.1.2 Ozone-initiated Particle Generation

Evidently, indoor ozone chemistry can generate a myriad of byproducts. Those byproducts with low vapor pressures can also increase the indoor particle concentrations by partitioning to particulate phase (Sarwar et al., 2003; Weschler and Shields, 1999). Hence, fine and ultrafine particles constitute another important class of ozone-initiated byproducts, a potential health concern.

Weschler and Shields (1999) observed particle generation from gaseous ozone/terpene reactions in experiments conducted in an office environment. Long et al. (2000) found that ozone/terpene reactions drastically increased (with a peak increase of 7–100 times) the particle number concentrations in Boston area homes. They also found that more than 50% of these particles (by volume) were ultrafine in nature. Morawska et al. (2009) measured ultrafine particles (UFPs) in three classrooms and found that art and cleaning activities led to a significant increase in indoor particle concentrations. They also conducted controlled experiments which showed that d-limonene (a monoterpene) emitted from the detergent reacted with ozone to generate particles.

A remarkably large number of investigations have studied ozone-initiated particle generation from gas-phase reactions of ozone with various terpenes and terpene-based consumer products under controlled conditions in environmental chambers (Coleman et al., 2008b; Sarwar and Corsi, 2007; Sarwar et al., 2004; Singer et al., 2006). These investigations have revealed details about the chemical and physical mechanisms of particle generation. It is now understood that ozone-initiated particles are generated through a burst of nucleation, which is followed by condensational growth towards larger sizes.

Several investigations have also studied particle generation from ozone reactions with terpenes applied to surfaces. For example, Destaillats et al. (2006) measured particle generation from ozone reactions with dried residues of terpene-based cleaners. Recently, Waring and co-workers measured ozone-initiated particle generation from reactions with surface-sorbed d-limonene and squalene (Wang and Waring, 2014; Waring and Siegel,

2013). These investigations have suggested that ozone reactions with surface-sorbed terpenes could potentially generate submicron particles in indoor environments.

The above review of literature on ozone-initiated particles showed that ozone/terpene reactions are an important source of submicron particles in indoor air. It is also well known that humans themselves constitute an important site for ozone reactions with their skin (Wisthaler and Weschler, 2010), hair (Pandrangi and Morrison, 2008), and clothing (Coleman et al., 2008a). These reactions are attributed primarily to squalene, which is a triterpene found in human skin oils(Wisthaler and Weschler, 2010). Hence, we can also expect ozone reactions with clothing soiled with skin oils to generate submicron particles, which was hypothesized by Fadeyi et al. (2013). However, to our knowledge there has been no investigation of particle generation from soiled clothing, which should be studied further.

2.2 Modeling Studies

The experimental studies discussed above have provided reliable results, but they are typically expensive and cumbersome. For this reason, a number of modeling studies have been attempted in order to provide a fast and convenient way to evaluate ozone's impact on indoor air quality. We have categorized these studies into two groups, according to whether they primarily address ozone-initiated VOC emissions or particle generation, and we discuss them one by one in the following subsections.

2.2.1 Ozone Consumption and Ozone-initiated VOC Emissions

Cano-Ruiz et al. (1993) developed an analytical model to determine the consumption of ozone at various indoor surfaces. They obtained an algebraic expression for computing the ozone removal rate under three different airflow conditions and also performed a numerical simulation to further analyze their results. Weschler and Shields (2000) developed a mass balance model to study the influence of ventilation rate on unimolecular and bimolecular chemical reactions occurring indoors under the assumption of well-mixed conditions. The results indicated that adequate ventilation is necessary, not only to remove pollutants generated indoors but also to limit chemical reactions in indoor

air. These analytical models provide a quick and simple way to estimate ozone contamination in indoor environments. However, it is difficult to analytically solve the model equations for complex indoor geometries and flow conditions without using the well-mixed assumption.

Hence, several computational fluid dynamics (CFD) studies on ozone have been performed. Some researchers have used CFD to analyze the volumetric and surface reactions of ozone in indoor settings (Russo and Khalifa, 2011, 2010; Sørensen and Weschler, 2002). They found significant spatial variations in the concentrations of reactants and products within a room and concluded that a well-mixed assumption might not be appropriate for many situations. Another CFD investigation by Rim et al. (2009) studied ozone reactions with an occupant under different indoor conditions and found that in the occupant's breathing zone, the concentration of ozone was 10–40% lower, and the concentration of ozone-initiated byproducts 1.2–6.0 times higher, than their corresponding bulk air concentrations. Thus, they concluded that these ozone reactions may reduce an occupant's exposure to ozone but would substantially increase exposure to ozone-initiated byproducts.

These CFD studies provide a method for extending analytical models to realistic indoor settings without using the well-mixed assumption. However, the CFD studies were performed for indoor environments with a simple geometry that required minimum validation. Recent advances in computing power have certainly made CFD methods attractive for studying the distributions of indoor contaminants. However, CFD requires thorough validation with experimental data because of numerical errors (discretization error, computer round-off error, etc.) and modeling errors (turbulence model errors, unknown boundary conditions, etc.).The limited availability of such experimental data in the existing research literature for indoor ozone reactions has hindered these modeling efforts.

2.2.2 Ozone-initiated Particle Generation

As discussed previously, ozone reactions are also an important source of indoor particles. Particle generation from ozone reactions is a complex phenomenon, and it involves the following steps: (1) production of ozone-initiated semi volatile organic compounds (SVOCs) in the vapor phase, which act as particle-forming precursors, and (2) the conversion of these vapor-phase compounds to the liquid phase through nucleation of new particles or condensation on pre-existing particles.

Therefore, in order to model particle generation, details of the ozone reaction chemistry need to be coupled with physical formulations of particle dynamics such as nucleation, condensation, etc. Several investigations have focused on modeling the chemical mechanisms without explicitly dealing with particle dynamics (Leungsakul et al., 2005; Sarwar et al., 2003). These models can provide reasonably good predictions of particle mass generation, but they cannot compute particle number concentrations and size distributions, which are essential indices for characterizing exposure to particles (Donaldson et al., 1998; Peters et al., 1997). A recent study by Ito and Harashima (2011) developed a sectional model for simulating particle generation from ozone/terpene reactions. Their model was based on physical formulations of particle dynamics, while omitting the detailed reaction chemistry. The model was able to predict particle generation and size distributions during the initial stages of generation. However, the model predictions were unsatisfactory in the later stages because they did not include the condensation growth of particles.

2.3 Literature Summary, Research Objectives, and Thesis Outline

A number of researchers have studied ozone consumption and ozone-initiated VOC emissions in different indoor environments, such as buildings and airliner cabins, and have identified human skin, hair, and clothing as significant sites for these reactions. However, very few researchers have studied the impact of environmental factors such as ozone concentration, relative humidity, and ventilation rate on ozone reactions. Therefore, our investigation first characterized the influence of these factors on ozone reactions with

clothing soiled by human skin oils through measurements in an environmental chamber, which is described in Chapter 3.

In addition to VOC emissions, we conjectured that ozone reactions with soiled clothing could generate submicron particles. Our hypothesis was based on the fact that ozone/terpene reactions were found to generate submicron particles under typical indoor conditions and the fact that squalene (a terpene) is a major component of human skin-oils. However, our literature review did not find any studies of particle generation from ozone/clothing reactions. Therefore, we also utilized the environmental chamber setup to examine the possibility of particle generation from ozone reactions with clothing, as discussed in Chapter 4.

The literature review also showed that in contrast to the large number of experimental investigations, only a few modeling studies have been performed. These studies indicate that CFD is a good method for studying ozone reaction chemistry and its impact on indoor air quality, but experimental data is needed to validate the CFD results. We therefore developed a CFD model for simulating the ozone consumption and ozone-initiated VOC emissions in an aircraft cabin. The CFD model was based on existing models in the literature for studying ozone consumption, together with new empirical models developed for computing VOC emissions on the basis of our chamber measurements. The performance of the CFD model was critically analyzed by comparing its results with experimental measurements available in the literature. The CFD modeling technique for simulating ozone consumption is explained in Chapter 5, and for VOC emissions in Chapter 6.

Finally, we developed a model to study particle generation from ozone reactions with soiled clothing on the basis of our chamber measurements. Unlike the modeling approaches typically found in the literature, which focus on either the chemical mechanism of particle generation or the details of particle dynamics, we combined the two. The resulting model was useful for further exploring the potential of ozone/clothing reactions to generate particles under realistic indoor conditions, as discussed in Chapter 7.

CHAPTER 3. OZONE REACTION WITH CLOTHING AND ITS INITIATED VOC EMISSIONS IN AN ENVIRONMENTAL CHAMBER

The introductory chapters discussed that the ozone reactions with various indoor materials can produce secondary emissions of VOCs such as formaldehyde, acetaldehyde, 4-oxopentanal (4-OPA), etc. Human exposure to these VOCs was found to be a greater health risk than the exposure to ozone itself. It was also identified that human surfaces (skin, hair, etc.) and their clothing are important sites for such ozone reactions and the associated VOC emissions. Out of these, human clothing is predominant because of its largest surface area. Hence, this investigation studied the ozone reactions with human clothing under different indoor conditions by conducting experiments in an environmental chamber. These experiments measured the ozone consumption and its initiated VOC emissions from the ozone reactions with a T-shirt with/without human skin-oils. The experiments were designed to characterize the effect of some important factors such as ozone concentration, humidity, soiling degree of clothing by skin-oils, and air change rate on the ozone reaction chemistry.

3.1 Experimental Setup

This investigation used a stainless-steel chamber with dimensions of 1.8 m × 1.7 m × 1.7 m to conduct experiments as shown in Figure 3.1. A steel box of 0.2 m × 0.4 m × 1.2 m with an internal heat source to maintain a surface temperature at 31±1°C was placed at the center of the chamber as a human simulator. The temperature was determined from a previous experimental study by Rim et al. (2009), which seems reasonable since the comfortable skin temperature for humans under sedentary conditions is about 33–34°C (ASHRAE, 2009). A cotton T-shirt (area ≈ 0.9 m^2) with/without human skin-oils was stretched over the human simulator and was the primary site for the ozone reactions. The T-shirt was washed in a fragrance- and dye-free detergent and its soiling by skin-oils was

achieved by a male subject's (26 years old Indian) sleeping in it unless otherwise mentioned. Note that the cotton T-shirt came from a set of identical T-shirts and we used the same method of laundering in all experiments. The T-shirt was stored in a clean metal-foil bag (storage time was usually less than three hours) and handled with gloves during laundering, storage, and placement inside the environmental chamber. The chamber was supplied with outdoor air with an air change rate of either 0.5 h^{-1} or 2.7 h^{-1}, and was maintained with an exhaust air temperature of approximately 24^{o}C.

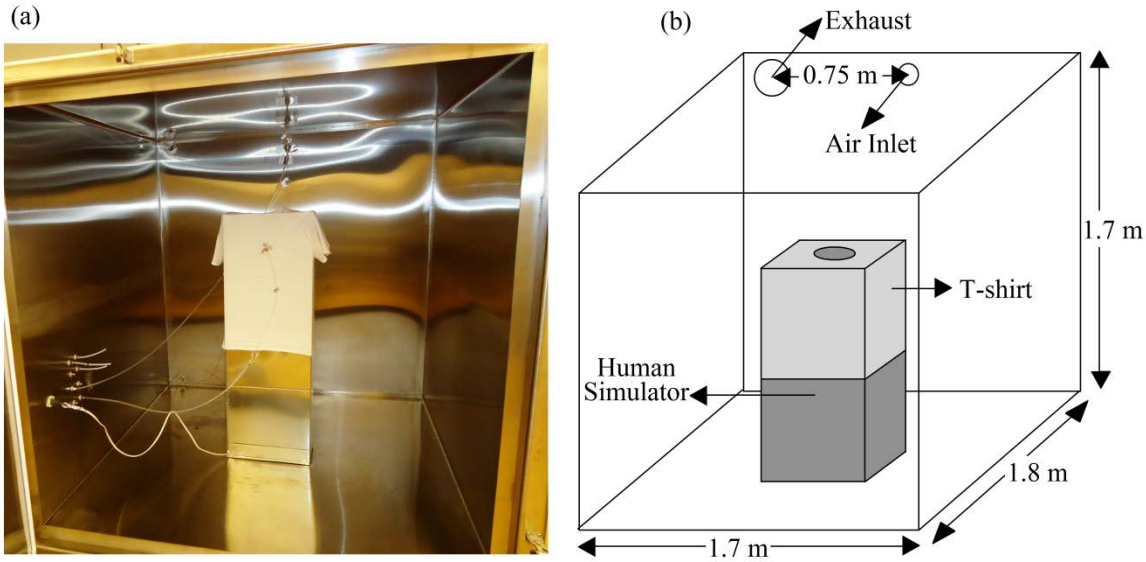

Figure 3.1. Setup of the environmental chamber used to study the ozone reactions with a T-shirt on a human simulator.

The detailed schematic of the experimental setup is shown in Figure 3.2. As shown in that figure, ozone was generated outside the chamber using UV irradiation and injected together with the supply air. A dynamic dilution calibrator (Model 700, Teledyne Instruments) was used for ozone generation in most cases, and a high capacity ozone generator (Model 610, Jelight Company, Inc.) was used in cases (Cases 4, 9, 10, 10D, and 11) that required high ozone levels. The ozone depleted inside the chamber due to its reactions with the T-shirt, human simulator, and chamber walls and produced VOCs as reaction byproducts. We measured the concentration of ozone at the inlet, near the T-shirt, and exhaust by using a three-point solenoid switching system that changed the sampling location (from inlet, to near T-shirt, to exhaust) every five minutes. The VOC

concentrations were measured before and after the ozone injection. The schematic also shows a Scanning Mobility Particle Sizer (SMPS), which was used for particle measurements discussed in Chapter 4.

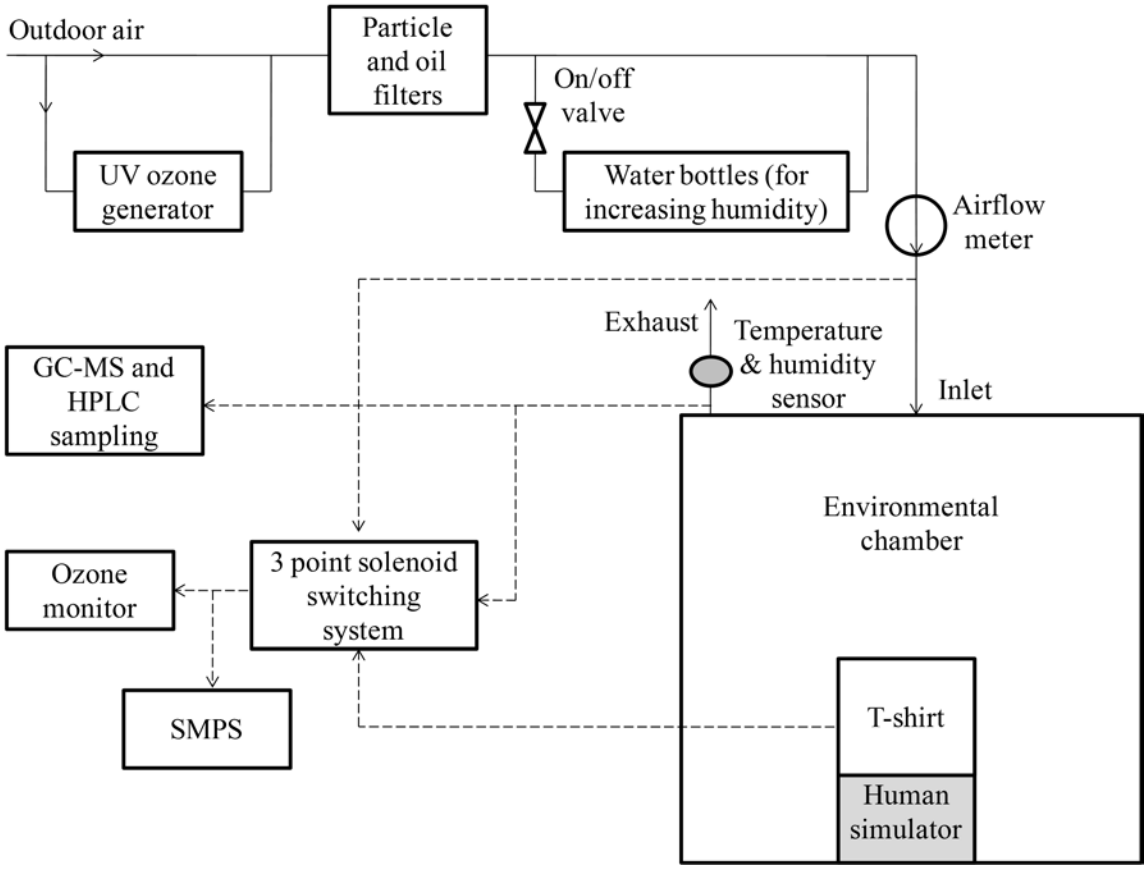

Figure 3.2. Schematic of the experimental setup used to study the ozone reactions with a T-shirt on a human simulator.

The ozone concentration was monitored with a photometric ozone analyzer (Model 202, 2B Technology), which has a precision equal to the greater of 1.5 ppb or 2% of the reading. The air samples were collected on Tenax® TA filled tubes and DNPH (2,4-Dinitrophenylhydrazine) cartridges using a sampling pump at the exhaust. The Tenax® TA samples were collected in duplicates at a sampling airflow rate of 100 ml/min for 2 hours (i.e., with a sampling volume of 12 L). These duplicate samples were analyzed by thermal desorption gas chromatography-mass spectrometry (TD-GC/MS) for C6–C10 straight-chain saturated aldehydes, 4-oxopentanal (4-OPA), 6-methyl-5-hepten-2-one (6-

MHO), and geranyl acetone according to ASTM-D6196 (ASHRAE, 2009b). The DNPH samples were collected at an airflow rate of 500 ml/min for 2.5 hours (i.e., with a sampling volume of 75 L), extracted with acetonitrile, and analyzed by high performance liquid chromatography (HPLC) for formaldehyde, acetaldehyde, and acetone as specified in ASTM-D5197 (ASHRAE, 2009c). Note that the sampling durations were different for Tenax® TA and DNPH samples to satisfy the sampling volume requirements under recommended sampling flow rates.

3.2 Experimental Procedure

We designed 13 test cases, as shown in Table 3.1 to systematically study ozone consumption and VOC production from human-worn clothing. The first three cases (Cases 1–3) were designed to identify individual contributions of the chamber, laundered T-shirt, and soiled T-shirt surfaces on the ozone removal and VOC emissions. The next eight cases (Cases 4–11) studied the effects of ozone concentration, relative humidity, soiling degree of the T-shirt, and air change rate. The last two cases replicated building conditions (i.e. lower ozone and higher relative humidity than the other test cases). Additionally, we also conducted duplicate Cases 3D and 10D, which had chamber conditions almost identical to those of Cases 3 and 10, respectively, to study the repeatability of the results. Note that most cases were conducted at low air change rate (0.5 h^{-1}) and moderate ozone (~ 50 ppb) conditions to produce sufficiently high VOC concentrations in the chamber, which reduced uncertainties in their measurements.

Table 3.1. Details of the experimental conditions in the chamber used for studying the ozone reactions with clothing.

Case	Ozone concentration (ppb)		Relative humidity (%)	Hours the T-shirt was worn (h)	Air change rate (h^{-1})
	Inlet	Exhaust			
1	74	42	15	No T-shirt	0.5
2	158	46	17	Laundered T-shirt	0.5
3	191	40	12	6	0.5
4	530	148	20	6	0.5
5	274	54	44	6	0.5
6	247	70	23	2	0.5
7	254	57	24	12	0.5
8	244	53	27	6 hours by a different human subject	0.5
9	86	75	12	No T-shirt	2.7
10	87	48	10	6	2.7
11	224	133	11	6	2.7
12	97	22	28	6	0.5
13	105	24	49	6	0.5
3D	191	44	11	6	0.5
10D	87	51	11	6	2.7

In all the above cases, the chamber was ventilated overnight with outdoor air to remove any leftover VOCs from previous experiments. Then, a T-shirt was placed inside the chamber and it was further ventilated for 1.5 hours (about 3 air changes). Next, we set the air change rate to the desired value (0.5 h^{-1} or 2.7 h^{-1}) and switched on the heating system of the manikin, and waited half an hour for the chamber airflow to stabilize. Subsequently, the background levels of ozone and VOCs were measured for 2.5 hours. The background ozone concentration was typically less than 5 ppb and the VOC concentrations are given in Table A.1. After background measurements, ozone was constantly injected through the inlet and the system was allowed to reach a steady state, which was assumed to prevail after 3 air changes (6 hours at 0.5 h^{-1} air change rate or

1.25 hours at 2.7 h^{-1} air change rate). Finally, the VOC concentrations were measured at the steady state and the experiment was completed.

3.3 Evaluation Parameters

This study defined several parameters to evaluate the ozone removal and VOC emissions for the cases shown in Table 3.1. The parameters were ozone removal, ozone removal rate, contribution to the ozone removal rate, deposition velocity, and molar yield.

3.3.1 Ozone Removal (α)

The ozone removal (α) quantifies the total ozone loss in the chamber due to surface and gas phase reactions. Under steady state, α is given by:

$$\alpha = \lambda_{total}\left(C_{inlet} - C_{exhaust}\right), \tag{3.1}$$

where λ_{total} is the total air change rate and C_{inlet} and $C_{exhaust}$, the ozone concentrations at the chamber inlet and exhaust, respectively.

3.3.2 Ozone Removal Rate (β_{total})

The total ozone removal rate (β_{total}) quantifies the total ozone loss in the chamber due to surface and gas phase reactions per unit chamber ozone concentration. At steady state, the β_{total} can be approximated by:

$$\beta_{total} = \lambda_{total}\frac{(C_{inlet} - C_{exhaust})}{C_{exhaust}}. \tag{3.2}$$

Note that the above equation is strictly valid only when the chamber and exhaust concentrations are same, i.e., for well-mixed conditions.

3.3.3 Contribution to the Ozone Removal Rate (β_s)

The contribution to the ozone removal rate (β_s) identifies the ozone removal by a surface. It can be estimated by adding one reacting surface at a time and measuring the β_{total} in each case. For example, Case 1 had only chamber surfaces , Case 2 was added with a laundered T-shirt (clean T-shirt), and Case 3 had a soiled T-shirt (with skin-oil on it). The $\beta_{s,\ chamber\ surfaces}$ was approximated as:

$$\beta_{s,\ chamber\ surfaces} = \beta_{total,\ Case\,1}. \tag{3.3}$$

The β_s for the laundered T-shirt and the soiled T-shirt with the skin-oils were calculated, respectively, as:

$$\beta_{s,\ laundered\ T\text{-}shirt} = \beta_{total,\ Case2} - \beta_{total,\ Case1}, \tag{3.4}$$

$$\beta_{s,\ soiled\ T\text{-}shirt} = \beta_{total,\ Case3} - \beta_{total,\ Case1}. \tag{3.5}$$

Note that Eqs. (3.3)–(3.5) assume that the gas phase reactions are negligible and that the ozone deposition on one surface does not affect the deposition on other surfaces.

3.3.4 Deposition Velocity (v_d)

We also computed the deposition velocity for the soiled/laundered T-shirt, which quantifies the ozone mass transfer coefficient and can be compared to those reported in the literature for similar airflow conditions. It is defined as:

$$v_d = \frac{\beta_{s,\ T\text{-}shirt} \times V_{chamber}}{A_{T\text{-}shirt}}, \tag{3.6}$$

where $A_{T\text{-}shirt}$ is the area of the T-shirt surface and $V_{chamber}$ the chamber volume.

3.3.5 Molar Yield (Y)

The molar yield of VOC_i (Y_i) is defined as the moles of VOC_i generated per mole of ozone consumed by a reacting surface (Weschler et al., 2007). Hence, it characterizes the conversion efficiency of ozone to VOC_i.

$$Y_i = \frac{\Delta VOC_i}{(C_{inlet} - C_{exhaust})}, \tag{3.7}$$

where ΔVOC_i is the increase in concentration of the VOC_i after ozone injection. Note that the above equation was used in this study to compute molar yields for the T-shirt surface by assuming that the VOC generation by the chamber surfaces was negligible.

We defined Y_{fabric} as the sum of molar yields of C6–C10 straight-chain saturated aldehydes. This parameter quantifies the efficiency of ozone conversation to C6–C10 aldehydes from its reactions with the T-shirt fabric because C6–C10 aldehydes were predominantly generated by the fabric (as shown in Section 3.4.1). We also computed $Y_{skin\text{-}oil}$ by summing the molar yields of acetone and 4-OPA. It quantifies the efficiency of ozone conversion to acetone and 4-OPA due to its reactions with the skin-oils on the T-shirt, since these compounds were generated by the skin-oils (as shown in Section 3.4.1). Additionally, the molar yield for total VOCs (Y_{total}) was also computed, which indicates the overall conversion efficiency of ozone to VOCs.

3.4 Results

This section first presents the results of Cases 1, 2, and 3, which were to identify the contributions of different surfaces to the ozone removal and its initiated VOC emissions. Then, the results of Cases 4–11 are presented, which analyze the influence of various factors on the ozone reaction chemistry. Finally, the ozone-initiated chemistry in indoor conditions similar to those in buildings is presented. The key results have been summarized in Table 3.2 and will be discussed in the following subsections. Detailed results for the individual VOC concentrations can be found in the Table A.1.

Table 3.2. Key results from the study of VOC generation from ozone reactions with human clothing.

Case	α (ppb/h)	β_{total} (h^{-1})	v_d (cm/s)	Y_{fabric}	$Y_{skin\text{-}oil}$	Y_{total}
1	16±1	0.38±0.03	-	-	-	-
2	55±2	1.18±0.05	0.13±0.01	0.19±0.03	-	0.21±0.03
3	75±2	1.86±0.09	0.23±0.02	0.12±0.02	0.12±0.01	0.28±0.03
4	195±5	1.31±0.04	0.15±0.01	0.18±0.01	0.09±0.01	0.30±0.01
5	107±2	1.98±0.07	0.25±0.02	0.39±0.02	0.16±0.01	0.57±0.02
6	91±2	1.31±0.04	0.15±0.01	0.35±0.02	0.13±0.01	0.52±0.02
7	99±2	1.74±0.06	0.21±0.02	0.28±0.02	0.16±0.01	0.46±0.02
8	97±2	1.82±0.07	0.23±0.02	0.34±0.02	0.18±0.01	0.54±0.02
9	30±7	0.40±0.09	-	-	-	-
10	107±7	2.3±0.2	0.29±0.03	0.15±0.08	0.27±0.05	0.5±0.1
11	250±10	1.9±0.1	0.23±0.02	0.22±0.04	0.18±0.02	0.44±0.05
12	40±1	1.9±0.1	0.23±0.03	0.23±0.04	0.23±0.03	0.49±0.06
13	40±1	1.6±0.1	0.20±0.02	0.29±0.04	0.22±0.03	0.54±0.05
3D	75±2	1.72±0.08	0.21±0.02	0.11±0.02	0.11±0.01	0.23±0.03
10D	100±7	2.0±0.1	0.25±0.03	0.11±0.09	0.20±0.06	0.4±0.1

α is the ozone removal, β_{total} the total ozone removal rate, v_d the deposition velocity for the T-shirt, Y_{fabric} the molar yield of C6–C10 straight-chain saturated aldehydes, $Y_{skin\text{-}oil}$ the molar yield of squalene oxidation products (acetone and 4-OPA), and Y_{total} the total molar yield of VOCs. The measurement uncertainties were estimated from an error propagation analysis and reported as plus/minus one standard deviation ($\pm\sigma$). Case numbers followed by 'D' are duplicate experiments.

3.4.1 Effect of Different Surfaces on Ozone Reactions

Cases 1, 2, and 3 were designed to identify the contributions of individual surfaces (the chamber, laundered T-shirt, and soiled T-shirt) on the ozone removal and VOC emissions by adding reacting surfaces one at a time.

Table 3.2 shows that α in Case 1 was the smallest since it only had the chamber surfaces. The α increased in Case 2 because of additional ozone removal by the T-shirt. The α further increased in Case 3, which was due to the extra ozone removed by the skin-oils in the soiled T-shirt. According to Eqs. (3.3)–(3.5) and the data shown in Table 3.2, β_s from the chamber surfaces was 0.38 h^{-1}, from the laundered T-shirt was 0.80 h^{-1}, and from the

soiled T-shirt was 1.48 h^{-1}. We also calculated the deposition velocities (v_d) for the laundered and soiled T-shirts as shown in Table 3.2. The v_d for the T-shirt compared well with those measured by Tamas et al. (2006), who reported values between 0.19 and 0.27 for soiled T-shirts stretched over seat backs in a Boeing-767 aircraft cabin mockup.

Figure 3.3 shows the ozone-initiated VOCs emissions for Cases 1 to 3. Without the T-shirt (Case 1), the concentrations of VOCs did not increase much with ozone, but with the T-shirt (Cases 2 and 3) they did. Without the T-shirt, only formaldehyde and acetaldehyde concentrations increased slightly with ozone. With the laundered T-shirt (Case 2), the ozone led to a slight increase in formaldehyde concentration as in the previous case, but not acetaldehyde. A small amount of increase in C6–C8 straight-chain saturated aldehydes (~ 2 ppb) and a significant increase in nonanal and decanal concentrations (> 5 ppb) were observed with ozone injection, when compared to Case 1. This indicates that these VOCs were ozone reaction byproducts with the laundered T-shirt fabric. With the T-shirt soiled with human skin-oils (Case 3), the increase in aldehyde concentrations was about the same as in Case 2. The concentrations of acetone and 4-OPA increased considerably (> 5 ppb) with ozone when compared to Case 2, which means that these are the ozone reaction byproducts with the human skin-oils. Wisthaler and Weschler (2010) pointed out that acetone and 4-OPA were the major oxidation products of the unsaturated compound squalene present in the human skin lipids. The other squalene oxidation products such as 6-MHO and geranyl acetone were not detected, probably due to their low concentrations. Our results are in qualitative agreement with the study by Coleman et al. (2008a), which measured the ozone-initiated VOC emissions from soiled and laundered clothing fabrics. They reported emissions of straight-chain saturated aldehydes from ozone reactions with both laundered and soiled fabrics, but the squalene oxidation products (acetone and 6-MHO) were mainly produced with soiled fabrics.

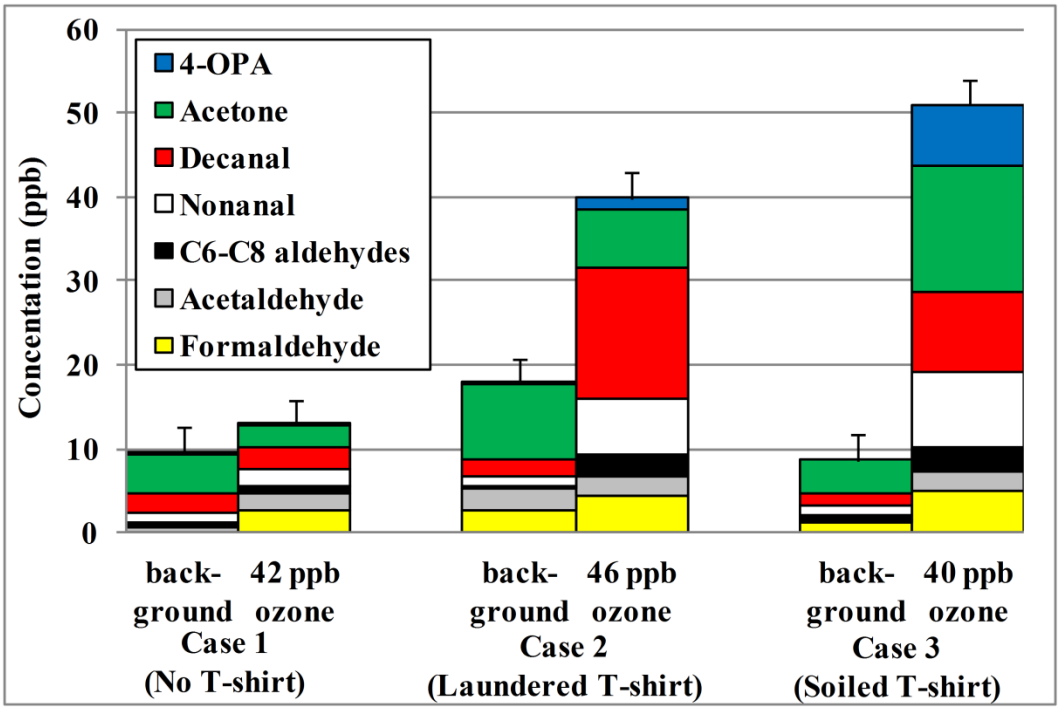

Figure 3.3. Effect of the chamber, laundered T-shirt, and soiled T-shirt surfaces on the ozone-initiated VOC emissions. Error bars indicate plus one standard deviation.

Table 3.2 shows that the Y_{fabric} was significantly higher in Case 2 than in Case 3 because of the lower ozone consumption in Case 2, although the generation of C6–C10 aldehydes was approximately the same in both the cases. The $Y_{skin\text{-}oil}$ was approximately zero in Case 2 since no squalene oxidation products (acetone and 4-OPA) were generated from the ozone reactions with the laundered T-shirt surface. The Y_{total} was higher in Case 3 than in Case 2, indicating that the overall efficiency of the ozone conversion to VOCs was higher with the soiled T-shirt.

3.4.2 Effect of Different Factors on Ozone-initiated Chemistry

This investigation designed Cases 4 to 11 to identify the influence of several key factors on the ozone reaction chemistry by using Case 3 as a reference case. This required that only one factor would vary in Cases 4–11 and that the other factors would be identical to the reference case. However, it was difficult to achieve this with the current experimental setup, which made comparisons with the reference case unsuitable while analyzing the effect of T-shirt soiling. Hence, to isolate the influence of T-shirt soiling, we compared

Cases 6, 7, and 8 which had different soiling levels, but otherwise similar conditions (ozone and relative humidity).

3.4.2.1 Effect of Ozone Concentration

In order to identify the effect of ozone concentration, this investigation compared Case 4 (148 ppb ozone) with Case 3 (40 ppb ozone), given in Table 3.1. These cases had roughly identical chamber conditions except for the large difference in the ozone concentrations.

Table 3.2 shows that the β_{total} and v_d were about 30% lower in Case 4 than in Case 3. However, the β_{total} (and v_d) should be constant for different ozone levels since the ozone reactions with surfaces that have large amounts of reactant species generally follow a first-order mechanism (Tamás et al., 2006). Hence, the decrease in β_{total} (and v_d) at high ozone concentrations shows that the reaction was probably saturated (ozone was in excess) and limited by the availability of skin-oils on the T-shirt surface. The α was higher in Case 4 than in Case 3, due to the high ozone concentration in Case 4 ($\alpha = C_{exhaust} \times \beta_{total}$).

Figure 3.4 shows that total VOC emissions more than doubled when the soiled T-shirt was exposed to higher ozone (148 ppb in Case 4 versus 40 ppb in Case 3). However, Coleman et al. (2008a) found that ozone-initiated VOC emissions from cotton fabric only increased ~ 30% when the chamber ozone concentration was increased from 45 ppb to 213 ppb ozone (Figure 5 in Coleman et al. (2008a)). Compared with their experiment, our chamber was 50 times larger in volume and the air change rate was 40 times lower, which created a spatial ozone gradient in our experiments. For example, the ozone concentrations near the T-shirt surface were about 15 ppb and 66 ppb in Cases 3 and 4, respectively, where the exhaust concentrations were 40 ppb and 148 ppb. The chamber used by Coleman et al. (2008a) likely did not have such a gradient, which means that the ozone concentrations near the soiled fabric were close to the chamber concentrations (45–213 ppb). Hence, it is possible that the high ozone concentrations near the fabric already saturated the reaction in their study, and there was insignificant influence of ozone concentration on the VOC emissions.

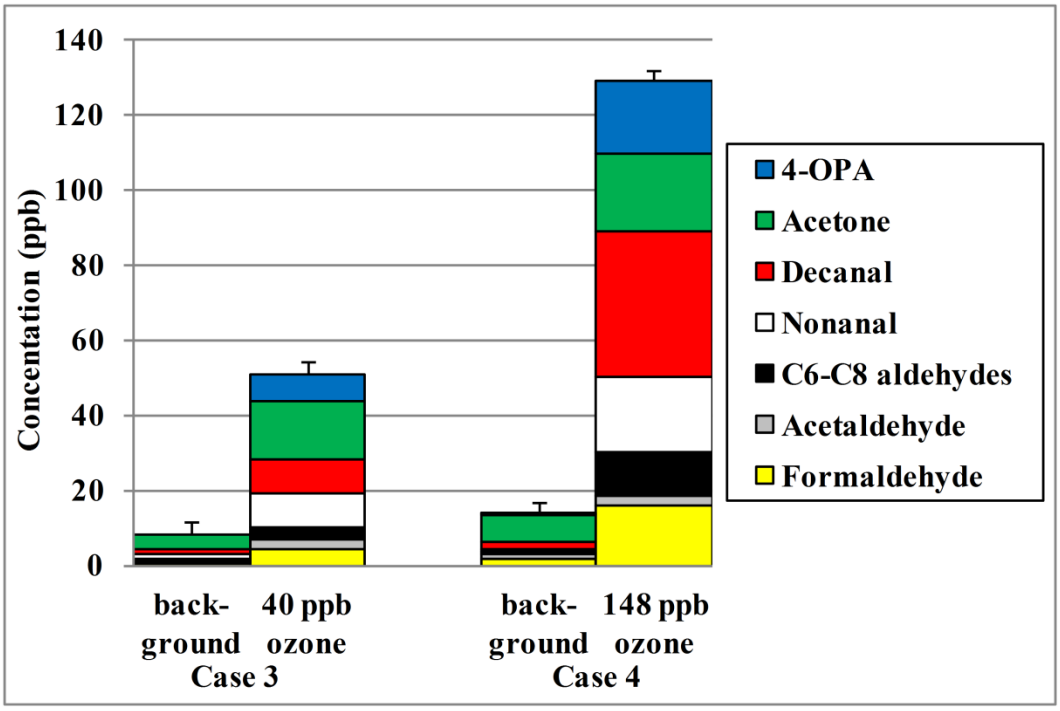

Figure 3.4. Effect of ozone concentration on the VOC emissions from its reactions with the soiled T-shirt at an air change rate of 0.5 h^{-1}. Error bars indicate plus one standard deviation.

Table 3.2 shows that the Y_{fabric} was significantly higher in Case 4 than that in Case 3, which indicates that the high ozone concentration in Case 4 enhanced the ozone conversion efficiency to aldehydes from the T-shirt fabric. However, the $Y_{skin\text{-}oil}$ was lower in Case 4, probably because the reaction was already saturated due to the high ozone concentration. The Y_{total} was approximately equal in both cases.

Table 3.2 further shows the impact of ozone concentration on Y_{fabric}, $Y_{skin\text{-}oil}$, and Y_{total} at a higher air change rate of 2.7 h^{-1} (Cases 10 vs. 11), which was similar to that observed at 0.5 h^{-1} air change rate. Under the high air change rate, Figure 3.5 shows much lower VOC concentrations when compared with Figure 3.4, which is discussed in the Section 3.4.2.4. To avoid the VOC concentrations becoming lower than our equipment detection limit or causing a high measuring error, most of our measurements used a lower air change rate at 0.5 h^{-1}.

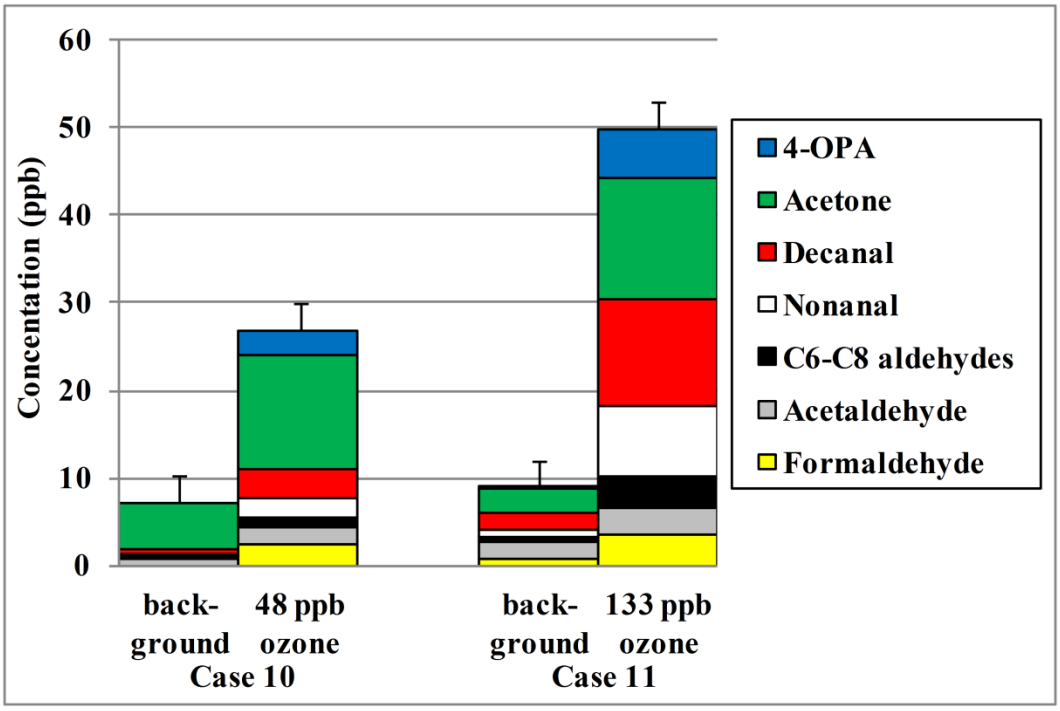

Figure 3.5. Effect of ozone concentration on the VOC emissions from its reactions with the soiled T-shirt at an air change rate of 2.7 h^{-1}. Error bars indicate plus one standard deviation.

3.4.2.2 Effect of Relative Humidity

This investigation used Cases 3 and 5 to study the impact of different humidity conditions on the ozone reactions. Case 5 had a relative humidity of 44% while Case 3 had 12%. The ozone concentration was slightly higher in Case 5 as it was difficult to control it during our experiment, but this should not play a major role in this comparison.

Table 3.2 shows that β_{total} and v_d were about the same in both cases, and the humidity did not have much effect. The α was significantly higher in Case 5 than that in Case 3 since it varies linearly with ozone concentration for a constant β_{total} ($\alpha = C_{exhaust} \times \beta_{total}$). Ozone-initiated VOC emissions except for formaldehyde and acetaldehyde were much higher in Case 5 than in Case 3, as shown in Figure 3.6. The most significant increase was in the emissions of C6–C8 aldehydes, nonanal, and decanal, which were 3–6 times higher at the higher humidity level in Case 5. These results agreed qualitatively with those by Coleman et al. (2008a), who found that ozone-initiated VOC emissions with a laundered cotton

fabric increased by raising the relative humidity from 10% to 50%. The Y_{fabric} in Case 5 was about three times higher than in Case 3, and the $Y_{skin\text{-}oil}$ and Y_{total} also increased in Case 5, as shown in Table 3.2. This indicates that the high relative humidity increased the conversion efficiency of ozone (to VOCs) from the soiled T-shirt, especially from the cotton fabric.

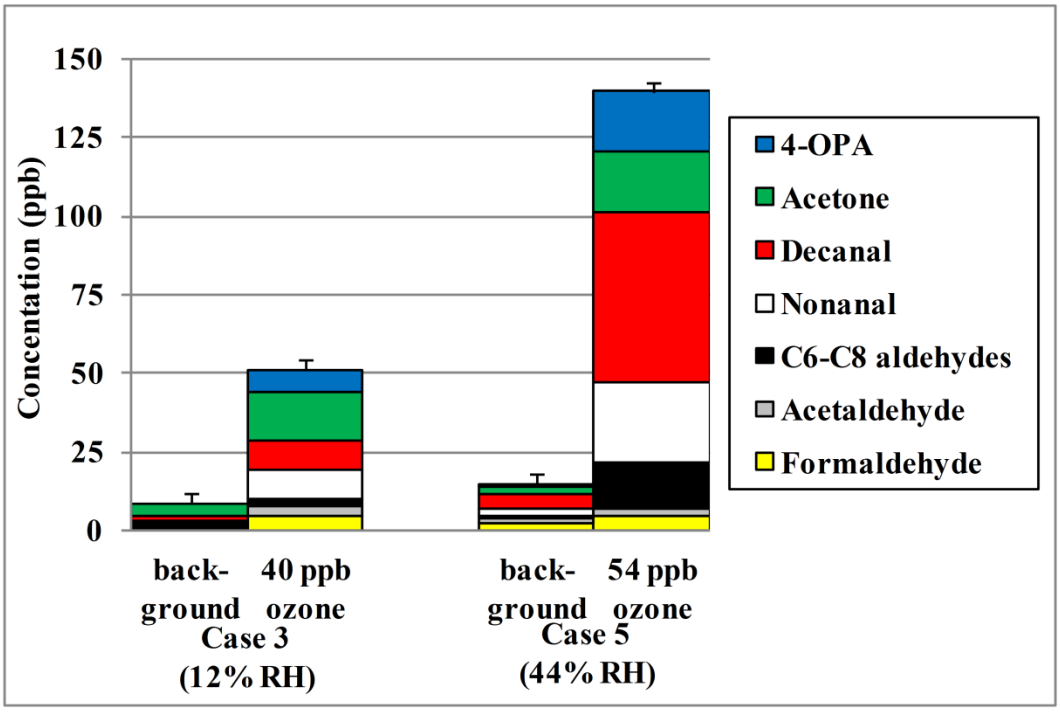

Figure 3.6. Effect of relative humidity on the ozone-initiated VOC emissions with the soiled T-shirt. Error bars indicate plus one standard deviation.

3.4.2.3 Effect of T-shirt Soiling

This study compared Cases 6 and 7 to characterize the effect of soiling amount of T-shirt by human skin oils on ozone removal and its initiated VOC emissions. The different soiling levels in these cases were achieved by having a person sleep in the T-shirt for 2 h in Case 6 and 12 h in Case 7. Note that the ozone concentration in the two cases also differed slightly.

Table 3.2 shows that β_{total} and v_d were significantly lower in Case 6 compared to that in Case 7, probably due to incomplete soiling of the T-shirt surface by human skin-oils. The

α was also low in Case 6 despite the higher ozone concentration since the β_{total} was low ($\alpha = C_{exhaust} \times \beta_{total}$). Figure 3.7 shows the effect of the soiling amount of the T-shirt on the ozone-initiated VOC emissions. The C6–C10 aldehyde emissions were the same between Cases 6 and 7 since these were primarily reaction byproducts of the ozone with the cotton T-shirt and were not affected by the soiling of the T-shirt. The emissions of squalene oxidation products (acetone and 4-OPA) were slightly lower in Case 6 than in Case 7 because the T-shirt had not become completely soiled by the skin-oils in 2 hours. Table 3.2 shows that the Y_{fabric} and Y_{total} were higher in Case 6 than in Case 7 due to the low ozone consumption in Case 6. The $Y_{skin\text{-}oil}$ was smaller in Case 6 because of the lower emissions of squalene oxidation products.

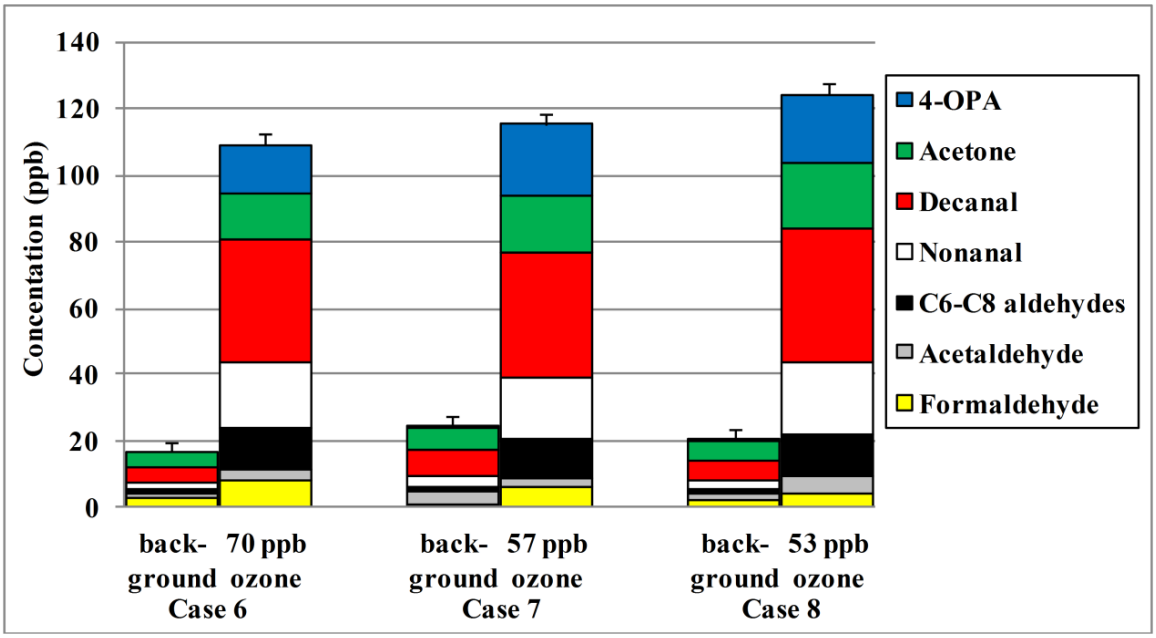

Figure 3.7. Effect of T-shirt soiling by skin-oils on the ozone-initiated VOC emissions. Error bars indicate plus one standard deviation.

To understand the effect of the skin-oils from the human subject on the ozone reactions with the T-shirt, this study used a T-shirt in Case 8 worn by a female subject (middle-aged American). The results were compared with those from Case 7 since both cases had similar chamber conditions (i.e., exhaust ozone and humidity levels).

The α, β_{total}, and v_d were nearly the same between Cases 7 and 8, as shown in Table 3.2. Figure 3.7 shows that the VOC emissions were slightly higher in Case 8, which made the Y_{fabric}, $Y_{skin\text{-}oils}$, and Y_{total} also slightly higher. Hence, it seems that the ozone reaction chemistry with the soiled T-shirt was not affected by different human subjects sleeping in the T-shirt.

As stated previously, this investigation did not used the reference case (Case 3) to analyze the effect of T-shirt soiling (studied in Cases 6, 7, and 8) since the ozone and relative humidity levels were quite low in Case 3 compared with those in Cases 6, 7, and 8. However, it is noteworthy that the ozone-initiated VOC emissions more than doubled in Cases 6, 7, and 8 compared to Case 3. Such high VOC emissions were likely due to the combined effects of high ozone and relative humidity levels in Cases 6, 7, and 8.

3.4.2.4 Effect of Air Change Rate

Cases 9 and 10 were performed with an air change rate of 2.7 h^{-1}. Case 9 did not have a T-shirt in the chamber, while Case 10 had a soiled T-shirt. Cases 9 and 10 can be compared to Cases 1 and 3, which had the lower air change rate of 0.5 h^{-1}.

Table 3.2 shows that α was higher in Cases 9 and 10 than in Cases 1 and 3, respectively, because of higher β_{total} and ozone concentrations ($\alpha = C_{exhaust} \times \beta_{total}$). Ozone removal rate by the chamber surfaces ($\beta_{s,\ chamber\ surfaces}$) under different air change rates was the same (0.40 h^{-1} for Case 9 and 0.38 h^{-1} for Case 1). However, ozone removal rate by the T-shirt ($\beta_{s,\ T\text{-}shirt}$) increased with the air change rate (2.3 h^{-1} – 0.4 h^{-1} = 1.9 h^{-1} for Case 10, and 1.86 h^{-1} – 0.38 h^{-1} = 1.48 h^{-1} for Case 3.), and also its deposition velocity (v_d) given in Table 3.2. Ozone removal rate (and deposition velocity) by a surface depends on (1) the fluid motion and ozone diffusion that transport ozone molecules to the surface and (2) the ozone chemical reactions on the surface (Cano-Ruiz et al., 1993). For relatively low-reactivity surfaces (such as the chamber walls), ozone removal is limited by ozone reactions at the surface. For highly reactive surfaces (soiled T-shirt surfaces), ozone uptake by the surface is limited by the rate at which ozone can be transferred to the surface (and hence air change rate).

The ozone-initiated VOC emissions were very low in Case 9 without the T-shirt, and the total concentration of VOCs only increased by about 4 ppb after ozone injection (results not shown). Figure 3.8 compares the VOC emissions in Case 10 with those in Case 3. In Case 10, the air change rate was 5 times higher, but the VOC concentrations only reduced by a factor of 2, which means that the VOC emission rate was approximately 2.5 times higher than Case 10 compared with Case 3. The higher emission rate was probably because Case 10 had a thin boundary layer compared with Case 3 (due to the higher air change rate), which could have enhanced the convective transport of VOCs from the T-shirt surface to the chamber air. Hence, Y_{fabric}, $Y_{skin\text{-}oil}$, and Y_{total} in Case 10 were also higher than those in Case 3, as shown in Table 3.2. The most significant increase was in $Y_{skin\text{-}oil}$, which more than doubled in Case 10.

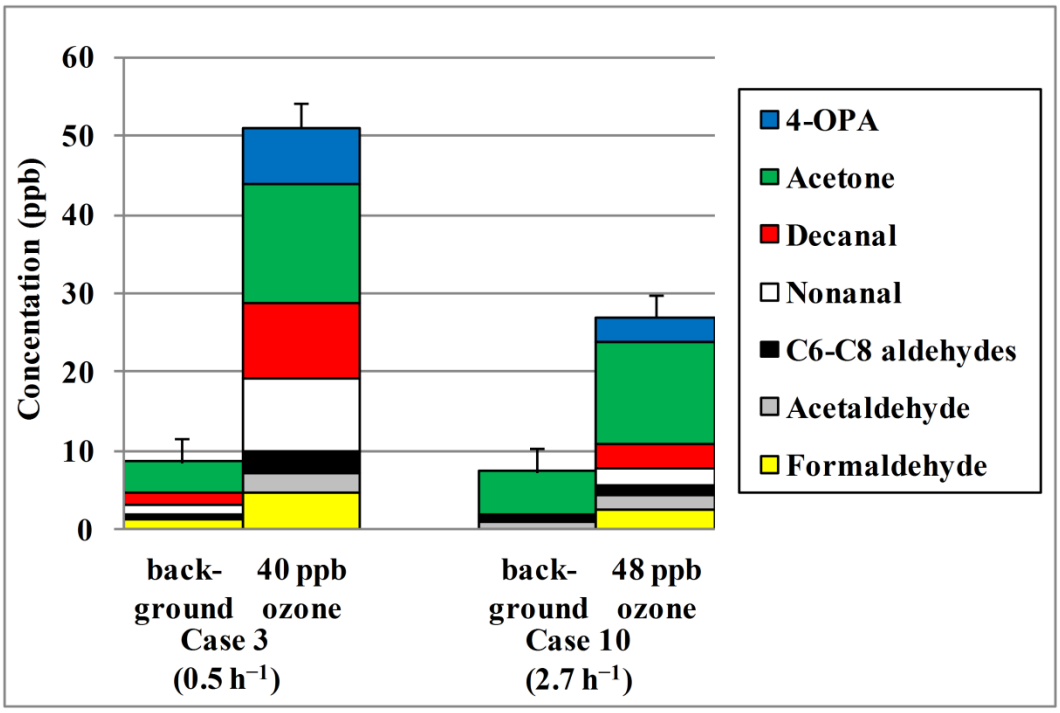

Figure 3.8. Effect of air change rate on the ozone-initiated VOC emissions with the soiled T-shirt. Error bars indicate plus one standard deviation.

3.4.3 Ozone Reaction Chemistry under Typical Building Conditions

Since this investigation used 0.5 h^{-1} air change rate for most of the cases, the ventilation rate corresponded to that in buildings. Of course, the ozone concentration in buildings is

normally not very high. Cases 12 and 13 simulated environmental conditions that could be found in buildings on a poor air-quality day. The ozone concentration was about 22 ppb. This investigation studied the ozone reactions under two different relative humidity conditions, 28% for Case 12 and 49% for Case 13.

The β_{total} and v_d in Case 13 was about 10% lower than in Case 12. However, the α in both cases was almost the same because the ozone concentration was higher in Case 13 ($\alpha = C_{exhaust} \times \beta_{total}$). Figure 3.9 shows that both the cases had significant ozone-initiated VOC emissions despite the low ozone concentrations. The VOC emissions were slightly higher in Case 13 compared to those in Case 12 probably due to the higher humidity level, which is also consistent with the results when comparing Case 3 with Case 5. The Y_{fabric} and Y_{total} were also higher in Case 13 compared with those in Case 12, but the $Y_{skin\text{-}oil}$ was approximately equal.

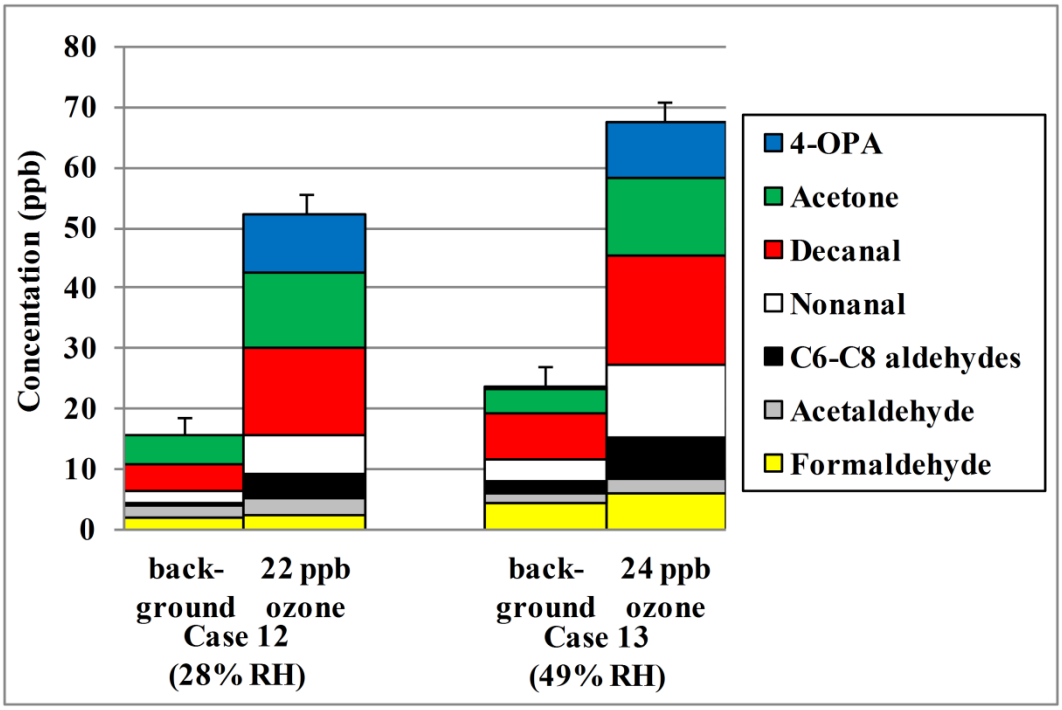

Figure 3.9. Ozone-initiated VOC emissions with soiled T-shirt under typical building conditions with different relative humidity levels. Error bars indicate plus one standard deviation.

3.5 Discussion

There were several sources of uncertainties in the experiment such as measurement errors of ozone monitors, GC-MS, and HPLC; uncertainties in soiling of T-shirts; random errors; etc. For example, this study did not quantify the amount of skin-oils on the T-shirt surface, which means there would be no assurance that the amount of soiling would be the same even if the same human subject slept in the T-shirt for the same amount of time. Hence, this investigation conducted duplicate experiments 3D and 10D for chamber conditions almost identical to Cases 3 and 10, respectively, to analyze the repeatability of the results. The β_{total} was 1.72 h^{-1} in Case 3D, which was about 8% lower than in Case 3. The β_{total} was 2.0 h^{-1} in Case 10D, which was about 12% lower than in Case 10. The production of the ozone-initiated VOCs was similar between the duplicate pairs of experiments as shown in Figure 3.10. Hence, there was reasonable repeatability between the duplicate pairs of experiments despite the experimental uncertainty.

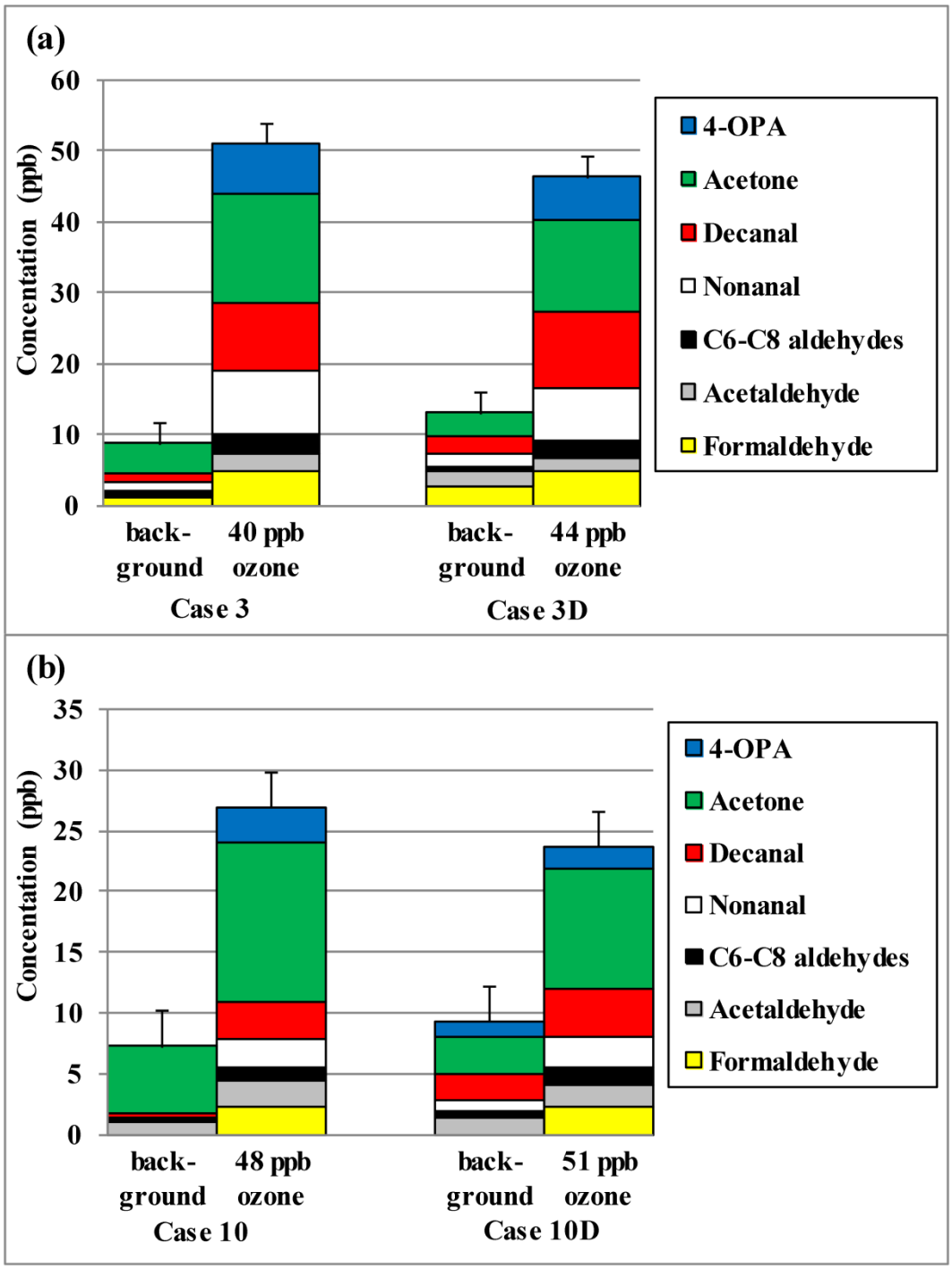

Figure 3.10. The ozone-initiated emissions of VOCs in duplicate experimental measurements, (a) for Case 3 (b) for Case 10. Error bars indicate plus one standard deviation.

3.6 Conclusions

This chapter experimentally studied ozone reactions with a cotton T-shirt in a middle-scale environmental chamber under different factors. The factors considered were ozone concentration, relative humidity, soiling degree of the T-shirt by human skin-oils, and air change rate. The study measured the ozone consumption and its initiated VOC emissions and came to the following conclusions:

The ozone reactions with the T-shirt consumed ozone and generated VOCs. The C6–C10 straight-chain saturated aldehydes were the major byproducts of the ozone reaction with the cotton T-shirt fabric. Acetone and 4-OPA were mainly produced due to the ozone reaction with the human skin-oils in the T-shirt.

These reactions were significantly affected by the chamber conditions. The ozone removal rate by the T-shirt and its deposition velocity increased with the increasing soiling level and air change rate, decreased at high ozone concentrations, and was relatively unaffected by the humidity.

The ozone-initiated VOC emissions were generally higher at higher ozone, humidity, soiling of T-shirt, and air change rates. The total molar yield for most cases was 0.5 as shown in Table 3.2, which means that for every two moles of ozone removed by the T-shirt surface, one mole of VOCs were produced.

CHAPTER 4. OZONE REACTION WITH CLOTHING AND ITS INITIATED PARTICLE GENERATION IN AN ENVIRONMENTAL CHAMBER

The previous chapter studied the ozone-initiated VOC emissions from its reactions with a T-shirt. Some of those VOC emissions were attributed to the ozone reactions with squalene, which is a triterpene found in the human skin-oils. Several researchers have also shown that the ozone reactions with terpene-based consumer products are important sources of submicron particles in the indoor air (Coleman et al., 2008b; Destaillats et al., 2006; Sarwar et al., 2004; Singer et al., 2006). Hence, it is conceivable that the ozone reactions with human skin-oils (which contains a triterpene) could also generate submicron particles. However, to our knowledge there was no investigation of particle generation from skin-oils. Therefore, we conducted measurements to investigate particle generation from ozone reactions with clothing with/without human skin-oils under different indoor conditions as discussed in this chapter. We studied the effect of various factors such as ozone concentration, relative humidity, degree of soiling of a T-shirt with skin-oils, and air change rate on the particle generation.

4.1 Method

This investigation conducted experiments in the environmental chamber (see Figures 3.1 and 3.2) that was described in the previous chapter. In addition to measurements of ozone and VOCs (reported in Chapter 3), we also measured the time-varying particle concentrations at the inlet, near the T-shirt, and exhaust. Particle concentrations were monitored by a Scanning Mobility Particle Sizer (SMPS) (Model 3936 by TSI), which measured the number concentrations of particles between 9.65 and 421.7 nm in diameter and separated them into 105 bins (or 64 bins per decade of particle diameter). The SMPS software also calculated the particle mass concentrations by:

$$M = \rho_p \frac{\pi}{6} Dp_m^3 N, \tag{4.1}$$

where ρ_p is the particle density; Dp_m the geometric midpoint diameter of the particle size bin; N the particle number concentration; and M the particle mass concentration. The particle density was taken as 1.2 g/cm^3 as suggested by Turpin and Lim (2001), who derived their results by using the data of Rogge et al. (1993) for atmospheric organic aerosols. Note that the particle number concentrations are approximate values since the SMPS was not calibrated before making the measurements, and the existing factory settings were used. Hence, the mass concentrations also bear large uncertainties since it was derived from the number concentrations by using Eq. (4.1).

To examine the particle generations due to ozone reactions with clothing and identify the effect of different factors on these generations, we used the same cases that were described in Table 3.1. However, some of those cases could not be used for studying the particle generations due to malfunctioning of the SMPS. Hence, Table 4.1 lists those cases (from Table 3.1) that measured the particle generations. Note that these cases have been renumbered in Table 4.1 (from Case 1–12) to carry out an orderly discussion of the results for this chapter.

Table 4.1. Details of the experimental conditions in the chamber used for studying particle generation from ozone reactions with human clothing.

Case	Corresponding case in Table 3.1	Ozone concentration (ppb)	Relative humidity (%)	Hours the T-shirt was worn (h)	Air change rate (h^{-1})
1	1	42	15	No T-shirt	0.5
2	2	46	17	Laundered T-shirt	0.5
3	3	40	12	6	0.5
4	4	148	20	6	0.5
5	5	54	44	6	0.5
6	6	70	23	2	0.5
7	7	57	24	12	0.5
8	8	53	27	6 hours by a different human subject	0.5
9	9	75	12	No T-shirt	2.7
10	10D	51	11	6	2.7
11	11	133	11	6	2.7
12	12	22	28	6	0.5

4.2 Results

This section first presents the results from Cases 1, 2, and 3, which were used to identify the effects of different surfaces on ozone-initiated particle generation. Next, the results of Cases 4–12 were used to analyze the influence of different factors on these particle generations and also to study them for typical building conditions. Table 4.2 summarizes the key results.

Table 4.2. Key results from the study of particle generation from ozone reactions with human clothing.

Case	$N_{max, exhasut}$ (#/cm^3)	Time at $N_{max, exhaust}$ (hours)	GMD at $N_{max, exhaust}$ (nm)	GSD at $N_{max, exhaust}$	Particle number concentrations at the end of experiment (#/cm^3)		Particle mass concentrations at the end of experiment (μg/m^3)	
					Inlet	Exhaust	Inlet	Exhaust
1	1212	8.2	20	2.2	271	509	0.15	0.30
2	2180	5.2	28	1.8	512	1235	0.28	0.49
3	8034	4.2	31	1.4	138	1408	0.08	0.79
4	23326	3.7	31	1.4	134	2212	0.07	1.10
5	8639	4.0	35	1.5	102	1819	0.07	1.86
6	3762	4.7	34	2.3	878	1404	0.62	2.09
7	8929	4.2	32	1.5	240	1886	0.14	1.29
8	5527	4.5	36	1.6	200	1293	0.15	1.32
9	323	6.0	19	2.3	217	208	0.17	0.16
10	781	1.7	19	2.2	159	192	0.05	0.17
11	714	0.5	20	2.2	140	171	0.08	0.11
12	1185	6.5	36	1.7	62	591	0.04	0.18
$N_{max, exhaust}$ is the peak particle number concentration at exhaust; GMD and GSD are the geometric mean diameter and standard deviation of particle size distributions, respectively.								

4.2.1 Effect of Different Surfaces on the Ozone-initiated Particle Generation

This subsection discusses particle generation due to ozone reactions with the steel chamber, laundered T-shirt, and soiled T-shirt surfaces. Figure 4.1 shows that the exhaust particle concentrations were very low in Cases 2 and 3 without ozone injection ($t < 2.5$ h). The particle concentrations were not measured without ozone in Case 1 because of a malfunction of the SMPS. After ozone injection ($t > 2.5$ h), the exhaust particle concentration did not show a significant increase without the T-shirt (Case 1) if it is assumed that the conditions for Cases 2 and 3 for $t < 2.5$ h applied to Case 1. However, the particle concentration increased significantly when the T-shirt was present (Cases 2 and 3). Compared with the laundered T-shirt (Case 2), the particle concentration was much higher with the soiled T-shirt (Case 3) after ozone injection. These results show

that the ozone reactions with the T-shirt generated particles, which were enhanced by the soiling of the T-shirt with human skin-oils, probably due to the ozone reactions with human skin-oils as suggested by Fadeyi et al. (2013).

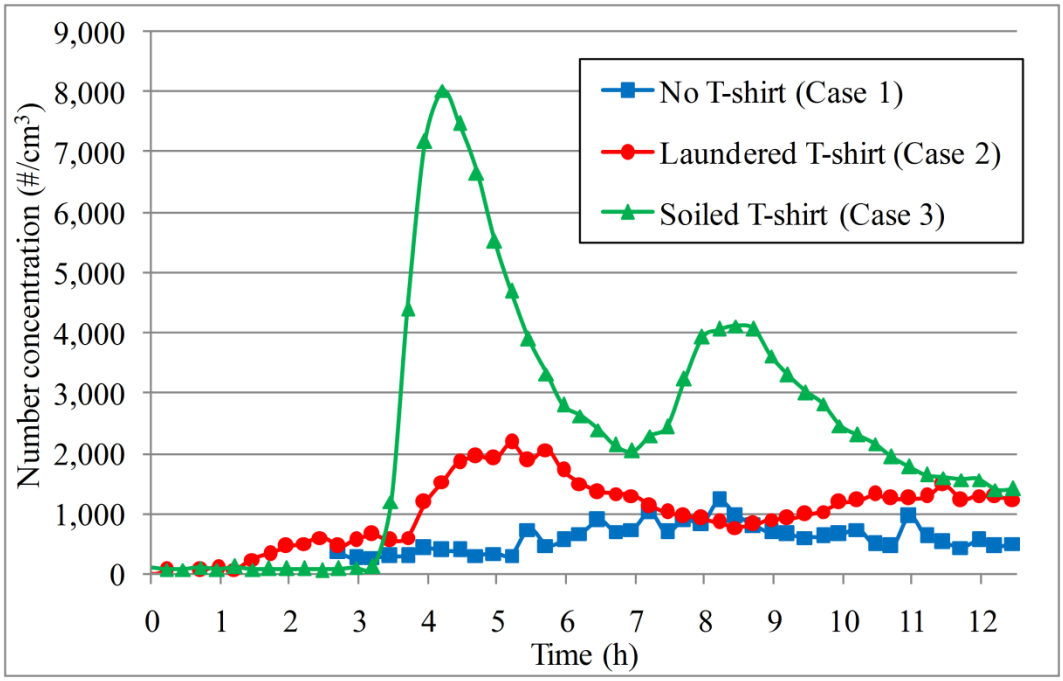

Figure 4.1. Effect of chamber, laundered T-shirt, and soiled T-shirt surfaces on the ozone-initiated particles measured at the exhaust.

We further analyzed particle generation due to ozone reactions with the soiled T-shirt (Case 3) since it was the most significant. Figure 4.2 shows the temporal variations of particle number and mass concentrations at the inlet and exhaust for Case 3. The corresponding particle size distributions at the exhaust are shown in Figure 4.3 for some important points in time. The exhaust particle concentrations were low from t = 0–2.5 h as shown in Figures 4.2 and 4.3(a), due to the low inlet concentrations. From t = 2.5 h, ozone was continuously injected in the chamber, but the particle concentrations were still low even after 40 minutes (t = 3.2 h) as shown in Figure 4.3(b). At t = 3.5 h, a primary burst of ultrafine particles (UFPs) with a geometric mean diameter of approximately 18 nm was measured, as shown in Figure 4.3(c). This one-hour delay after the ozone injection was probably due to the time required for the generation of sufficient precursors

from the ozone reactions (low-vapor-pressure oxidation products), which can form particles.

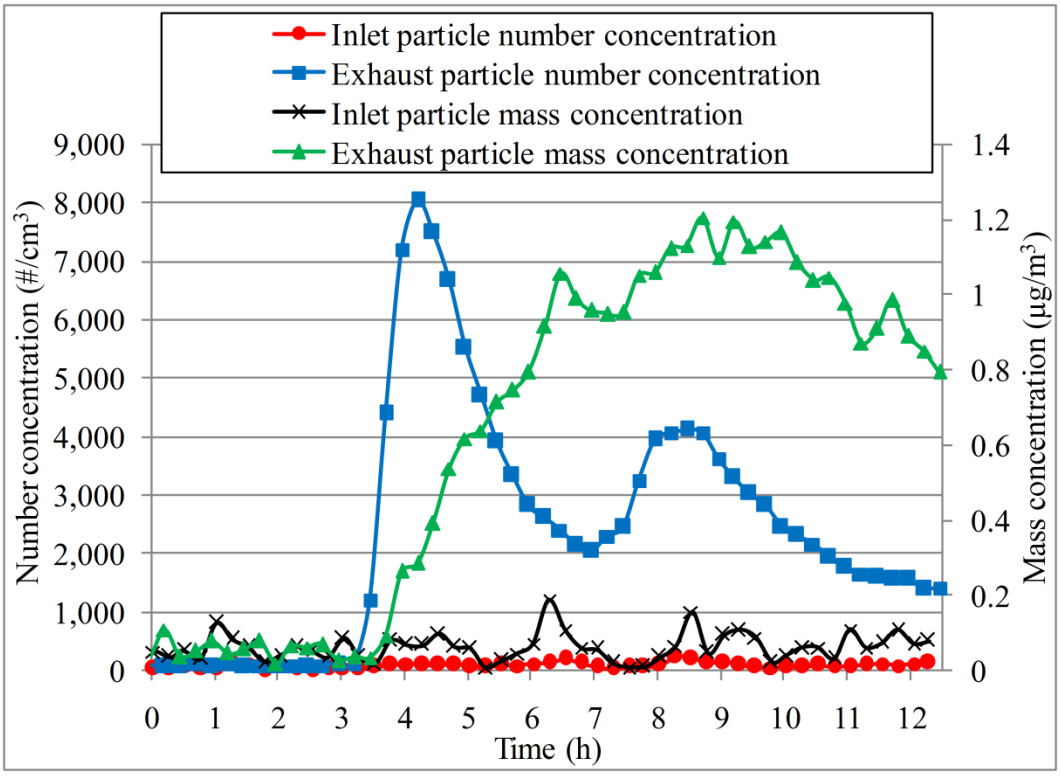

Figure 4.2. Temporal variations of particle number and mass concentrations at the inlet and exhaust for the ozone reactions with the soiled T-shirt in Case 3.

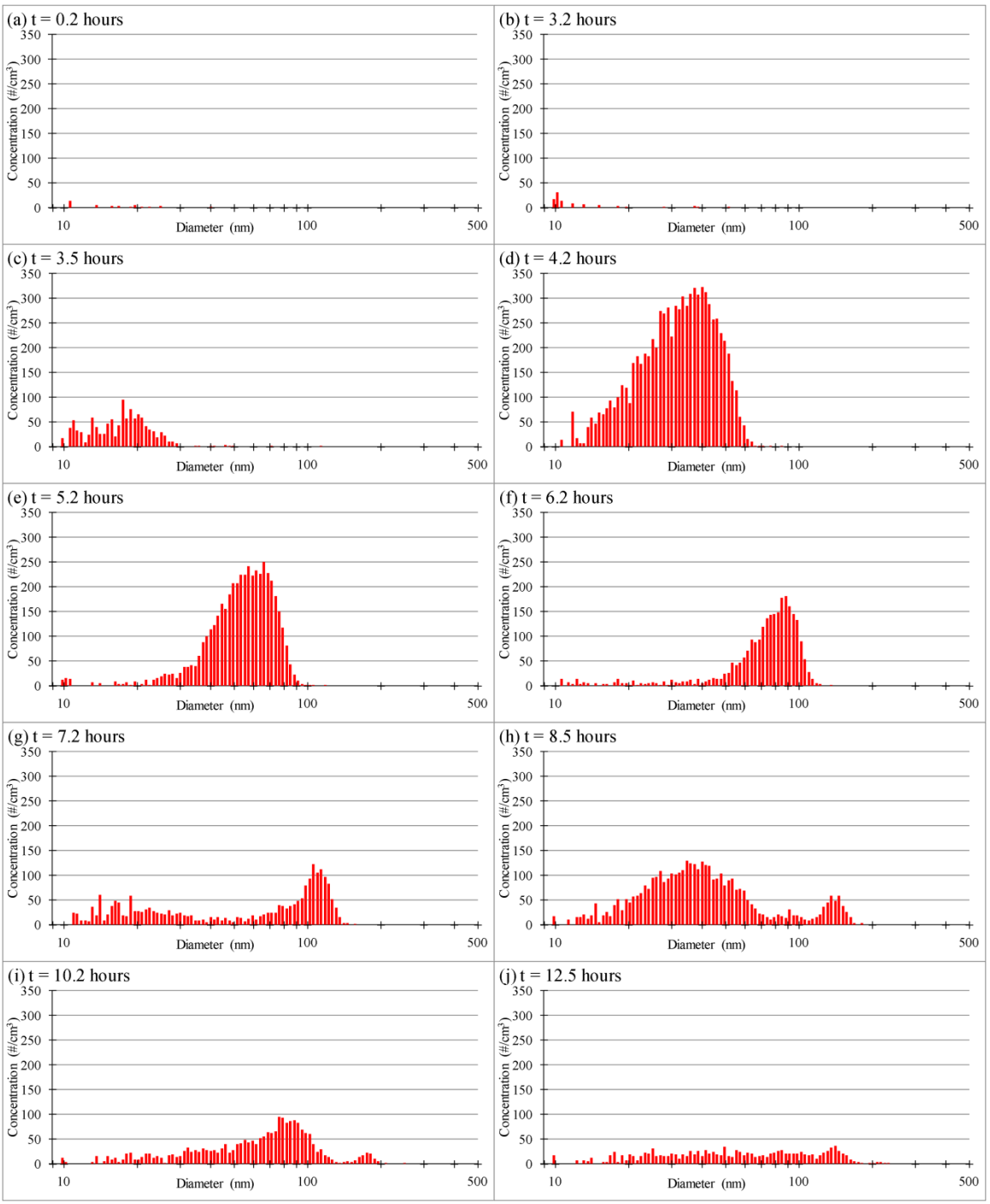

Figure 4.3. Evolution of particle size distributions at the exhaust for the ozone reactions with the soiled T-shirt in Case 3.

The primary burst could be attributed to nucleation (which forms new particles) or condensation (which leads to particle growth) on smaller existing particles, which grew

to sizes measurable by SMPS. However, nucleation seems more likely, since condensation on existing particles should also produce particle bursts in higher sizes as suggested by Sarwar et al. (2003). After the primary burst, the number and mass concentrations increased for about 45 minutes (until t = 4.2 h), and the particles sizes also grew as shown in Figures 4.2 and 4.3(d). Hence, nucleation, condensation, and coagulation mechanisms seemed to prevail. The number concentrations then decayed (until t = 7.0 h), which suggests that new particles formed at a slower rate as compared to the removal of existing particles by ventilation and deposition. However, the mass concentrations and particle sizes continued to increase, indicating that particle generation by condensation was dominant, as shown in Figures 4.2, 4.3(e), and 4.3(f). Coagulation of particles could also be responsible for some of the particle growth, but it cannot account for the increasing mass concentrations, suggesting that growth by condensation was more significant.

A secondary burst of UFPs was observed at t = 7.2 h as shown in Figures 4.2 and 4.3(g). Hence, it seems that new particles were formed by nucleation, since insufficient particles were left in the chamber which reduced the surface area available for condensation as shown in Figure B.1. A similar phenomenon was also observed by Coleman et al. (2008b) during ozone-initiated particle generations from terpene-rich household products. The particle concentrations and sizes continued to increase until t = 8.5 h, probably as a result of nucleation, condensation, and coagulation mechanisms as shown in Figures 4.2 and 4.3(h). Finally, the particle number concentrations decayed until the end of the experiment because of ventilation and deposition. The mass concentrations also decayed, probably because of a decrease in particle generation rate or particle growth beyond the measuring range. Figures 4.3(i) and (j) illustrate the particle size distributions towards the end of the experiment. We did not observe another burst of particles toward the end of the experiment despite the number concentrations (and surface area) being lower than that at which the secondary burst was observed. Hence, it seems that the particle generation rate declined towards the end, probably as a result of depletion of skin-oils from the T-shirt surface.

4.2.2 Effect of Different Factors on the Ozone-initiated Particle Generation

This study used Cases 4 to 11, given in Table 4.1 to identify the effect of different factors on particle generation resulting from ozone reactions with the soiled T-shirt. These cases were originally designed by keeping Case 3 as the reference and varying one factor at a time to isolate its effect on particle generation. However, it was difficult to control the chamber conditions precisely, and sometimes more than one factor varied from the reference case, which made the reference case unsuitable for comparison. Hence, we compared those cases which had roughly identical conditions except for the factor to be examined. The factors examined were ozone concentration, relative humidity, soiling degree of the T-shirt, and air change rate.

4.2.2.1 Effect of Ozone Concentration

This investigation compared Cases 3 and 4, which had 40 ppb and 148 ppb ozone, respectively, in order to identify the effect of ozone on particle generation. The other conditions were similar between the two cases.

Figures 4.4(a) and (b) compare the particle number and mass generation, respectively, from the ozone reaction with the soiled T-shirt in Cases 3 and 4. In both the cases, the inlet particle concentrations were very low throughout the experiment. A primary and secondary burst of UFPs was measured at exhaust after ozone was injected at t = 2.5 h, and the particle generation mechanisms were also similar. However, the primary burst of particles occurred earlier in Case 4 (148 ppb ozone), and the particle number and mass concentrations were also generally higher. Hence, it seems that the high ozone concentration in Case 4 increased the production of particle-forming precursors from its reactions with the soiled T-shirt. The secondary burst of particles happened later in Case 4 than that in Case 3, since the high particle concentrations (and high surface areas) in Case 4 probably sustained condensation for a longer period of time.

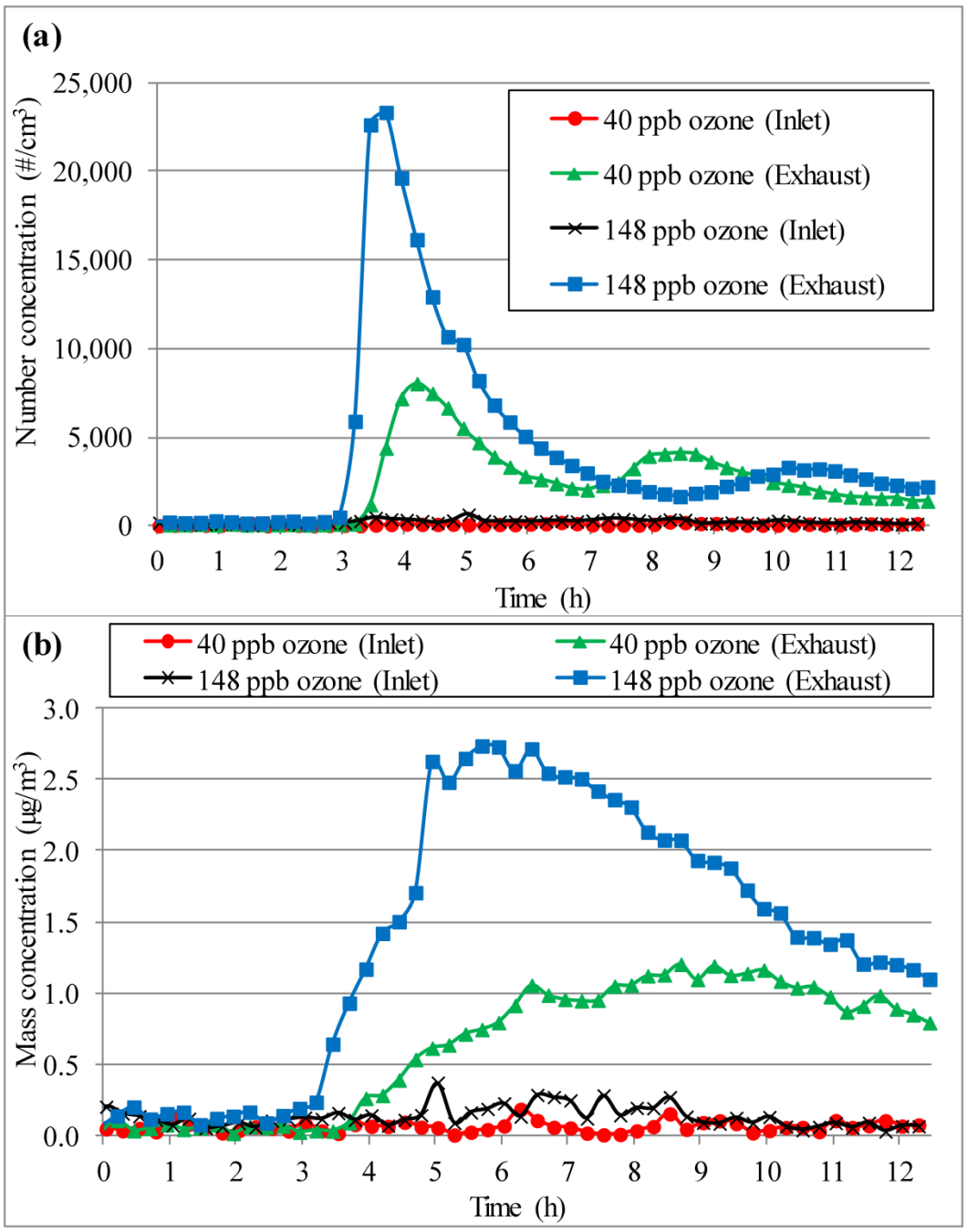

Figure 4.4. Effect of ozone concentration on (a) particle number generation and (b) particle mass generation when the ozone reacted with the soiled T-shirt.

4.2.2.2 Effect of Relative Humidity

This study used Case 5 with a relative humidity of 44% to study the impact of relative humidity on particle formation, by comparing it with Case 3 with a relative humidity of 12%. The other conditions were roughly similar for the two cases.

The inlet and exhaust particle number concentrations over time were approximately the same in Cases 3 and 5 as shown in Figure 4.5(a), except that the secondary burst was less pronounced in Case 5. The secondary burst was less significant in Case 5 because condensation was dominant over nucleation due to the large surface area of existing particles as shown in Figure B.2. The particle mass concentrations were also significantly higher in Case 5 (44% RH), as shown in Figure 4.5(b), because of larger particle sizes. Such an increase in sizes was reported by Dua and Hopke (1996) for some indoor particles at high relative humidity conditions, and was attributed to hygroscopic growth. Hence, it seems that the particles generated by ozone reactions with the soiled T-shirt were hygroscopic in nature, and their sizes increased at high relative humidity, which also increased their masses.

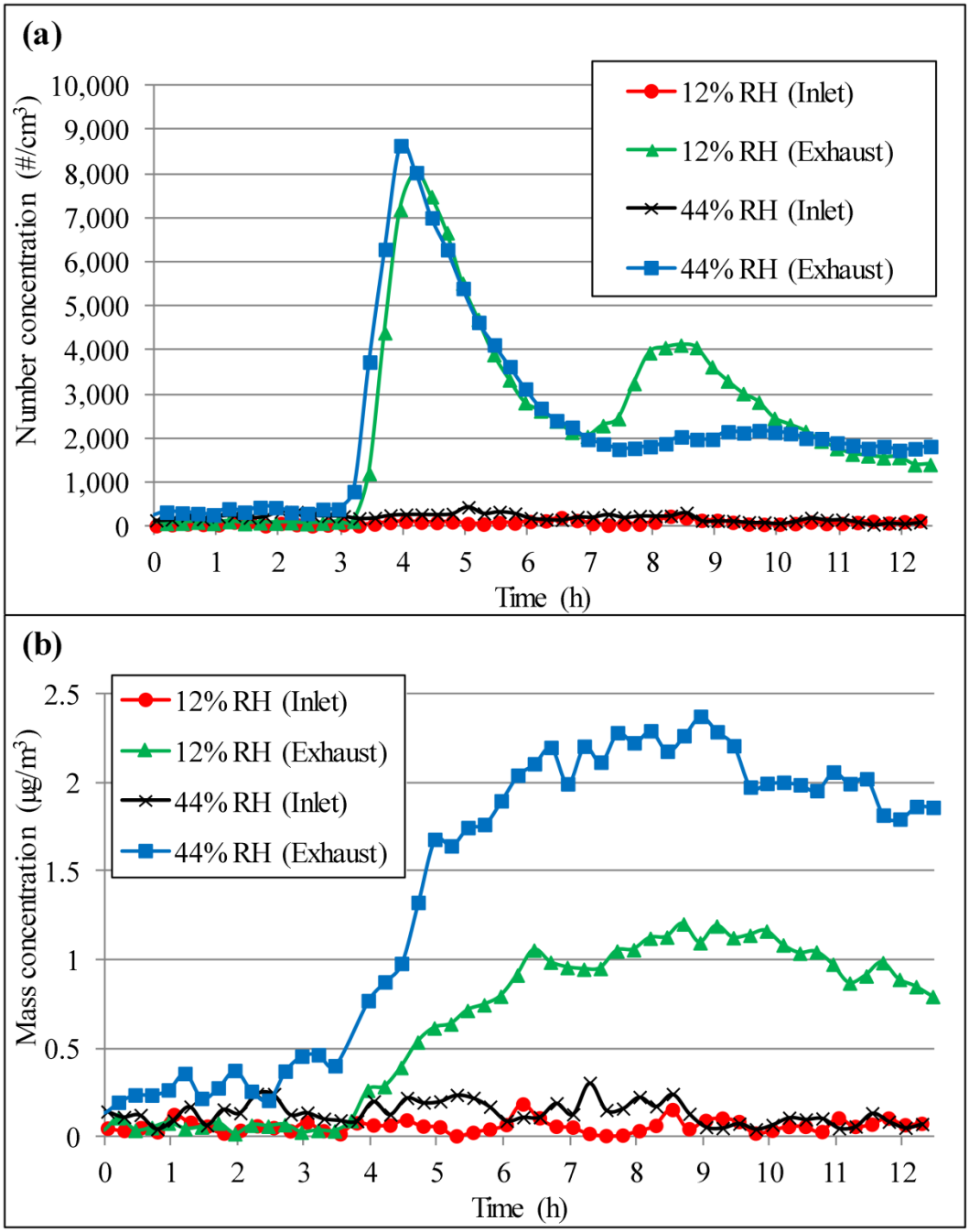

Figure 4.5. Effect of relative humidity on (a) ozone-initiated particle number generation and (b) ozone-initiated particle mass generation with the soiled T-shirt.

4.2.2.3 Effect of T-shirt Soiling

This investigation used Cases 6 and 7 given in Table 4.1, which had different soiling levels of the T-shirt but otherwise similar conditions, to identify the effect of soiling level

on particle generation. The different soiling levels of the T-shirt were achieved by a human subject's sleeping in it for 2 hours and 12 hours in Cases 6 and 7, respectively.

Initially, the exhaust particle number and mass concentrations with the 2-hour soiled T-shirt in Case 6 were higher than those with the 12-hour soiled T-shirt in Case 7 because of the high inlet concentrations as shown in Figures 4.6(a) and (b). From t = 2.0 h to t = 3.5 h, the exhaust concentrations in Case 6 further increased because of an increase in the inlet particle concentrations. For t > 3.5 h the exhaust concentrations continued to increase, but not the inlet concentrations. This indicates that the particles were generated from the ozone reactions in Case 6 because the ozone was injected at t = 2.5 h. Since the inlet particle concentrations for Case 7 were relatively stable and small, it is much easier to see particle generation from the ozone reaction after the ozone was injected at t > 2.5 h.

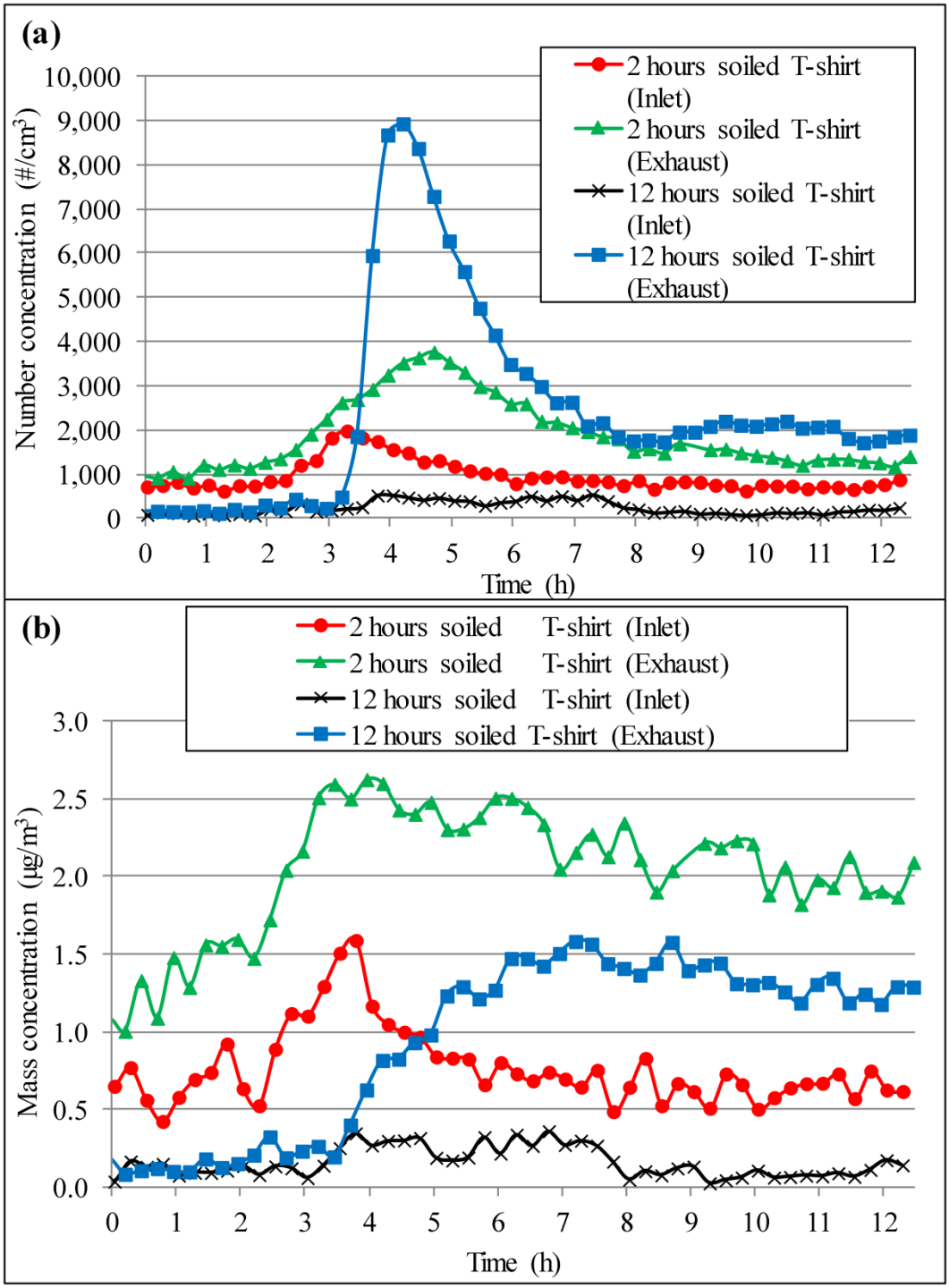

Figure 4.6. Effect of the soiling level of the T-shirt by skin-oils on (a) ozone-initiated particle number generation and (b) ozone-initiated particle mass generation.

After ozone injection, the particle number concentration in Case 7 was significantly higher than that in Case 6. The lower particle concentration in Case 7 before ozone injection could have promoted much higher nucleation of new particles compared to that in Case 6. Such a phenomenon was also reported by Sarwar et al. (2003), who found that low initial particle concentrations (and low surface areas) supported nucleation of new particles, whereas high initial concentrations (and high surface areas) favored condensation on existing ones. The particle mass generation in Case 7 was lower than that in Case 6 as shown in Figure 4.6(b), probably because the 2-hour soiling level was sufficiently high for the reaction and the reaction was already saturated.

In order to characterize the effect of skin-oils from different human subjects on particle generation, this investigation used a T-shirt soiled by a female subject (middle-aged American) in Case 8. The results were compared with those of Case 7 under similar conditions.

Figure 4.7(a) shows the particle number concentrations at the inlet and exhaust for the two cases. Before the ozone injection ($t < 2.5$ h), the exhaust particle concentration in Case 8 was greater than that in Case 7 because of high inlet concentration. However, after the ozone injection, the exhaust number concentration was higher in Case 7, probably because of higher nucleation of new particles resulting from low initial concentrations, which was discussed when comparing Cases 6 and 7. The particle mass generation was similar for both cases as shown in Figure 4.7(b), which indicates that it was unaffected by the different human subjects in these cases.

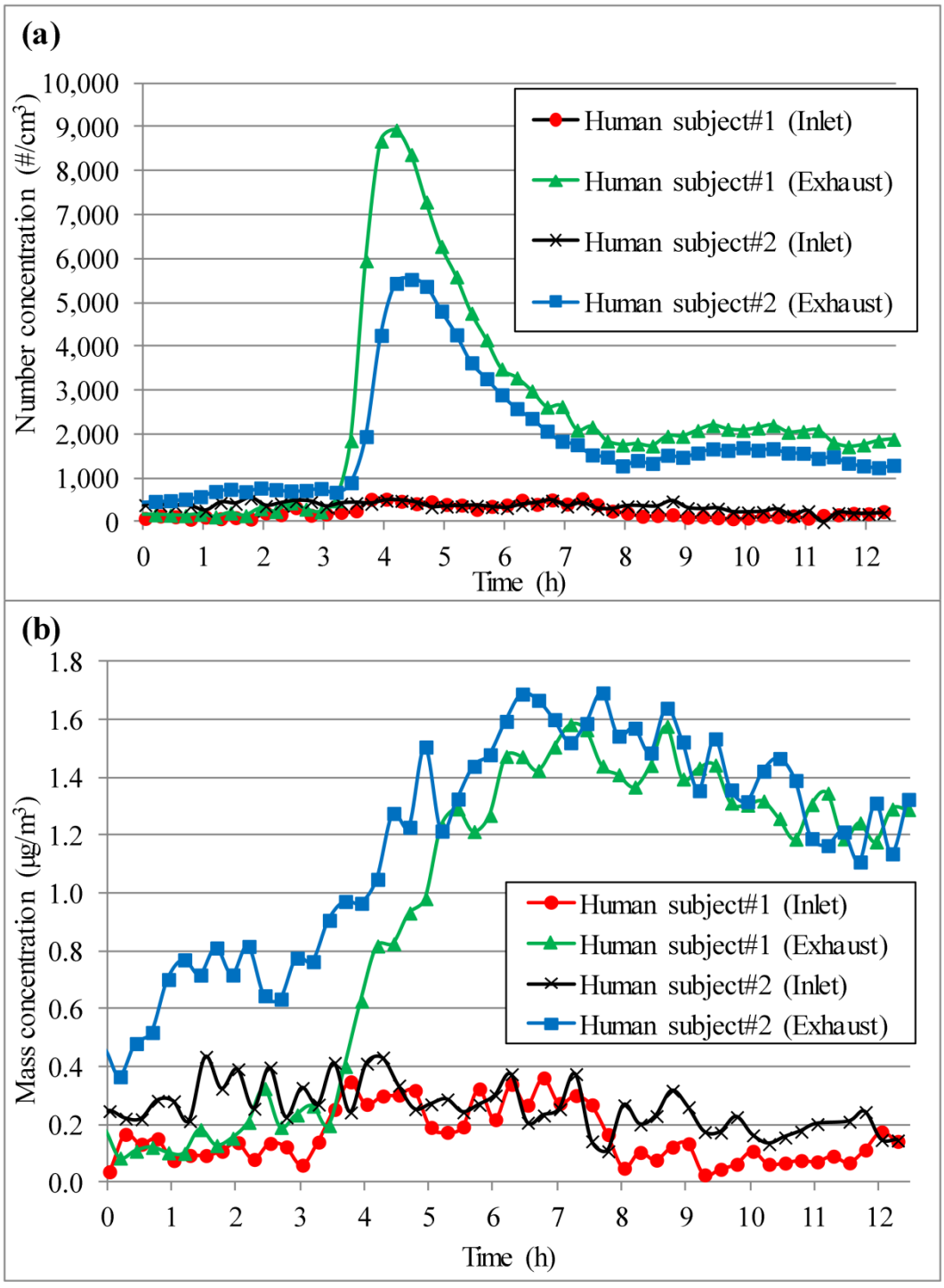

Figure 4.7. Effect of T-shirt wearing by different human subjects on (a) ozone-initiated particle number generation and (b) ozone-initiated particle mass generation.

4.2.2.4 Effect of Air Change Rate

Cases 9 to 11, given in Table 4.1, were at a higher air change rate of 2.7 h^{-1}. Case 9 was without a T-shirt; Case 10 with a soiled T-shirt at 51 ppb ozone; and Case 11 with a soiled T-shirt at 133 ppb ozone. In all of these cases, particle generation due to ozone reactions was not observed because the exhaust and inlet particle concentrations were approximately the same, as illustrated in Table 4.2. It seems that there was insufficient time for particle formation at the high air change rate, since the high ventilation could quickly remove the particle-forming precursors from the chamber. These results are in qualitative agreement with a previous study by Weschler and Shields (2003), who measured particle generation from gas phase ozone reactions with d-limonene (a terpene) under different air change rates. They found that ozone-initiated particle generations decreased when the air change rate was increased, and finally that no excess particles were detected at air change rates exceeding 12.0 h^{-1}.

4.2.3 Ozone-initiated Particle Generation under Typical Building Conditions

Most of the cases studied (Cases 1 to 8) were with an air change rate of 0.5 h^{-1}, which corresponded to typical ventilation conditions in buildings. However, these cases had high ozone concentrations when compared with about 10 ppb as typically found in buildings. The high concentration, in fact, helps us accurately characterize the effect of different factors on the ozone reactions, since a low ozone concentration would considerably increase the experimental uncertainties. Nevertheless, we conducted Case 12 as a low-ozone case with only 22 ppb concentration, which can be found in buildings on a poor air quality day.

Figure 4.8 shows the ozone-initiated particle number generation for Case 12. The particle mass generation is not shown here; it was very low because of the small number concentrations, which led to high fluctuations in the estimation of mass concentrations from Eq. (4.1) Nevertheless, the particle generation mechanism seemed similar to previous cases. A primary burst of UFPs was observed at about one hour after ozone injection, which was followed by particle growth. Finally, the particle number

concentration attained a steady value of about 600 #/cm^3 with most particles lying in the ultrafine region (diameters < 100 nm). Hence, it seems that the ozone reactions with human clothing can become a possible source for indoor UFPs, which is further discussed in the next section.

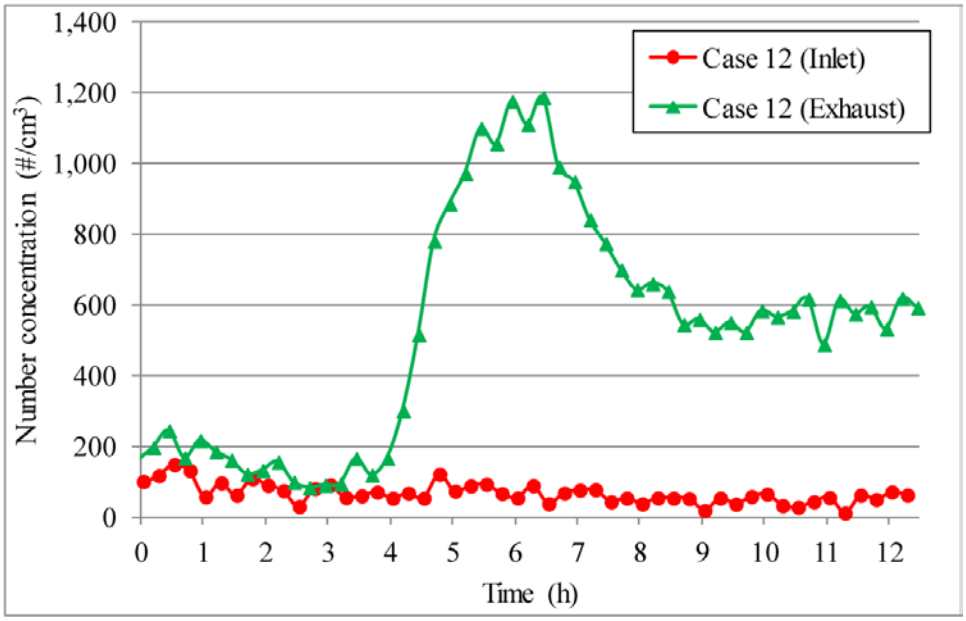

Figure 4.8. Ozone-initiated particle number generation under typical building conditions.

4.3 Discussion

UFPs are presumably responsible for the association between the exposure to particulate matter and morbidity and mortality (Donaldson et al., 1998; Seaton et al., 1995; Sioutas et al., 2005). Wallace and Ott (2011) estimated the indoors exposure to UFPs as 2373 #/cm^3 when no sources were present, and the total daily intake was estimated to be 172000 #-h/cm^3 for typical suburban locations. We calculated that the ozone reactions with human surfaces can contribute between 80–160 #/cm^3 UFPs for typical building conditions on a poor air quality day (See Appendix B for details), which corresponds to a daily intake of 1760–3520 #-h/cm^3 UFPs for 22 hours spend indoors. Hence, such ozone reactions can account for approximately 5% of the indoor UFPs and 2% of the total daily intake. Note that the above calculations had some simplifying assumptions and only provide a very rough estimate of exposure to ozone-initiated UFPs from human surfaces.

The ozone-initiated particle generation from human surfaces seems quite small when compared with that from ozone reactions with common consumer products such as fragrances and cleaners. For example, Long et al. (2000) observed a peak increase of 7–100 times in particle number concentrations in Boston-area homes due to the ozone reactions with a commercial cleaning agent. However, other human surfaces such as skin and hair could potentially react with ozone and generate particles at much higher rates compared to that by clothing, since human skin-oil seems to be an important ingredient for the particle generation. Such particle generation could become significant in indoor settings with high occupancy and ozone levels such as airliner cabins, which is further analyzed in Chapter 7.

4.4 Conclusions

This chapter studied the particle generation due to ozone reactions with clothing (a T-shirt) in an environmental chamber under typical indoor conditions. The study identified the effect of some important factors such as ozone concentration, relative humidity, degree of soiling of the T-shirt with human skin-oils, and air change rate on the particle generation. The study led to the following conclusions:

The ozone reactions with T-shirt with/without human skin-oils led to generation of sub-micron particles. Particle generation was significantly higher when the T-shirt was soiled with skin-oils. Those particles were initially generated in the ultrafine region and then grew to larger sizes.

The particle generation increased with increasing ozone concentrations. A higher relative humidity did not increase the particle number generation, but led to hygroscopic growth of particles to larger sizes, which increased their masses. The particle generation was relatively unaffected by an increase in soiling level of T-shirt from 2 hours to 12 hours or by different human subjects. At a higher air change rate, few particles were formed due to short residence time of the air. The ozone reactions with clothing were identified as another potential source of UFPs in the indoor environment.

CHAPTER 5. SIMULATIONS OF OZONE DISTRIBUTIONS IN AN AIRCRAFT CABIN USING COMPUTATIONAL FLUID DYNAMICS

It was reviewed in Section 2.2.1 that a few studies have utilized computational fluid dynamics (CFD) to show that significant gradients can exist in the indoor ozone concentration due to its gas-phase and surface reactions occurring in the indoor environment. These CFD studies also found that the bulk air measurements of ozone were insufficient to accurate quantify its exposure to humans. However, these studies had limited validation. Therefore, to better assess the exposure to ozone we developed a CFD model to simulate the ozone distributions in an aircraft cabin and also conducted detailed analysis for validating the CFD model, which is discussed in this chapter.

5.1 Method

This investigation used CFD to model the ozone transport and consumption by different surfaces in an aircraft cabin since it is inexpensive and informative. The CFD model solved the Reynolds-averaged Navier-Stokes equations with the re-normalization group (RNG) k-ε turbulence model (Yakhot and Orszag, 1986). Zhang et al. (2009) recommended using the RNG k-ε turbulence model since it can effectively predict the turbulent features of the airflow in an aircraft cabin. The ozone concentration distribution was solved by the following species transport equation:

$$\nabla.(\rho\vec{u}C) = \nabla.((\rho D_{ozone} + \frac{\mu_t}{Sc_t})\nabla C), \tag{5.1}$$

where ρ is air density, $\vec{u}$ the air velocity vector, C the ozone concentration, D_{ozone} the binary diffusion coefficient of ozone in air, μ_t the turbulent viscosity, and Sc_t the turbulent Schmidt number.

This investigation used the second-order upwind discretization scheme for solving all the variables except pressure. Pressure discretization was based on the PRESTO! (Pressure staggering option) scheme (FLUENT, 2009). The Boussinesq approximation was used to account for the buoyancy effects. The governing equations were solved using the SIMPLE algorithm (Patankar, 1980) in the commercial CFD software FLUENT (FLUENT, 2009).

5.1.1 Surface Deposition

In order to solve the ozone distribution in an aircraft cabin by using Eq. (5.1), it is necessary to have an appropriate model to compute the ozone deposition (or consumption) at cabin and human related surfaces. The surface ozone deposition depends on (1) fluid motion and ozone diffusion that transport ozone molecules to the surfaces and (2) the ozone chemical reactions on the surfaces. The ozone deposition flux at surface J_{ozone} is given by (Cano-Ruiz et al., 1993):

$$J_{ozone} = -\gamma \frac{< v >}{4} C\Big|_{y=\frac{2}{3}l}, \tag{5.2}$$

where γ is the mass accommodation coefficient (or reaction probability) between the ozone and the deposition surface and is defined as the fraction of all ozone molecules collision with the surface that results in deposition, <v> Boltzmann velocity for ozone (360 m/s at 293 K), C ozone concentration, and l mean molecular free path (6.5×10^{-8} m at 293 K and 1 atm). Eq. (5.2) can be used to calculate the ozone flux at cabin and human related surfaces. However, Eq. (5.2) requires CFD to use an extremely fine grid size near the deposition surface (comparable to l). To increase the grid size near the surface, this study used the following flux model (Sørensen and Weschler, 2002):

$$J_{ozone} = \frac{-\gamma . \frac{< v >}{4}}{1 + \gamma . \frac{< v >}{4} . \frac{\Delta y_1}{D_{ozone}}} . C\Big|_{y=\Delta y_1}, \tag{5.3}$$

where Δy_1 is the distance of the first cell center from the surface. Note that Eq. (5.3) is valid only when the first grid point is very close to the surface (ideally $y^+ < 1$).

This study used Eq. (5.3) to determine the ozone flux at cabin surfaces such as the carpet and seats. Since ozone reacts significantly with human related surfaces such as skin, hair, and clothing (Pandrangi and Morrison, 2008; Weschler et al., 2007; Wisthaler et al., 2005), the ozone concentration is expected to be very low at those human related surfaces (Pandrangi and Morrison, 2008). Hence, this study set zero ozone concentration at human related surfaces, as suggested by Rim et al. (2009).

5.1.2 Mass Accommodation Coefficient (γ)

The γ for different surfaces is a necessary input for the CFD model to compute the ozone deposition using Eq. (5.3). The γ was calculated by using the two-resistor model developed by Cano-Ruiz et al. (1993):

$$\gamma = \left[\frac{< v >}{4} \left(\frac{1}{v_d} - \frac{1}{v_t} \right) \right]^{-1}, \tag{5.4}$$

where v_d is the ozone deposition velocity and defined as the ozone flux normalized by a characteristic ozone concentration; v_t the transport limited deposition velocity and defined as the deposition velocity when γ equals one.

The v_d for the different surfaces was available from the experimental data of Tamas et al. (2006). The v_t was estimated using CFD as follows:

- The v_d is equal to v_t, when the surface resistance to the ozone deposition becomes zero; i.e., the surface becomes a perfect sink.
- Hence, in order to estimate v_t for a surface, we performed CFD simulations by setting the ozone concentration equal to zero at that surface.
- The v_d (which equals to v_t) was calculated by the following equation:

$$v_d = \frac{Q}{A}\frac{(C_{inlet} - C_{exhaust})}{C_{avg}}, \tag{5.5}$$

where Q is the supply airflow rate to the cabin; A the area of the ozone deposition surface; and C_{inlet}, $C_{exhaust}$, and C_{avg} the inlet, exhaust, and volume averaged cabin ozone concentrations, respectively. Note that the above equation is valid for a cabin with only one deposition surface, one inlet, and one exhaust, under steady state.

The γ for the carpet surface is 8.4×10^{-6} by using the above-mentioned method. The value is lower than that of some previous measurements made for carpet surfaces (Coleman et al., 2008a; Morrison and Nazaroff, 2000), where γ was found to be between 10^{-4} and 10^{-5}. The study by Morrison and Nazaroff (2000) also found that all carpet specimens exhibited the phenomenon of "aging" since the γ decreased after a long period of ozone exposure. The γ obtained in this investigation is comparable to that of carpet surfaces obtained after 48-hour ozone exposure (Morrison and Nazaroff, 2000). A direct comparison between these different γ values should be avoided as different studies used different carpet specimens that had a wide variety of storage and usage history.

The γ for seat surfaces was determined to be 1.9×10^{-5}, which is lower than that obtained experimentally by Coleman et al. (2008a) for a soiled seat fabric ($\gamma = 1.4\times10^{-4}$). Again, the differences could be attributed to the differences in seat fabric and usage history. Nevertheless, the γ for seat surfaces is higher than that for carpet since the seat fabric is soiled with human skin-oils to some extent. These γ values for carpet and seat surfaces have been used in this study to compute the ozone deposition by using Eq. (5.3).

5.2 Case Setup

This investigation used CFD to simulate the ozone distributions in an aircraft cabin mockup for which detailed experimental data were available (Tamás et al., 2006). The cabin mockup was a section of Boeing-767 (3 rows, 21 seats) as shown in Figure 5.1, which was 4.9 m wide, 3.2 m long, and 2.0 m high in the center with a total volume of $28.5 m^3$. The experimental setup injected the air containing ozone to the cabin from the two overhead air-supply slots along the longitudinal direction (12 mm × 3200 mm each)

with a velocity of 2.6 m/s and a flow rate of 200 L/s. The ozone concentration in the cabin mockup was measured at its center and varied from 41–341 ppb depending on the experimental conditions and objectives, but this investigation used only a constant ozone concentration of 100 ppb at the inlets. Note that the species transport equation (Eq. (5.1)) and the CFD boundary conditions used in this investigation were homogeneous (if ‘C’ is a solution, then all its multiples will also be solutions) with respect to the ozone concentration except the inlet condition. Hence, the absolute level of ozone would be determined by the inlet concentration and all the results can be normalized with the volume averaged cabin ozone concentration for comparison against the experimental data.

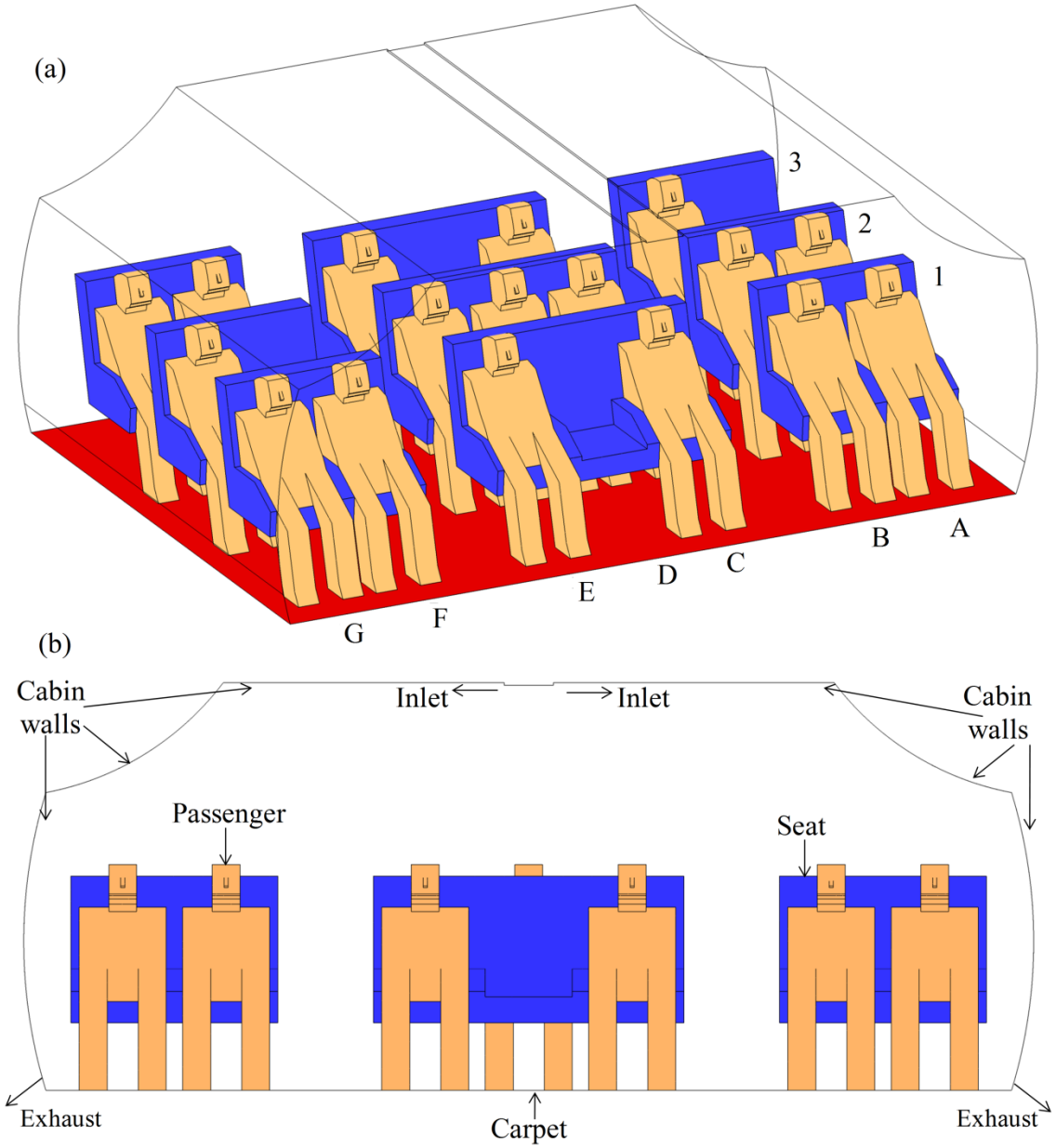

Figure 5.1. The occupied cabin setup for Case 5, (a) the schematic of the case and (b) boundary surfaces in the cabin mockup.

In the experiment, the air containing ozone entered the cabin mockup through the air supply system. The ozone in the cabin depleted due to its reaction with various surfaces (carpet, seats, human skin, and clothing) and gas phase compounds. The ozone removal by surface reaction versus gas phase reactions was governed by the outdoor air change rate. The high outdoor air change rate (between 3.0 and 8.8 h^{-1}) in the cabin reduced the

time available for gas phase reactions because the residence time of the gases in the cabin was low. At such high outdoor air change rates, only unsaturated organic compounds can undergo gas phase reactions with ozone. Weschler et al. (2007) measured the level of unsaturated organic compounds in the cabin mockup at outdoor air change rates of 4.4 and 8.8 h^{-1} in the absence of ozone (ozone concentration less than 2 ppb). They found that the concentration of unsaturated organic compounds was very low (less than 2 ppb) for any significant loss of ozone through gas phase reactions. Thus, the high air change rate in the cabin coupled with the low concentration of unsaturated organic compounds prevented the ozone removal by gas phase reactions. Hence, the present investigation only modeled the ozone removal by surface reactions.

In order to separate the influence of each surface on the ozone concentration, this investigation designed five different cases as illustrated in Table 5.1. The cabin setup in the design varied systematically, such as the presence or absence of seats and people and soiled T-shirts. The gradual changes in the complexity of the boundary conditions in these cases enabled us to make a step-by-step comparison with the experimental data for validating the CFD model. The occupied cabin cases (Cases 4 and 5) were designed to gain an understanding of the exposure to ozone of passengers seated at different locations in the cabin as well as the overall ozone distribution in the cabin environment. The boundary conditions in the CFD model are presented in Table 5.2. The enhanced wall treatment model (FLUENT, 2009) was used to solve the airflow near the walls. The inlet temperature was 24°C for Cases 1, 2, and 3 and 21.2°C for Cases 4 and 5. The lower temperature in Cases 4 and 5 was to maintain the same cabin air temperature by offsetting the heat generated by the passengers. Figure 5.1 shows the schematic and its boundary surfaces for Case 5, which represented the most complex scenario. Figure 5.2 shows the grid used for Case 5. The grid consisted of 2.43 million elements where tetrahedral elements were used for the bulk volume, and layers of extruded triangular prisms were created on ozone reactive surfaces. The prism elements were used near the ozone reactive surfaces to accurately capture the boundary layer flow and ozone deposition. The initial height of the prism layer was kept very small (~ 2 mm) to ensure that the y^+ was small (~ 5) near the ozone reactive surfaces, and the deposition model (Eq.

(5.3)) was valid. The average y^+ for the other cabin surfaces was around 15 and the maximum value was less than 100 in all the cases. This meshing strategy was used for all the cases.

Table 5.1. Description of the five cases used in studying the ozone reaction in a cabin mockup.

Case	Description	Ozone reaction surfaces
1	Empty cabin	Carpet
2	Cabin with seats	Carpet and seats
3	Cabin with seats and T-shirts	Carpet, seats, and T-shirts
4	Occupied cabin with simple human geometry (block model)	Carpet, seats, and passengers
5	Occupied cabin with detailed human geometry	Carpet, seats, and passengers

Table 5.2. The thermal, ozone, and turbulence boundary conditions used for the five cases.

Surfaces	Temperature	Ozone	Turbulence
Inlet	Case specific	100 ppb	$k = 3/2(0.1U_{in}^2)$, $\varepsilon = (C_\mu k^{3/2})/L_{in}$; $C_\mu = 0.09$, L_{in} = (Air supply slot width)/7
Cabin walls	18°C	Zero flux	$\partial k/\partial y = 0$, ε: local equilibrium hypothesis
Exhausts	Outflow	Outflow	Outflow
Carpet	18°C	Flux calculated with Eq. (5.3)	$\partial k/\partial y = 0$, ε: local equilibrium hypothesis
Seats	Adiabatic	Flux calculated with Eq. (5.3)	$\partial k/\partial y = 0$, ε: local equilibrium hypothesis
T-shirts	Adiabatic	Zero concentration	$\partial k/\partial y = 0$, ε: local equilibrium hypothesis
Passengers	31°C	Zero concentration	$\partial k/\partial y = 0$, ε: local equilibrium hypothesis
where k is the turbulent kinetic energy, ε the turbulence dissipation rate, C_μ a constant used in the k- ε turbulence model, U_{in} the air velocity at the inlet, and y the local coordinate normal to the surface.			

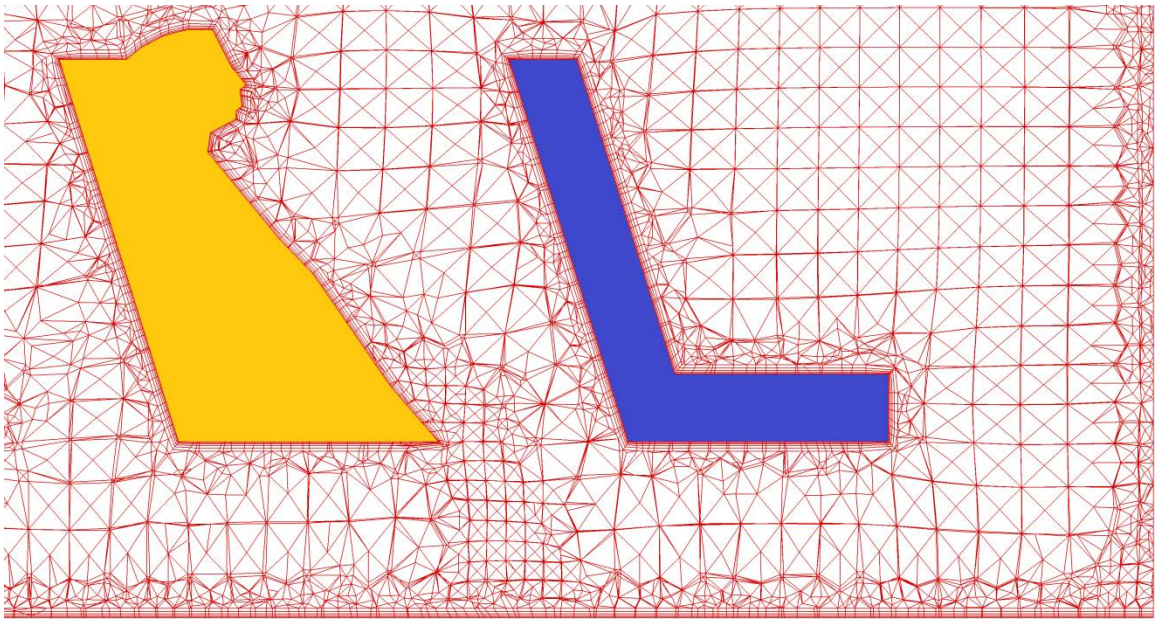

Figure 5.2. Mesh distribution in the longitudinal section through the cabin center for Case 5.

Our study simulated the passengers by two different human geometry models for the occupied cabin cases. Case 4 used a simple block model, while Case 5 used a more detailed representation of human shape, as shown in Figure 5.3. The two geometric models were designed to identify whether the simple block model was sufficient for CFD modeling. Figure 5.3 also depicts a breathing zone of 500 cm^3 volume below the nose since this investigation assessed the ozone dose inhaled by the passengers by calculating the volume-averaged concentration in the breathing zone as suggested by Rim et al. (2009). The volume of breathing zone was chosen larger than the hemispherical volume suggested by Brohus (1997) to account for the face movements of passengers.

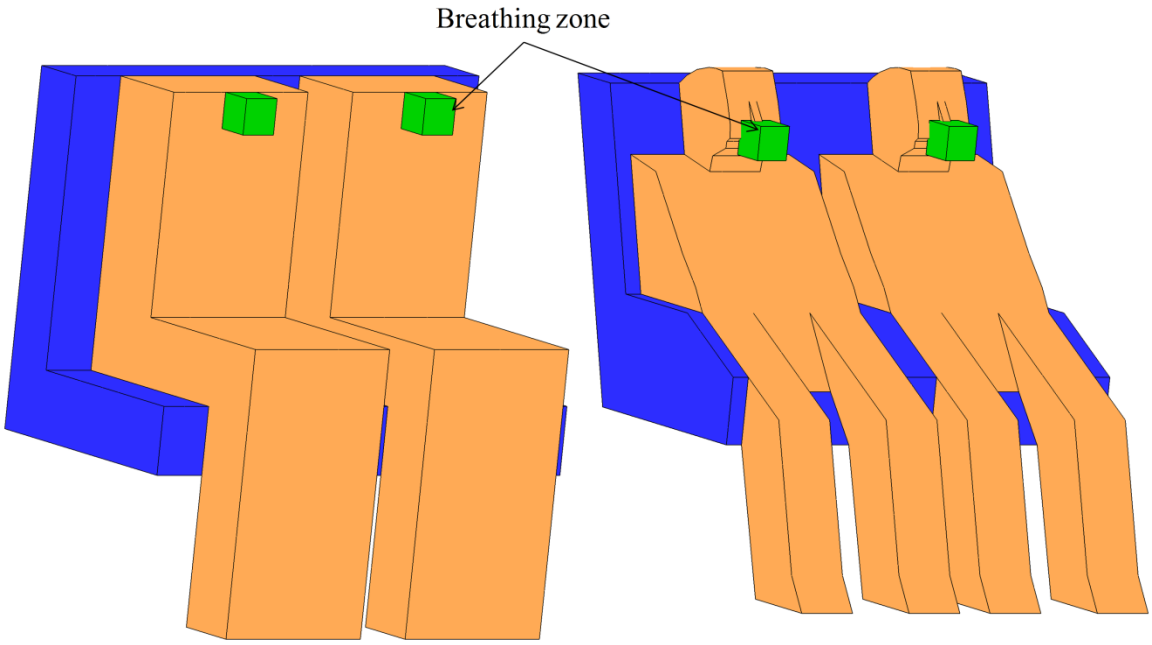

Figure 5.3. Occupant geometries and breathing zones for Cases 4 and 5.

5.3 Evaluation Parameters

This section defines some important parameters for evaluating the cabin air quality for the cases designed in the previous section. These parameters help evaluate the CFD results against the available experimental data.

5.3.1 Ozone Removal Rate (β_{total})

The ozone removal rate (β_{total}) was defined in Section 3.3.2 and can be used to quantify the total ozone loss in the cabin environment due to surface and gas phase reactions by using Eq. (3.2). The β_{total} can also be obtained by measuring the first order decay of ozone inside the cabin. In this method, ozone is injected into the cabin until a reasonable ozone concentration (roughly around 50–100 ppb) is reached. The ozone injection is then stopped and the cabin ozone concentration is measured with respect to time. The ozone decay in the cabin is quantified by a best fit to an exponential decay equation given by:

$$C_t = C_{t=0}.e^{-(\lambda_{outdoor}+\beta_{total})t}, \quad (5.6)$$

where C_t is the ozone concentration at time t; $C_{t=0}$ is the concentration at the time when the ozone injection was stopped; $\lambda_{outdoor}$ is the outdoor air change rate. The decay constant ($\lambda_{outdoor} + \beta_{total}$) in the above equation can be used to determine β_{total} when the $\lambda_{outdoor}$ is known. The experimental study by Tamas et al. (2006) obtained the β_{total} primarily by using Eq. (5.6), and Eq. (3.2) was used when steady state conditions were achieved.

5.3.2 Contribution to the Ozone Removal Rate (β_s)

The contribution to the ozone removal rate (β_s) quantifies the ozone removal by an individual surface. It is defined as:

$$\beta_s = \frac{\int J_{ozone} dA}{C_{avg} V_{cabin}}, \tag{5.7}$$

where V_{cabin} is the volume of the air inside the cabin. The β_s definition implies that it can be calculated from CFD but cannot be directly measured, since the surface ozone deposition (the numerator in Eq. (5.7)) is difficult to quantify. Therefore, to determine β_s, a reacting surface should be added one at a time as discussed in Section 3.3.3. This is why the investigation designed five cases. In Case 1, the β_s was approximated as follows if the gas phase reactions of ozone are neglected:

$$\beta_{s,\,carpet} = \beta_{total,\,Case1}. \tag{5.8}$$

By adding the reacting surfaces one at a time in Cases 2, 3, and 4, the β_s for seats, T-shirt, and passengers was estimated as:

$$\beta_{s,\,seats} = \beta_{total,\,Case2} - \beta_{s,\,carpet}, \tag{5.9}$$

$$\beta_{s,\,T\text{-}shirts} = \beta_{total,\,Case3} - \beta_{s,\,carpet} - \beta_{s,\,seats}, \tag{5.10}$$

$$\beta_{s,\,passengers} = \beta_{total,\,Case4} - \beta_{s,\,carpet} - \beta_{s,\,seats}. \tag{5.11}$$

Hence, the experimental β_s values can be compared with those obtained from CFD (Eq. (5.7)).

5.3.3 Ozone Deposition Velocity (v_d)

The deposition velocity (v_d) characterizes the intensity of ozone surface reactions and can be compared to those reported in the literature. It is analogous to the heat transfer coefficient as:

$$v_d = \frac{J_{ozone}}{C_{avg}}, \tag{5.12}$$

where J_{ozone} and C_{avg} are analogous to the heat flux and temperature difference. According to Eq. (5.12), v_d will vary across a surface as the ozone flux (J_{ozone}) will vary depending on the position. Hence, it is convenient to define v_d by using the average ozone flux over a surface (or multiple surfaces) as:

$$v_d = \frac{\left(\int J_{ozone} dA\right) / A}{C_{avg}}. \tag{5.13}$$

Similar to β_s, the v_d can also be calculated from CFD, but cannot be measured directly. Hence, by combining Eqs. (5.7) and (5.13), v_d can be determined as:

$$v_d = \frac{\beta_s V_{cabin}}{A}. \tag{5.14}$$

which is similar to the expression used for v_d in Section 3.3.4.

5.3.4 Retention Ratio (θ)

The retention ratio (θ) is a parameter that indicates the ozone loss in the aircraft due to reactions in the cabin and the air supply system in the absence of ozone converters. It is defined as:

$$\theta = \frac{C_{avg}}{C_{ambient}}, \tag{5.15}$$

where $C_{ambient}$ is the ambient ozone concentration. If the ozone reactions in the air supply system are neglected, then $\lambda_{total}C_{inlet} = \lambda_{outdoor}C_{ambient} + \lambda_{recirculated}C_{exhaust}$. Eq. (5.15) can be rearranged to give:

$$\theta = \frac{\lambda_{outdoor}C_{avg}}{\lambda_{total}C_{inlet} - \lambda_{reciculated}C_{exhaust}}, \tag{5.16}$$

where $\lambda_{outdoor}$ is the outdoor air change rate; $\lambda_{recirculated}$ the recirculated air change rate. The experiment used Eq. (5.15) to determine θ from the measured C_{cabin} and $C_{ambient}$. However, this investigation used Eq. (5.16) to calculate θ, since the air supply system was not modeled.

5.3.5 Ozone Ratio (r_{ozone})

In order to quantify the ozone dose for different passengers, it is essential to calculate the ozone concentration in the breathing zone. This study used ozone ratio (r_{ozone}) to compare the inhaled ozone concentration with the average ozone concentration in the cabin:

$$r_{ozone} = \frac{C_{BZ}}{C_{avg}}, \tag{5.17}$$

where C_{BZ} is the ozone concentration in the breathing zone. The r_{ozone} can be used for assessing the ozone exposure of the passengers based on the average ozone concentration.

5.4 Results

The following section reports how the CFD was used to obtain the evaluation parameters defined in Section 5.3 and shows the comparison with the experimental data from Tamas et al. (2006).

5.4.1 Ozone Removal by Carpet and Seats (Cases 1 and 2)

Cases 1 and 2 were designed for identifying the ozone removal by the cabin surfaces (carpet and seats) by adding them one by one.

In Case 1, the carpet was assumed to be the only ozone reactive surface to determine its β_s and v_d. Hence, the measured β_{total} and the β_s calculated by Eq. (5.7) should be equal. This investigation calculated that the β_s for the carpet was 1.07 h^{-1}. The β_s calculated and the β_{total} measured were indeed nearly the same as shown in Figure 5.4. The v_d for the carpet was calculated by using Eq. (5.13) as 0.06 cm/s, which also agreed with the measurements as shown in Figure 5.5.

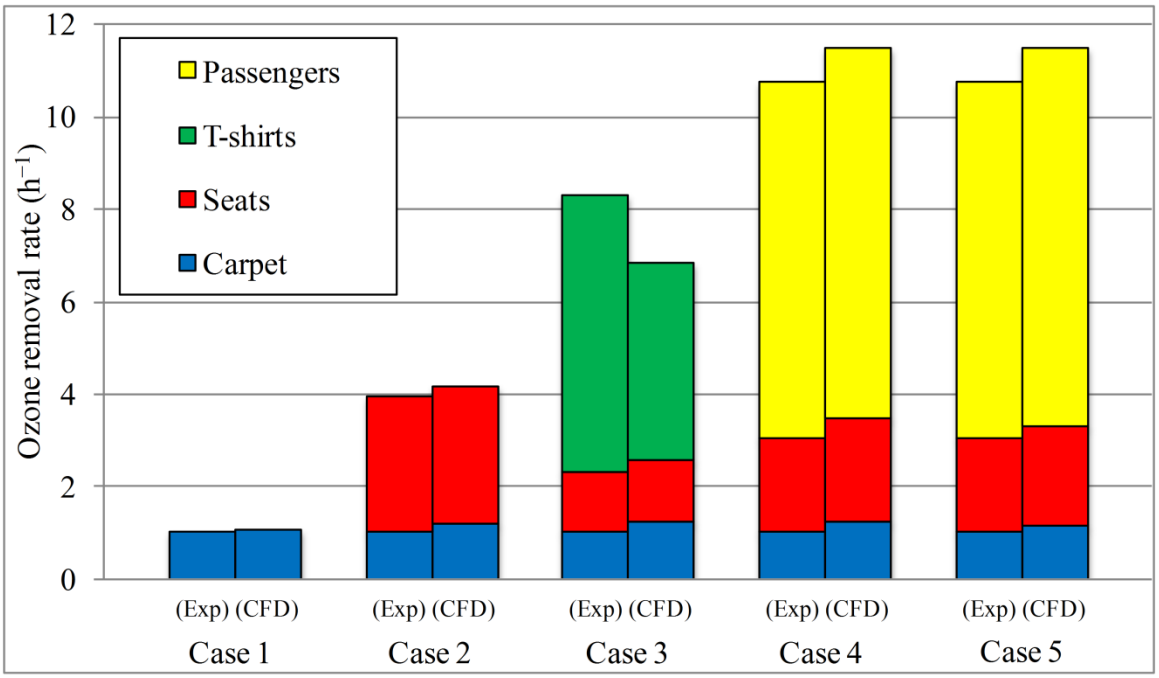

Figure 5.4. Comparison of the computed ozone removal rate with the corresponding experimental data from Tamas et al. (2006) for various cabin and human related surfaces.

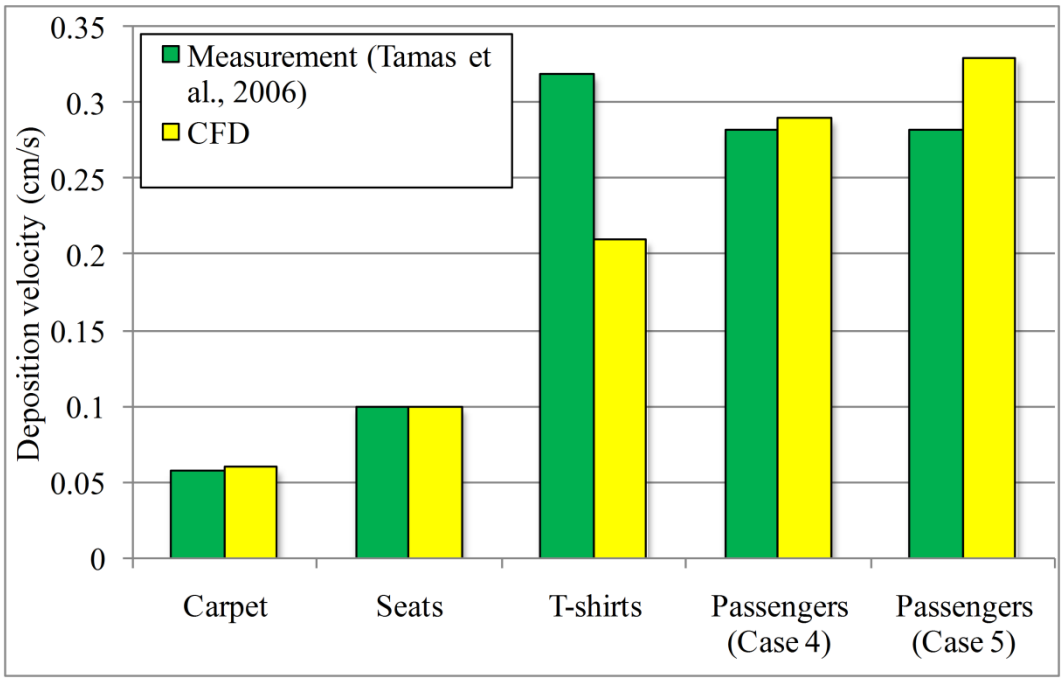

Figure 5.5. Comparison of the computed deposition velocity with the corresponding experimental data from Tamas et al. (2006) for various cabin and human related surfaces.

In Case 2, the seats were also placed in the cabin together with the carpet. This was done in the experiment to determine the β_s for the seats by using Eq. (5.9) since the β_s for the carpet was assumed to be known from the previous case. This investigation calculated the β_s for the carpet and seats as 1.19 h^{-1} and 2.97 h^{-1}, respectively, by using Eq. (5.7). The seats had a higher β_s than the carpet because they had a larger surface area for reaction and also a higher reactivity. The β_{total} in Case 2 was greater than that in Case 1 because of the additional ozone removal by the seats. The computed β_s and β_{total} agreed with the measured data as shown in Figure 5.4. The v_d for the carpet and seats was calculated by using Eq. (5.13) as 0.06 cm/s, and 0.10 cm/s, respectively, which also agreed with the measurements as shown in Figure 5.5. Hence, the "measured" β_s and v_d for the seats seem correct, and the CFD results are also reliable.

The β_{total} and v_d for Case 2 (which represents a typical unoccupied cabin setup) can also be compared to those in buildings to better understand the ozone depletion in the cabin and the reactivity of the cabin surfaces. Lee et al. (1999) measured the average β_{total} as 2.80±1.30 h^{-1}, and v_d as 0.049±0.017 cm/s in the living rooms of 43 Southern California

homes. The v_d measured by Lee et al. (1999) included all indoor surfaces (including both ozone reactive and inert surfaces). If the same method is applied to this cabin, the v_d for both ozone reactive and inert surfaces is 0.04 cm/s. Note that although the v_d for the cabin was almost the same as that for the homes, the β_{total} for the cabin was 1.5 times higher than that for the homes. This is because the V/A in Eq. (5.14) for the cabin was lower than that for the homes.

5.4.2 Ozone Removal by T-shirts Soiled with Human Skin-oil (Case 3)

This case was designed for identifying the ozone removal by clothing soiled with human skin-oil. The cabin in Case 3 was identical to the one in Case 2, except that the seat backs were covered with T-shirts. The T-shirts were soiled with human skin-oil as male subjects had slept in them overnight.

The β_s for the carpet, seats, and T-shirts were 1.23 h^{-1}, 1.34 h^{-1}, and 4.29 h^{-1}, respectively, calculated by Eq. (5.7). The area of the T-shirts was approximately 40% of all the surface areas, but it removed about 60% ozone due to the high reactivity of ozone with squalene in human skin-oil. The β_{total} was higher than that in previous cases because of the addition of the T-shirts. The experiment used Eq. (5.10) to determine $\beta_{s,\ T\text{-shirts}}$, with $\beta_{s,\ carpet}$ and $\beta_{s,\ seats}$ from Cases 1 and 2. However, it is not appropriate to use the $\beta_{s,\ seats}$ obtained in Case 2 to calculate $\beta_{s,\ T\text{-shirts}}$, since a large area of the seats was covered with the T-shirts and was not part of the ozone reaction in Case 3. Thus, this investigation used the following procedure to determine the "measured" $\beta_{s,\ T\text{-shirts}}$:

- The $\beta_{s,\ seats}$ for Case 3 was assumed to be proportional to the exposed area, which was available for ozone reactions.
- Since the exposed area of the seats was unknown, it was assumed to be equal to that used in the CFD investigation, which was about 45% of the total area.
- The "measured" $\beta_{s,\ seats}$ was determined by using $\beta_{s,\ seats,\ Case3} = \beta_{s,\ seats,\ Case2} \times (A_{exposed} / A_{total})$, where $A_{exposed}/A_{total}$ is the ratio of the exposed area to the total area of the seats.

- The "measured" $\beta_{s,\ \text{T-shirts}}$ was then determined from the $\beta_{s,\ \text{seats}}$ obtained in the previous step by using Eq. (5.10).

The comparisons between the "measured" β_s obtained using the above procedure and the CFD results are shown in Figure 5.4. The computed $\beta_{s,\ \text{carpet}}$ and $\beta_{s,\ \text{seats}}$ agreed well with the measurements but the computed $\beta_{s,\ \text{T-shirts}}$ and β_{total} were underestimated by CFD. A possible reason for these discrepancies could be that when ozone reacted with the human skin-oil present in T-shirts, some of the volatile byproducts that entered the gas phase reacted further with the ozone (Weschler et al., 2007). This gas phase chemistry could have contributed to the additional ozone removal in the experiment, but was not considered in the CFD analysis.

The computed v_d for the T-shirts was 0.21 cm/s by using Eq. (5.13), and the computed v_d for the carpet and seats remained the same as in the previous cases (0.06 cm/s and 0.1 cm/s, respectively). The high value of v_d for the T-shirts shows that the ozone reaction intensity was very high at the surfaces. In order to compare the CFD results with the measurements, this investigation used the "corrected" $\beta_{s,\ \text{T-shirts}}$ to calculate the "measured" $v_{d,\ \text{T-shirts}}$ by using Eq. (5.14). Since the CFD underpredicted the $\beta_{s,\ \text{T-shirts}}$, the $v_{d,\ \text{T-shirts}}$ was also lower than the measured one, as shown in Figure 5.5.

5.4.3 Ozone Removal by Passengers (Cases 4 and 5)

Cases 4 and 5 were designed for identifying the ozone removal in an occupied cabin mockup. The only difference between them was: Case 4 represented passengers by simple block models, whereas Case 5 had a more detailed representation of human geometry, as shown in Figure 5.3. Despite the differences in the human geometric presentation, the area available for ozone reaction remained approximately the same.

The β_s for the carpet, seats, and passengers calculated from Eq. (5.7) was 1.23 h^{-1}, 2.25 h^{-1}, and 8.03 h^{-1}, respectively, in Case 4; and it was 1.18 h^{-1}, 2.12 h^{-1}, and 8.18 h^{-1}, respectively, in Case 5. The small differences in β_s between Cases 4 and 5 show that the detailed representation of occupant geometry for the CFD studies was not important for evaluating the ozone removal rate as long as the reactive surface area was the same. The

β_{total} for the two cases was significantly greater than those in all the previous cases due to the large contribution of the passengers to ozone removal.

In order to compare the β_s with the experimental data, this investigation used the procedure described in Case 3 to correct the measured $\beta_{s,\ seats}$ and determine the "measured" $\beta_{s,\ passengers}$ by using Eq. (5.11). Figure 5.4 compares β_s and β_{total} obtained by CFD and the measurements. The computed $\beta_{s,\ carpet}$ and $\beta_{s,\ seats}$ agreed well with the measurements, but the CFD overpredicted the $\beta_{s,\ passengers}$ and β_{total} by 10%.

The v_d for the passengers was computed by using Eq. (5.13) to be 0.29 cm/s and 0.33cm/s for Cases 4 and 5, respectively. The computed v_d for the carpet and seats was the same as those in the previous cases (0.06 cm/s and 0.1 cm/s, respectively). Similar to $v_{d,\ T\text{-}shirts}$, the high v_d for the passengers showed that the ozone removal by the passengers was most important or the reactivity of the passengers was the highest. The "measured" $v_{d,\ passengers}$ was determined from the corrected $\beta_{s,\ passengers}$, based on the exposed surface area of the passengers (estimated at about 1.2 m^2 per passenger) and the volume of the cabin air (estimated at about 27 m^3) by using Eq. (5.14). Since the CFD results overpredicted the $\beta_{s,\ passengers}$, Figure 5.5 shows that the $v_{d,\ passengers}$ was also overpredicted.

This investigation computed θ as 0.42 for an outdoor airflow rate (8.8 h^{-1}) in Case 5 by using Eq. (5.16). The θ for Case 4 was approximately equal to Case 5. The calculated θ was less than that reported in the experiment (0.21) because the ozone removal in the air supply system was not modeled. The θ was smaller than the default value of 0.7 used by the Federal Aviation Administration (FAA) for determining the cabin ozone concentration and showing compliance with regulations. The low θ indicated that the cabin ozone concentration should be lower than that specified by the FAA. But this reduction in the cabin ozone levels was accompanied by the formation of even more harmful volatile byproducts (Weschler, 2004; Wisthaler et al., 2005). Hence, a low θ may reduce health risks from ozone inhalation, but would increase them from its byproducts.

Figure 5.6 shows the ozone distribution along the longitudinal plane through the center of the cabin in Case 5. It shows that ozone depleted near the carpet, seats, and breathing

zone of the passenger because of the surface chemical reactions. This investigation used r_{ozone} to quantify the breathing zone ozone concentration for the passengers as compared to in the average cabin concentration. The r_{ozone} varied between 0.77–0.93 in Case 4 and 0.77–0.99 in Case 5. The averaged r_{ozone} for all the passengers was 0.85 and 0.90 for Cases 4 and 5, respectively, which is in qualitative agreement with previous studies (Liu et al., 1994; Rim et al., 2009).The breathing zone concentration is generally lower than the average ozone concentration in the indoor environment ($r_{ozone} < 1$) because of reactions at the human surfaces. The r_{ozone} varied among the aircraft passengers due to the differences in the ozone transport and surface reactions at different locations. Figure 5.7 compares the r_{ozone} for different passengers between the two cases, which shows r_{ozone} being quite sensitive to human geometrical representations. Since most of the passengers inhaled an ozone concentration lower than the average one, it is better to use the local ozone concentration if one wants to accurately assess the health risks associated with the ozone exposure.

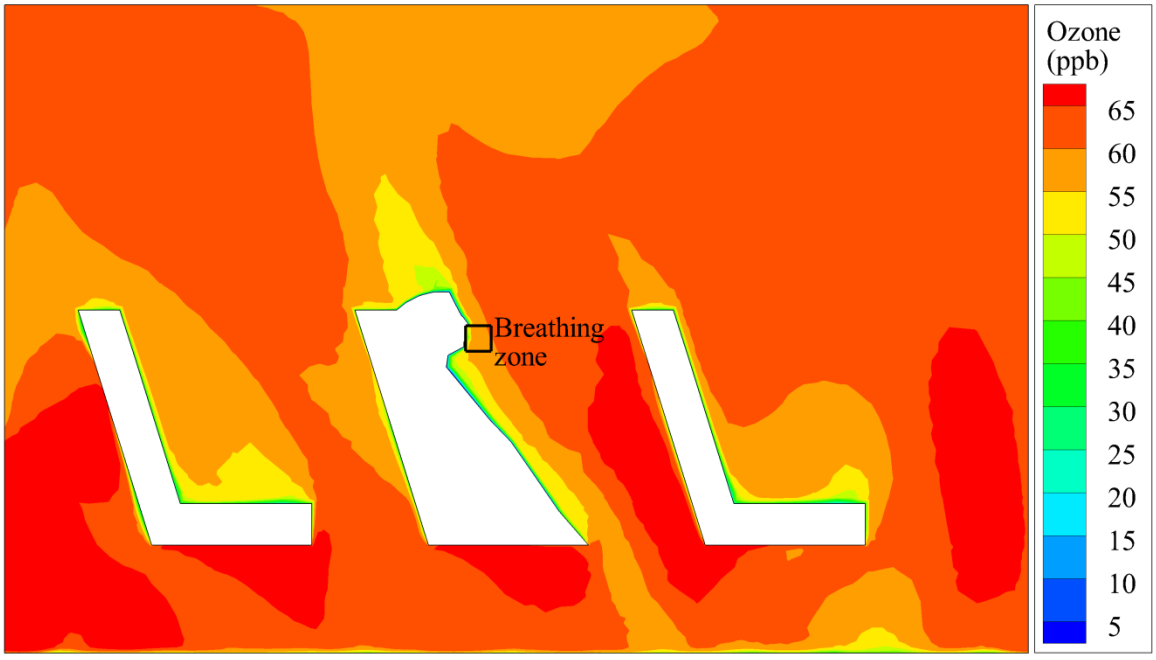

Figure 5.6. Ozone distribution in the longitudinal section through the cabin center.

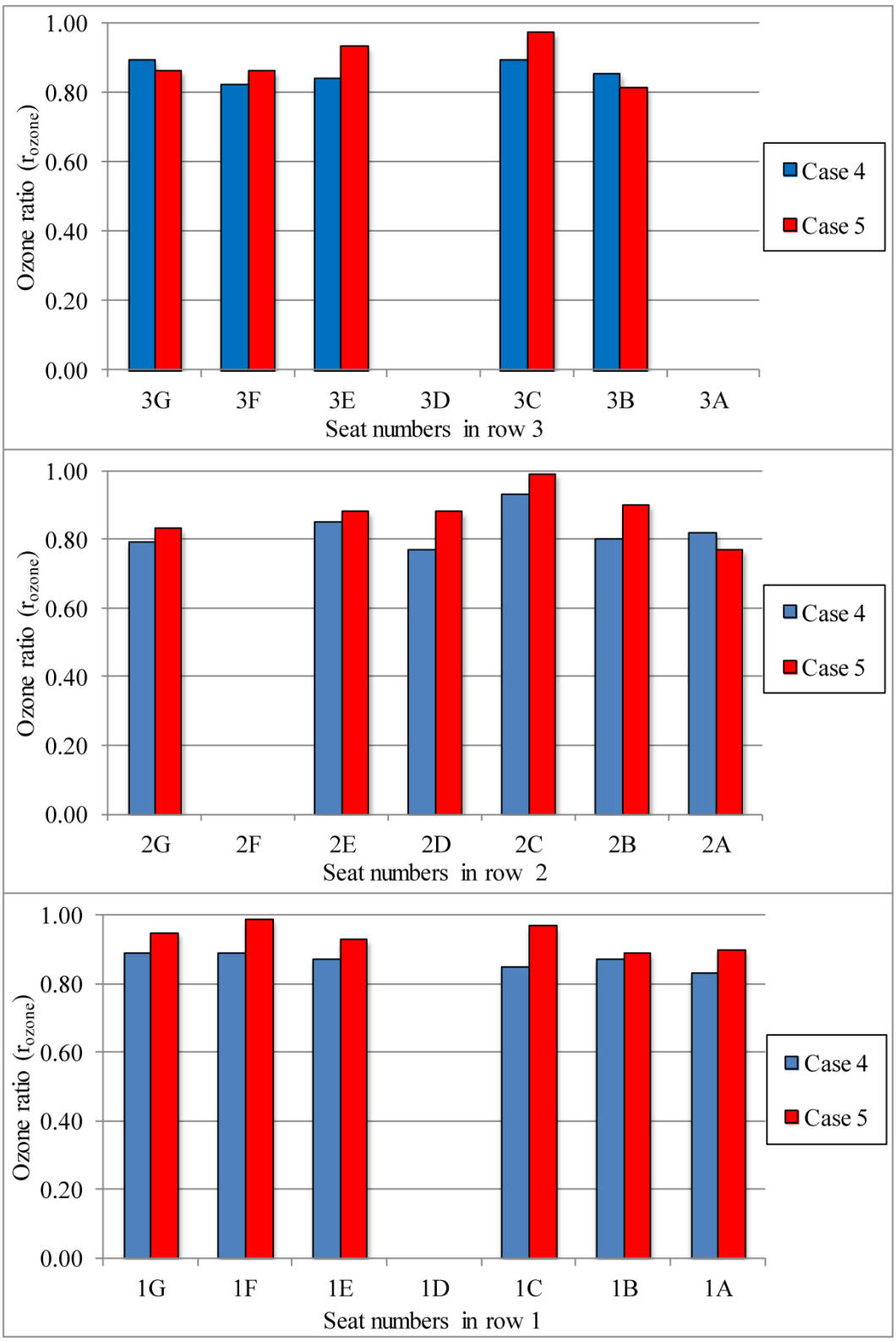

Figure 5.7. Comparison of ozone ratio (r_{ozone}) for the passengers in the breathing zone between Cases 4 and 5. Seats 1D, 2F, 3A, and 3D were unoccupied.

5.5 Discussion

The primary difficulty in computing the ozone distribution was that the γ for the ozone reactive surfaces was unknown. Hence, this investigation obtained the γ from the "measured" v_d and computed v_t by using Eq. (5.4). The flux model (Eq. (5.3)) was then used to compute the ozone removal by cabin surfaces. However, in the cases with the T-shirts and passengers, the flux model (Eq. (5.3)) was not used to compute the surface deposition since the v_d was found to be very close to v_t, and Eq. (5.4) was not suitable. Instead, a zero ozone concentration was assumed on the human related surface. Since the computed β_s and v_d agreed with the measured data, our method seems acceptable.

This study also performed grid independence analysis for the CFD simulations. For example, in Cases 2 and 3 where the cabin geometry was identical, this investigation used a coarse grid of 2.31 million elements and a fine grid of 4.96 million elements for the two cases. The initial prism layer height was 2 mm and 1 mm, for the coarse and fine grid, respectively. The velocity and ozone distributions obtained with the two grid sizes were similar and the difference between the computed ozone removal rates (β_{total}) was less than 5%. Thus, the coarse grid was selected for performing all CFD simulations reported in this chapter.

5.6 Conclusions

The investigation developed a CFD model to study the ozone reactions at different cabin and human related surfaces and simulate the ozone distributions in the cabin. The investigation led to the following conclusions:

- The study identified the individual contributions of cabin and human related surfaces to ozone removal and their deposition velocities. The results concluded that the human related surfaces (T-shirts and passengers) removed much more ozone than the cabin surfaces (carpet and seats).
- The ozone removal rate and deposition velocities calculated by the model were in good agreement with those measured by Tamas et al. (2006).

- The retention ratio predicted by the model was higher than the measured one (Tamás et al., 2006) since the air supply system was not modeled. The retention ratios were lower than the FAA recommended value, indicating a reduced risk directly from ozone inhalation but an increased risk from associated by-products.
- Ozone depleted more in the breathing zone compared to the average cabin concentration due to reaction at the human surfaces. To accurately assess the personal exposure to ozone, its concentration in the breathing zone should be used.

CHAPTER 6. NUMERICAL MODELING OF VOC EMISSIONS FROM OZONE REACTIONS WITH HUMAN-WORN CLOTHING IN AN AIRCRAFT CABIN

The previous chapter described CFD analysis for computing ozone consumption in an airliner cabin mockup from its reactions with different cabin surfaces and passengers. It was also discussed previously that such ozone consumption leads to secondary emissions of VOCs, which can be even more harmful to human health than ozone itself. Additionally, it was found that these secondary emissions were mainly attributed to ozone reactions with human-worn clothing under typical airliner cabin conditions. Therefore, this investigation developed models for computing secondary VOC emissions from ozone reactions with human-worn clothing based on the prevailing environmental conditions. Our objective was to compute common byproduct concentrations due to ozone/clothing reactions in an aircraft cabin mockup, such as acetone, 4-oxopentanal (4-OPA), nonanal, and decanal. Our study also integrated the models in CFD for computing the ozone-initiated VOC concentrations in breathing zones of passengers in an occupied airliner cabin mockup.

6.1 Method

To compute the secondary VOC emissions from surface reactions of ozone, we used the molar yield equation (Weschler et al., 2007), which calculates VOC emissions directly from ozone consumption as follows:

$$J_{VOCi} = Y_i J_{ozone}, \tag{6.1}$$

where J_{VOCi} and J_{ozone} are the molar fluxes of VOCi and ozone, respectively, on a particular surface; and Y_i is the molar yield of VOCi for that surface.

In the above equation, J_{ozone} can be computed as the product of the bulk air ozone concentration (C) and the measured/estimated ozone deposition velocity (v_d) for the surface (see Eq. (5.12)) , under the assumption of well-mixed conditions (Cano-Ruiz et al., 1993). Alternatively, J_{ozone} can be obtained by CFD analysis, which does not require the well-mixed assumption as described in Chapter 5. However, Y_i is generally unknown, and it depends on the environmental conditions under which ozone reacts with soiled clothing as shown in Chapter 3. Thus, it was reasonable to search for empirical equations connecting VOC yields to the environmental conditions for reactions with clothing. The equations can then be used to compute VOC yields and eventually their secondary emissions from Eq. (6.1). The procedure for determining these equations is discussed in the following subsection.

6.1.1 Selection of Empirical Equations

This investigation developed empirical equations for computing the yields of several major VOCs generated from ozone reactions with human-worn clothing based on the prevailing environmental conditions. The equations were developed from the chamber experiments discussed in Chapter 3. From the experimental cases, we choose the ones that had been conducted with soiled T-shirts (a total of 12 cases) because human-worn clothing would normally be soiled with skin-oils (see Table 3.1).

By analyzing the cases given in Table 3.1, it was found in Chapter 3 that air change rate (ACR), relative humidity (RH), and ozone concentration (C) were the major factors that influenced VOC yields. Therefore, we chose those factors as predictor variables for developing empirical equations connecting the VOC yields to the environmental conditions.

Among the predictors, humidity and ozone were used as continuous variables with linear (RH and C) and quadratic (RH^2 and C^2) terms since we had a range of conditions for these variables. ACR was used a dummy variable, and its value was set to zero or one for low or high ventilation conditions, respectively. We used ACR as a dummy variable because (1) in the measurements it had only two levels, an insufficient number for it to be

treated as a continuous variable, and (2) it was conjectured that ACR indirectly affected the yields of some VOCs by changing the airflow features and their resulting convective mass transport. For the cases given in Table 3.1, 0.5 h^{-1} and 2.7 h^{-1} were used as low and high air change rates, respectively. Another possible approach to account for the influence of airflow features on VOC yields could be to use the friction velocity (u*) as a predictor variable, which would account for the effects of indoor airflow intensity at the reaction surface. Such an approach was used by Lai and Nazaroff (2000) to characterize the influence of airflow features on particle deposition. However, this approach requires the value of the u*, which is very difficult to determine by either measurements or computations.

After the predictor variables had been selected, the yields of the major ozone-initiated VOCs were regressed on all the different linear combinations of these five variables (ACR, RH, RH^2, C, and C^2) for the 12 cases by using the SAS (Statistical Analysis System) statistical package. The resulting regression models (31 in total) were then categorized according to their complexity (i.e., the number of predictor variables). From each of these categories, the best model was identified as the one with the largest value of R^2_{adj} (adjusted R^2). Figure 6.1 shows the relationship between R^2_{adj} and the number of predictors for each VOC, along with the models that were finally selected. The finally selected models were the ones having a relatively large value of R^2_{adj} together with least complexity.

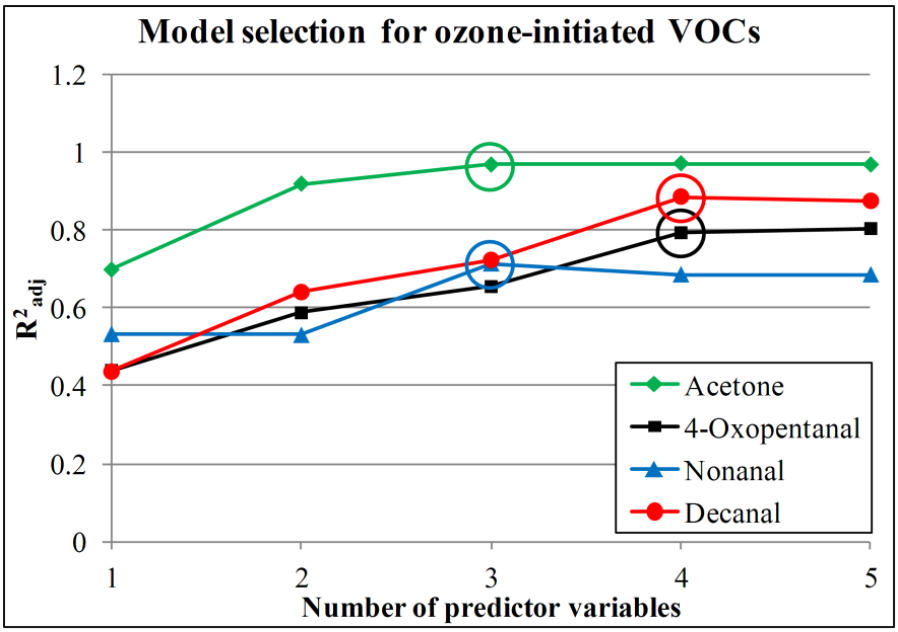

Figure 6.1. Model selections for the different VOCs based on the R^2_{adj} criterion. The circles identify the final model selections.

The selected regressions models are as follows:

$$Y_{ace} = 1.85\times10^{-1} + 1.35\times10^{-1}\,ACR - 2.45\times10^{-3}\,C + 9.72\times10^{-6}\,C^2, \quad (6.2)$$

$$Y_{4\text{-}OPA} = -3.71? \;\; 0^{-2} + 3.94\times10^{-2}\,ACR + 1.14\times10^{-2}\,RH - 3.49\times10^{-4}\,C... \\ ... - 1.61\times10^{-4}\,RH^2, \quad (6.3)$$

$$Y_{non} = -4.32\times10^{-2} + 2.52\times10^{-3}\,RH + 2.25\times10^{-3}\,C - 1.16\times10^{-5}\,C^2, \quad (6.4)$$

$$Y_{dec} = ? \;\; .48\times10^{-1} + 1.53\times10^{-2}\,RH + 5.18\times10^{-3}\,C - 1.80\times10^{-4}\,RH^2 - 2.70\times10^{-5}\,C^2, \quad (6.5)$$

where Y_{ace}, $Y_{4\text{-}OPA}$, Y_{non}, and Y_{dec} are the molar yield of acetone, 4-OPA, nonanal, and decanal, respectively. Eqs. (6.1) to (6.5) are the models for estimating secondary VOC emissions of acetone, 4-OPA, nonanal, and decanal, respectively, from ozone reactions with human-worn clothing. To use the above equations for computing VOC yields, the ozone concentration (C) must be inputted in ppb (on a molar basis). RH must be set to the value of the relative humidity without percentage. For example, if the relative humidity is 20%, the RH value must be set to 20. Finally, ACR value must be either zero or one

depending on low or high ventilation conditions. It is recommended to use an ACR value of zero for buildings since they usually have low ventilation rates, and a value of one for high ventilation settings such as airliner cabins.

The computed VOC emissions can then be incorporated in a simple mass balance analysis or used to provide boundary conditions for CFD analysis. The mass balance analysis can be used to estimate the contributions of human-worn clothing to bulk air concentrations of those VOCs, whereas the CFD analysis can provide a wealth of information about the concentration distributions. The next two subsections describe the mass balance and CFD modeling techniques, respectively.

6.1.2 Mass Balance Model

A simple mass balance can be used to compute the contributions of human clothing to ozone-initiated VOCs under indoor settings by assuming well mixed conditions, as follows:

$$C_{VOCi,\,clothing} = \frac{J_{VOCi} A_{clothing}}{V \lambda_{outdoor}}, \tag{6.6}$$

where $C_{VOCi,\,clothing}$ is the contribution of clothing to the concentration of VOCi, $A_{clothing}$ the clothing area, V the volume of the air in the indoor space, and $\lambda_{outdoor}$ the outdoor air change rate.

6.1.3 CFD Model

If the air distribution in a room cannot be assumed to be well-mixed, CFD should be used to compute the velocity, temperature, and ozone distributions as described in Chapter 5. The ozone and VOC distributions were obtained by solving the corresponding species transport equations. For example, the transport equation for VOCi takes the following form:

$$\nabla.(\rho\vec{u}C_{VOCi}) = \nabla.((\rho D_{VOCi} + \frac{\mu_t}{Sc_t})\nabla C_{VOCi}), \quad (6.7)$$

where ρ is the air density, $\vec{u}$ the air velocity vector, C_{VOCi} the concentration of VOCi, D_{VOCi} the binary diffusion coefficient of VOCi in air, μ_t the turbulent viscosity, and Sc_t the turbulent Schmidt number. These equations were solved by the use of commercial CFD software FLUENT (FLUENT, 2009).

6.2 Case Setup

We used the same Boeing-767 mockup that was used for validating our model for ozone consumption. The details of the cabin mockup were given in Section 5.2. In addition to the measurements of ozone consumption, this mockup was also used by Weschler's group for quantifying the ozone-initiated VOC emissions from different surfaces by adding them one at a time. For example, they first measured ozone-initiated VOC emissions in an empty cabin with carpet and seats only. Next, they stretched soiled T-shirts on the seat backs and repeated the VOC measurements. Finally, they conducted experiments with passengers in the cabin mockup. These arrangements enabled them to quantify the contributions to ozone-initiated VOC emissions from individual cabin surfaces, such as carpet and seats, soiled T-shirts, and passengers.

Because one of our aims was to evaluate our model performance for computing the secondary VOC emissions from human-surfaces, we studied those cases which contained human-worn clothing or passengers as given in Table 6.1. The environmental conditions for these cases are also summarized in Table 6.1. Case 1 was conducted with soiled T-shits stretched on seat backs as surrogates for humans, whereas Cases 2 and 3 were conducted with real human subjects.

Table 6.1. Description of the three cases used for studying ozone-initiated VOC emissions in a cabin mockup.

Case	Description	Ozone reaction surfaces	Average cabin ozone (ppb)	Relative humidity (%)	Air change rate (h^{-1})	
					Outdoor	Recirculated
1	Cabin with seats and T-shirts	Carpet, seats, and T-shirts	66	6.8	3.0	20.0
2	Occupied cabin	Carpet, seats, and passengers	75	10	8.8	12.2
3	Occupied cabin	Carpet, seats, and passengers	62	20	4.4	16.6

We have previously reported and validated detailed CFD modeling techniques for computing airflow, temperature, and ozone distributions for the cabin mockup in Chapter 5, but with a slightly higher air change rate. Therefore, we used similar meshing and solution techniques for computing the ozone-initiated VOCs.

Table 6.2 presents the boundary conditions for ozone and different VOCs in the CFD model for the occupied cabin cases. The inlet ozone concentration was unknown, and a value for this concentration was assumed in order to obtain the correct cabin ozone concentrations as measured in Cases 2 and 3. Correct concentrations in the cabin were essential for computing the flux of ozone (J_{ozone}) at reaction surfaces. The inlet VOC concentrations were calculated from those in the recirculated air because a portion of the exhaust air was recirculated. The outdoor air was assumed to have no VOCs. The VOC emissions from the cabin walls were assumed to be zero, and those from the carpet and seats were estimated from the measurements of Wisthaler et al. (2005), as the sum of both primary and secondary emissions. The primary VOC emissions from the human surfaces (clothing, skin, and hair) were neglected in accordance with the experimental measurements of Weschler et al. (2007). It was further assumed that all human surfaces had the same secondary emissions as the soiled cotton T-shirts, which was estimated from Eqs. (6.2)–(6.5). Because acetone is also present in human breath as a result of

metabolic processes (Fenske and Paulson, 1999), this study set its flux at the nose of occupants on the basis of experimental estimates of Weschler et al. (2007).

Table 6.2. The ozone and VOC boundary conditions used for this study.

Surfaces	Ozone	4-OPA, nonanal, and decanal	Acetone
Inlet	Case specific	Case specific	Case specific
Cabin walls	Zero flux	Zero flux	Zero flux
Carpet and Seats	Flux computed from Eq. (5.3)	Flux estimated from measurements	Flux estimated from measurements
Human surfaces (skin, hair, and clothing)	Zero concentration	Flux calculated with Eqs. (6.3), (6.4), and (6.5), respectively	Flux calculated with Eq. (6.2)
Passenger's nose	Zero concentration	Flux calculated with Eqs. (6.3), (6.4), and (6.5), respectively	Flux estimated from measurements
Exhausts	Outflow	Outflow	Outflow

6.3 Results

The following subsections present (1) the comparisons between our model predictions and the corresponding experimental data for the three cases shown in Table 6.1, and (2) the results obtained by conducting CFD analysis for the occupied cabin cases.

6.3.1 VOC Emissions

Case 1 was designed to study the contributions of the soiled T-shirts to ozone-initiated VOC emissions. In this case the VOC emissions mainly composed of primary and secondary emissions from the carpet and seats plus secondary emissions from the soiled T-shirts (Wisthaler et al., 2005). The contributions of cabin surfaces (carpet and seats) to VOCs (both primary and secondary) were isolated by means of another experiment performed in the same cabin mockup without T-shirts. It should then have been possible to estimate the contribution of the T-shirts to the overall concentration of VOCi in the cabin by simply subtracting the contribution of the cabin surfaces from the total VOCi concentration measured in Case 1. It should be noted, however, that because the T-shirts

were stretched on the seat backs in Case 1, about 55% of the seat surface was unavailable for VOC emissions. As a result, the VOCi emissions from the seats in Case 1 were probably 55% lower than in the similar case conducted without T-shirts. The above correction was incorporated in order to obtain the “measured” contributions of soiled T-shirts to the different VOCs in Case 1.

Figure 6.2 shows the contributions of the soiled T-shirts to the concentrations of different VOCs as computed by the mass balance model and their corresponding “measured” data for Case 1. The computed concentration of 4-OPA agreed well with the measurement. However, acetone, nonanal and decanal concentrations were considerably over-predicted by the model. The discrepancies between the model predictions and the measurements were caused primarily by the following factors. The regression models used to compute yields were developed on the basis of cotton T-shirts soiled by the same human subject in all but one of the cases, which means that the effects of fabric and of soiling by different human subjects could not be captured. The use of cotton T-shirts meant that VOC emissions were overestimated because soiled cotton fabric seems to have higher secondary emissions than the soiled wool or polyester fabrics, as demonstrated by Coleman et al. (2008a). The measured relative humidity in the mockup was 6.8%, which was outside the humidity range (10%–49% RH) used to develop the model. When the above factors are taken into account, the model’s performance does not seem to be poor.

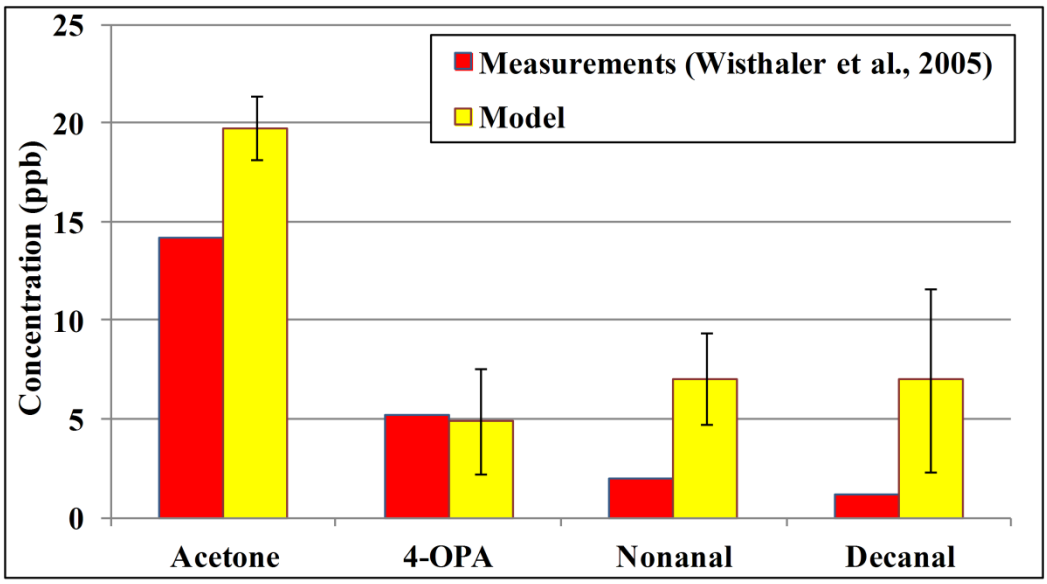

Figure 6.2. Ozone-initiated VOCs from reactions with soiled T-shirts: comparisons of the predicted and measured data for Case 1. The measurement errors are unknown, and the model error bars represent the 95% confidence intervals.

We also used the mass balance model to compute secondary VOC emissions from ozone/human-surface reactions in the occupied cabin mockup under high and low outdoor air change rate conditions (Cases 2 and 3, respectively). As in Case 1, the contributions of human surfaces were estimated from measurements by taking into account the portion of the seat backs that was covered by the passengers and unavailable for VOC emissions.

Figure 6.3 compares the computed contributions of ozone/human-surface reactions to VOC concentrations in the mockup with their corresponding experimental estimates at an air change rate of 8.8 h^{-1}. The computed VOC concentrations were higher than the measured data, especially for decanal. These discrepancies can be attributed to modeling deficiencies, as discussed above for Case 1. In addition, different passengers in the cabin can be expected to have different secondary VOC emissions because of differences in clothing, skin-oil composition, and usage of terpene-containing personal care products (such as perfumes and other fragrances). However, incorporating those details was beyond the scope of the current investigation.

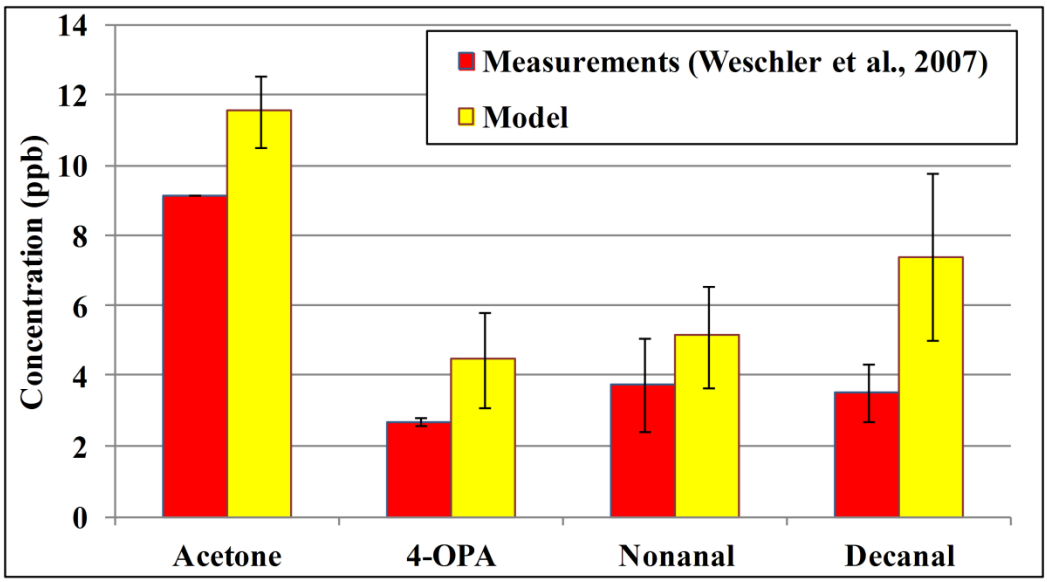

Figure 6.3. Ozone-initiated VOCs from reactions with human surfaces: comparisons of the predicted and measured data for Case 2. The measurement error bars represent the range, and the model error bars represent the 95% confidence intervals.

Figure 6.4 compares the contributions of human surfaces to the different VOCs in the cabin for Case 3. The "measured" and predicted contributions of human surfaces to different VOCs in the cabin were higher in Case 3 than in Case 2. Case 2 was conducted at 10% relative humidity, whereas in Case 3 the relative humidity was 20%. The VOC emission models (Eqs. (6.2)–(6.5)) are sensitive to changes in humidity, and they predicted a large increase in VOC emissions with increased humidity. A similar conclusion was obtained by Coleman et al. (2008a) for laundered cotton fabrics. In reality, an increase in relative humidity may not have a significant influence on the secondary emissions from other clothing fabrics. Unfortunately, there is no information available in the literature that could be used to verify our hypothesis.

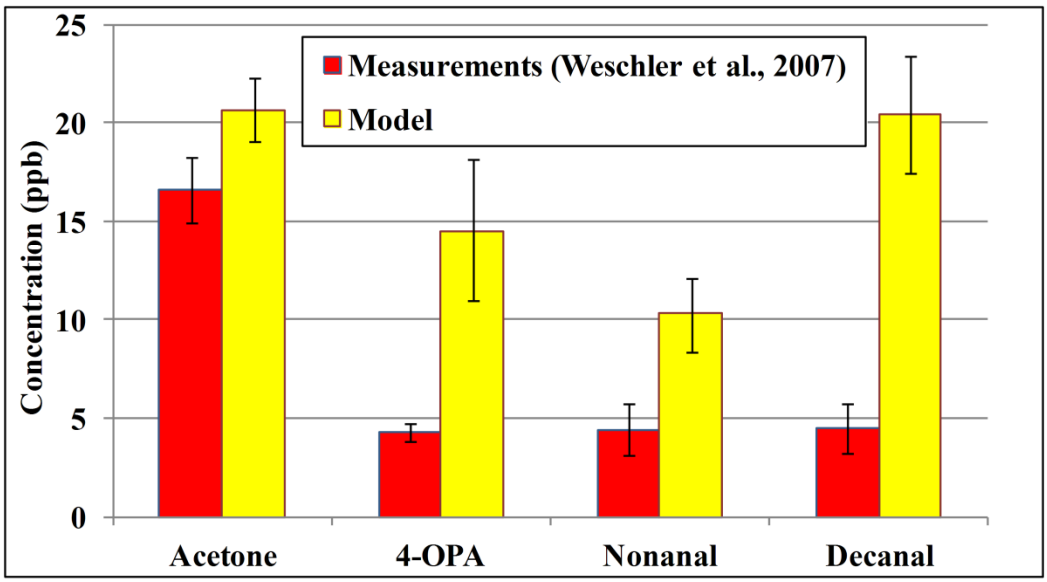

Figure 6.4. Ozone-initiated VOCs from reactions with human surfaces: comparisons of the predicted and measured data for Case 3. The measurement error bars represent the range, and the model error bars represent the 95% confidence intervals.

6.3.2 Distributions of Different VOCs in the Cabin Mockup

The previous subsections described modeling results for the concentrations of ozone-initiated VOCs from reactions with human surfaces under the assumption of well-mixed conditions. However, the well-mixed assumption might not be suitable because ozone/clothing reactions occur in rising thermal plumes, and the VOCs are expected to be enriched in the breathing zone. Hence, the actual exposure of passengers to VOCs could be higher than that calculated from a simple mass balance analysis under the well-mixed assumption. By using CFD modeling of VOC distributions, we can determine their concentrations in the breathing zone and make better risk assessments.

Figure 6.5 shows the distribution of 4-OPA normalized by its exhaust concentration along the longitudinal plane through the center of the cabin in Case 2. It can be seen that 4-OPA was enriched in the breathing zone of the occupant. The normalized distributions of nonanal and decanal were similar to the distribution of 4-OPA, and these compounds were also enhanced in the breathing zone. The distribution of acetone was qualitatively

similar to that of OPA, but its concentration was much higher near the breathing zone since it was also emitted in human breath.

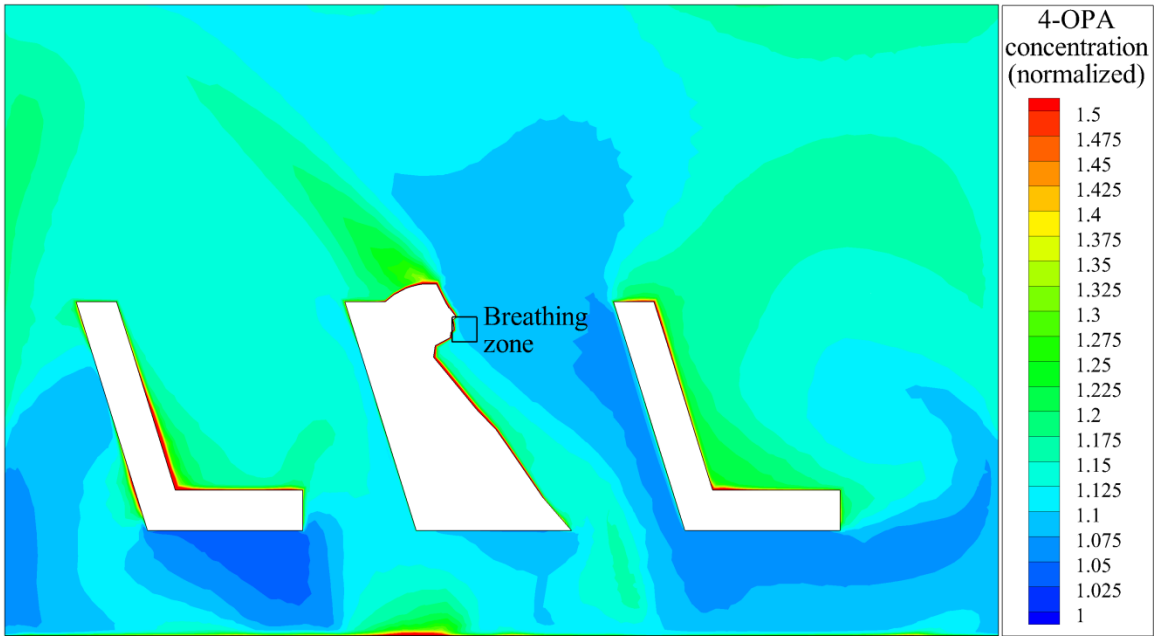

Figure 6.5. The 4-OPA distribution in the longitudinal section through the center of the occupied cabin mockup with an outdoor air change rate of 8.8 h^{-1} for Case 2.

The normalized 4-OPA distribution in Case 3 was qualitatively similar to that in Case 2, as shown in Figure 6.6. The normalized concentration in Case 3 was significantly lower than that in Case 2. This difference occurred because the exhaust concentration in Case 3 was much higher than that in Case 2 as a result of the lower outdoor air change rate, which was used for normalization.

Figure 6.6. The 4-OPA distribution in the longitudinal section through center of the occupied cabin mockup with an outdoor air change rate of 4.4 h^{-1} for Case 3.

To quantify the enhancement of VOC concentrations in the breathing zone, this investigation computed the VOC ratio (r_{VOCi}), which was defined as the VOC concentration in the breathing zone divided by its exhaust concentration. Figure 6.7 shows the r_{VOCi} for the different VOCs under the two air change rates for the middle row in the cabin mockup. The $r_{acetone}$, $r_{4\text{-}OPA}$, $r_{nonanal}$, and $r_{decanal}$ were 1.51±0.18, 1.22±0.05, 1.22±0.06, and 1.21±0.05, respectively, in Case 2; and 1.26±0.10, 1.11±0.03, 1.11±0.03, and 1.10±0.03, respectively, in Case 3. The r_{VOCi} values were higher in Case 2 than in Case 3 because the exhaust concentrations were much lower in Case 2 as a result of the higher air change rate. The $r_{acetone}$ was much higher than $r_{4\text{-}OPA}$, $r_{nonanal}$, and $r_{decanal}$ because acetone is also present in human breath and was consequently enriched in the breathing zone, as discussed previously.

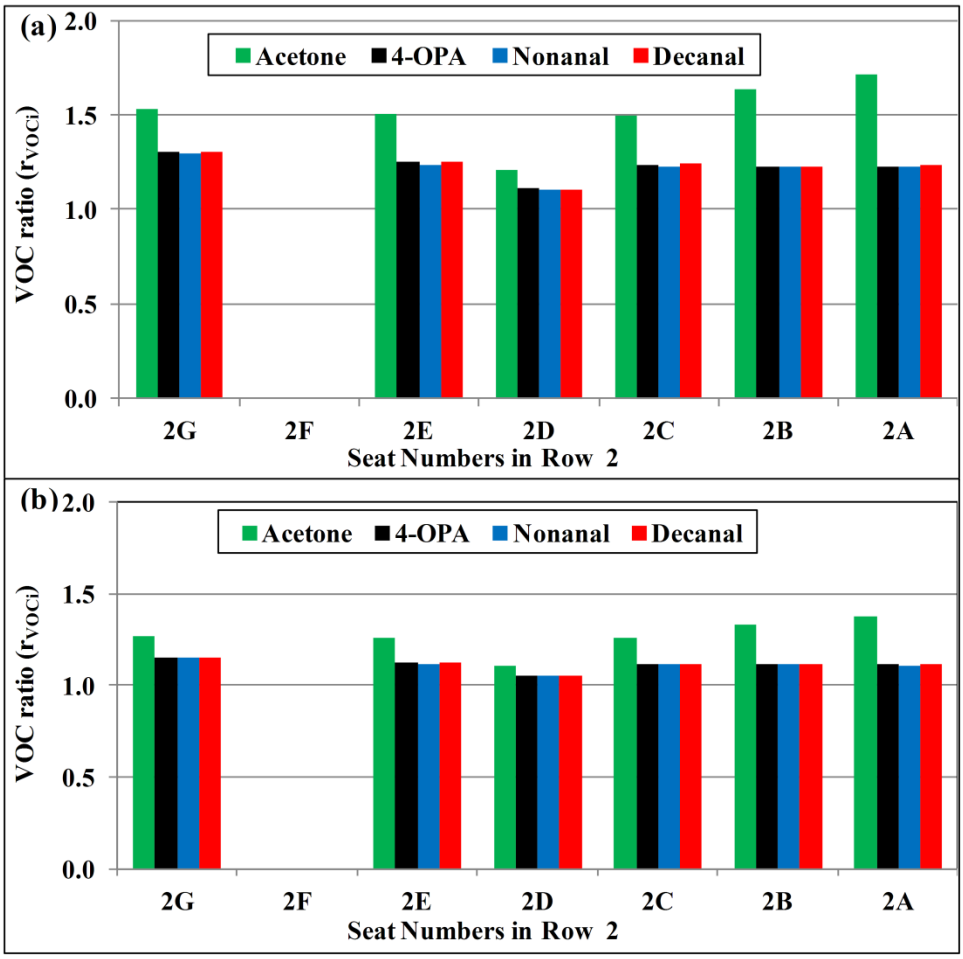

Figure 6.7. VOC ratio for different passengers seated in the middle row of the occupied cabin mockup under an outdoor air change rate of (a) 8.8 h^{-1} (Case 2) and (b) 4.4 h^{-1} (Case 3).

Overall, the ozone-initiated VOCs were found to be significantly enhanced in the breathing zones as compared with their corresponding exhaust concentrations, and thus the exhaust air measurements would have underestimated the inhalation dosage of the passengers. Hence, to accurately estimate passengers' exposure to such VOCs, their concentrations in the breathing zones should be used instead of those at the exhausts.

6.4 Discussion

This chapter demonstrated a method for estimating the contributions of human surfaces to the concentrations of several ozone-initiated VOCs in an aircraft cabin mockup. The method developed is a general one, and it can be extended to compute secondary

emissions from a variety of materials under given indoor conditions. The model development shows that experimental data obtained through chamber measurements constitutes the most important component of the model. The experimental dataset used in our investigation was rather small (only 12 cases), and it did not address the effects of clothing fabric or variations in soiling from different human subjects. These limitations were the major reasons for the discrepancies that were observed between the model predictions and experimental data. The model's performance may be improved by conducting additional experiments under a wide range of conditions. Nevertheless, the model is useful for estimating concentrations of ozone-initiated VOCs in indoor spaces.

6.5 Conclusions

This chapter studied ozone-initiated secondary emissions of acetone, 4-oxopentanal (4-OPA), nonanal, and decanal from reactions with human-worn clothing in an aircraft cabin mockup. The study was conducted by developing empirical models to compute the secondary VOC emissions from the prevailing environmental conditions (such as ozone concentration, humidity, and air change rate) based on experiments conducted in an environmental chamber.

These models were then used to compute the contributions of human surfaces (skin, hair, and clothing) to the ozone-initiated VOCs in an aircraft cabin mockup. The model predictions showed very good trends qualitatively, but with quantitative discrepancies when compared with the corresponding experimental data obtained in the mockup. A major reason for the discrepancies is that a limited dataset from the chamber was used for developing the model. Nevertheless, the models are promising and can be improved with more experimental data.

When the VOC emission models were integrated into a CFD model, much higher concentrations of the various VOCs were identified in the breathing zone of the passengers than in the mockup exhausts. The reason for this difference is that the VOC concentrations are not uniform, and the ozone/human-surface reactions occurring in the thermal plumes from passengers can enhance their concentrations. Therefore, it is more

accurate to assess the passengers' exposure risk by using the concentrations of the ozone-initiated VOCs in the breathing zone than those in the exhausts.

CHAPTER 7. NUMERICAL MODELING OF PARTICLE GENERATION FROM OZONE REACTIONS WITH HUMAN-WORN CLOTHING IN INDOOR ENVIRONMENTS

We observed sub-micron particle generation from the ozone reactions with clothing soiled by human skin-oils in Chapter 4. These reactions were identified as another potential source of indoor ultrafine particles (UFPs), a potential health hazard for humans. Therefore, to better understand particle generation from ozone reactions with human-worn clothing and human exposure to these particles, we developed a numerical model for computing size-resolved particle concentrations. The model was then used to compute concentrations of such ozone-initiated particles in various indoor environments such as buildings and airliner cabins.

7.1 Method

We simulated the generation of ozone-initiated particles from reactions with human-worn clothing measured in an environmental chamber. The measurements details were presented in Chapter 4. These measurements presented a well-controlled and challenging case study for developing models to study ozone-initiated particle generation from the reaction of ozone with clothing.

To model particle generation, this investigation assumed that ozone reacted with skin-oils on the T-shirt to produce a hypothetical semi-volatile organic compound (SVOC) in the vapor phase, as shown in Figure 7.1. The concentration of the SVOC vapor then increased in the chamber because its production rate from ozone/skin-oil reactions was higher than its removal rate by ventilation and deposition. The SVOC vapor concentration subsequently crossed its nucleation threshold, and new particles (liquid droplets of SVOC) were generated. Note that if ventilation and deposition rates were

sufficiently high, particle generation would not take place because the SVOC vapor concentration would never cross its nucleation threshold.

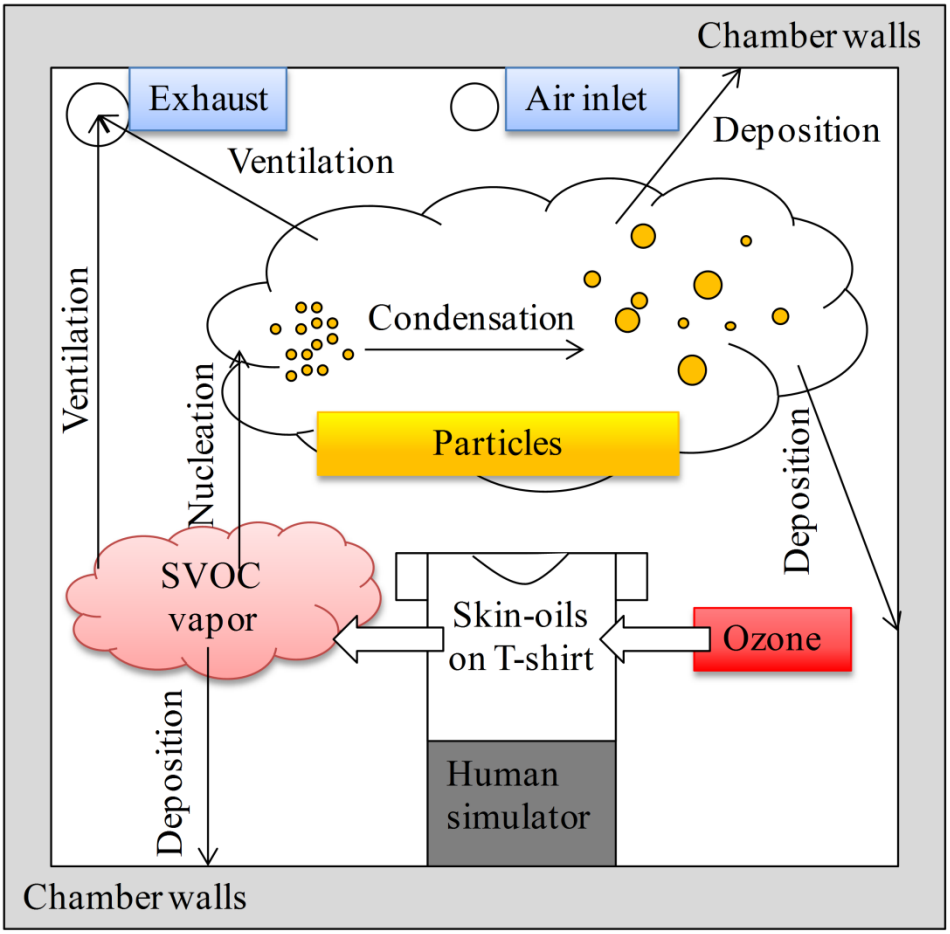

Figure 7.1. An illustration of the particle-generation mechanism.

These freshly nucleated particles then served as condensation sites for the SVOC vapor and subsequently reduced its concentration below the nucleation threshold, preventing further nucleation. From this time onward, condensation was predominant, which led to growth in particle size and consumption of the SVOC vapor. Furthermore, the number of particles in the chamber was also decreasing because nucleation had stopped and particles were continuously removed by ventilation and deposition, as illustrated in Figure 7.1. This in turn reduced the number of available condensation sites for the SVOC vapor, and its concentration started to increase again, producing another nucleation burst of particles. This cycle of particle generation, growth, and removal continued until the ozone/skin-oil

reactions could not generate sufficient SVOC vapor in the chamber. Note that coagulation of particles was ignored in the above description because the particle concentrations in most cases were too low for coagulation to have a significant influence (Hussein et al., 2009).

7.1.1 Model Formulation

As described above, the SVOC vapor was the primary driver of the particle generation cycle. The SVOC concentration in the chamber was assumed to be under well-mixed conditions because of the small particle size. The mass conservation equation for the SVOC is as follows:

$$\frac{dC_{SVOC}}{dt} = S_{gen} - \lambda_{outdoor} C_{SVOC} - \lambda_{d,SVOC} C_{SVOC} - CS \cdot C_{SVOC} - \rho_p \frac{\pi}{6} Dp_{nuc}^3 J_{nuc}, \quad (7.1)$$

where C_{SVOC} is the concentration of SVOC vapor, t the time, S_{gen} the SVOC production rate, $\lambda_{outdoor}$ the outdoor air change rate, $\lambda_{d,SVOC}$ the SVOC deposition rate coefficient on the chamber walls, CS the condensational sink of SVOC vapor on the existing particles, ρ_p the particle density, Dp_{nuc} the diameter of nucleating particles, and J_{nuc} the particle nucleation rate. The first term in the above equation is the rate of change of SVOC concentration in the chamber. The second term describes the production of SVOC from ozone/skin-oil reactions. The third and fourth terms describe SVOC removal by ventilation and deposition, respectively. The fifth and sixth terms are the SVOC conversion rates of particles from vapor to liquid droplets as a result of condensation and nucleation, respectively. Clearly, the above equation can be used to determine the time-varying SVOC vapor concentration in the chamber if the various terms on the right-hand side are computed. However, the equation is intrinsically coupled with the particle concentrations through the condensation and nucleation sink terms.

Therefore, it is necessary to introduce governing equations for particles. Just as the mass balance equation was used for the SVOC vapor, this investigation used the number balance equation to compute the particle number concentrations in the chamber. The

particles were first classified into different groups on the basis of diameter, and their number concentrations were computed by the following equations:

$$\begin{aligned} \frac{dN(Dp_i,t)}{dt} &= -\lambda_{outdoor}N(Dp_i,t) - \lambda_{d,p}(Dp_i)N(Dp_i,t) + J_{nuc} \quad (\text{for } i=1) \\ \frac{dN(Dp_i,t)}{dt} &= -\lambda_{outdoor}N(Dp_i,t) - \lambda_{d,p}(Dp_i)N(Dp_i,t) \qquad (\text{for } i=2,3,...) \end{aligned}, \tag{7.2}$$

where i is the group number, N the number concentration of particles with diameters Dp_i at time t, $\lambda_{d,p}$ their deposition rate coefficient, and Dp_{nuc} the diameter of nucleating particles. The first term in each of the above equations is the rate of change of particle number concentration with diameter Dp_i. The second and third terms describe the removal of particles by ventilation and deposition, respectively. The fourth term expresses particle generation by nucleation of SVOC vapor, which is a source of nucleating particles (i = 1 and $Dp_1 = Dp_{nuc}$) only. Note that the above equations do not include the incoming particles from ventilation and that we chose those experimental cases for which the inlet air contained negligible particles for comparison with the numerical results. Although inlet particles do not pose any theoretical problems and can be easily incorporated into Eq. (7.2), they increase computational costs drastically by increasing the number of groups in the model, and therefore they were not considered. We also did not account for coagulation in Eq. (7.2) because it was usually insignificant as a result of low particle concentrations.

To solve Eq. (7.2) for computing size-resolved particle concentrations, it is also necessary to account for particle size growth as described by Kumar and Ramkrishna (1997). The growth of particle diameters was governed by the condensation of SVOC vapor, which was computed by the following expression (Kulmala, 1988):

$$\frac{dDp_i}{dt} = \frac{4\beta_c D_{SVOC} C_{SVOC}}{\rho_p Dp_i}, \tag{7.3}$$

where D_{SVOC} is the diffusion coefficient of SVOC and β_c the transition correction factor (Fuchs and Sutugin, 1971).

Overall, Eqs. (7.1), (7.2), and (7.3) can be used for computing the time-dependent SVOC vapor concentration, particle number concentrations, and particle diameters, respectively. However, the various terms on the right-hand side of these equations needed to be determined, as described in the following subsections.

7.1.1.1 Modeling the SVOC Generation (S_{gen})

The ozone-initiated SVOC generation (S_{gen} in Eq. (7.1)) was estimated by assuming a first-order reaction between ozone and skin-oils on the T-shirt as follows:

$$\text{Ozone} + \text{Skin-oils} \xrightarrow{k_{ozone}} \text{SVOC}_{vapor} .$$

Thus, the generation rate of SVOC was expressed as:

$$S_{gen} = \frac{k_{ozone} A_{T\text{-shirt}} C_{skin\text{-}oils} C}{V_{chamber}}, \tag{7.4}$$

where k_{ozone} is the ozone/skin-oils reaction rate constant; $A_{T\text{-shirt}}$ the area of the T-shirt; $V_{chamber}$ the chamber volume; and C and $C_{skin\text{-}oils}$ the concentrations of ozone in the air and skin-oils on the T-shirt, respectively. The determination of ozone/skin-oils-reaction-generated SVOC was based on the assumption that the T-shirt was soiled with skin-oils because it was worn by a human subject. We calculated the time-varying concentration of skin-oils by solving the following equation:

$$\frac{dC_{skin\text{-}oils}}{dt} = -k_{ozone} C_{skin\text{-}oils} C, \tag{7.5}$$

Clearly, the above equation can be easily solved if the initial concentration of skin-oils on the T-shirt ($C_{0,skin\text{-}oils}$), C, and k_{ozone} are known. C was measured during the experiments; however, $C_{0,skin\text{-}oils}$ and k_{ozone} were not known beforehand. Therefore, this investigation fitted those two parameters by comparing the model predictions for ozone-initiated particles with their corresponding measurements, as described in Section 7.1.2. Finally, Eqs. (7.4) and (7.5) can be solved for computing S_{gen}.

The above calculation method for S_{gen} can be simplified if it is assumed that the T-shirt contained a large reservoir of skin-oils and that the reactions were controlled only by the ozone concentration in the chamber. Then the expression for S_{gen} becomes:

$$S_{gen} = \frac{k_{ozone\text{-}ex} A_{T\text{-}shirt} C}{V_{chamber}}, \tag{7.6}$$

where $k_{ozone\text{-}ex}$ is the ozone/skin-oils reaction rate constant with the assumption of excess skin-oils. Again, $k_{ozone\text{-}ex}$ can be estimated by comparing the model predictions with measurements as described in Section 7.1.2.

This study used both of the methods described above for computing S_{gen} and also compared their performance in simulating ozone-initiated particles, as analyzed in the results section. The calculation of S_{gen} from Eqs. (7.4) and (7.5) was termed the "skin-oils depletion" model, and the calculation of S_{gen} from Eq. (7.6) was termed the "excess skin-oils" model.

7.1.1.2 Modeling the Nucleation Rate (J_{nuc})

Nucleation governs the generation rate of new particles from ozone/skin-oil reactions. Hence, the aim of any nucleation model is to predict the generation rate of new particles given the physical properties of the nucleating species (SVOC vapor in this study), its super-saturation, and other environmental conditions. Various nucleation theories are described in detail in many texts (Seinfeld and Pandis, 2006), so our discussion here will be brief.

The nucleation rate can be determined experimentally if the generation of freshly nucleated particles is measured. However, such particles have extremely small sizes (on the order of a few nanometers) and usually cannot be detected by conventional measurement instruments such as a scanning mobility particle sizer (SMPS). Therefore, particles are measured only when they grow beyond the detection size limit, which is usually about ten nanometers. For example, the minimum detection limit for the SMPS used in our ozone/T-shirt experiments was 9.65 nm, which means that the true nucleation

rate was unknown. Nevertheless, these SMPS measurements can be used to compute the generation rate of the smallest detectable particles, also called the apparent nucleation rate (Kerminen and Kulmala, 2002).

To calculate the apparent nucleation rate, we summed Eq. (7.2) over all particle sizes and performed some algebraic manipulations as follows:

$$\sum_{Dp_i=Dp_{nuc}}^{\infty}\frac{dN}{dt}=-\lambda_{outdoor}\sum_{Dp_i=Dp_{nuc}}^{\infty}N-\sum_{Dp_i=Dp_{nuc}}^{\infty}\lambda_{d,p}N+J_{nuc}$$

$$\Rightarrow\sum_{Dp_i=Dp_{nuc}}^{Dp_i=Dp_{SMPS}}\frac{dN}{dt}+\sum_{Dp_i=Dp_{SMPS}}^{\infty}\frac{dN}{dt}=-\lambda_{outdoor}\sum_{Dp_i=Dp_{nuc}}^{Dp_i=Dp_{SMPS}}N-\lambda_{outdoor}\sum_{Dp_i=Dp_{SMPS}}^{\infty}N...$$

$$...-\sum_{Dp_i=Dp_{nuc}}^{Dp_i=Dp_{SMPS}}\lambda_{d,p}N-\sum_{Dp_i=D_{SMPS}}^{\infty}\lambda_{d,p}N+J_{nuc}$$

$$\Rightarrow\sum_{Dp_i=Dp_{SMPS}}^{\infty}\frac{dN}{dt}=-\lambda_{outdoor}\sum_{Dp_i=Dp_{SMPS}}^{\infty}N-\sum_{Dp_i=Dp_{SMPS}}^{\infty}\lambda_{d,p}N...$$

$$...+\left[J_{nuc}-\lambda_{outdoor}\sum_{Dp_i=Dp_{nuc}}^{Dp_i=Dp_{SMPS}}N-\sum_{Dp_i=Dp_{nuc}}^{Dp_i=Dp_{SMPS}}\lambda_{d,p}N-\sum_{Dp_i=Dp_{nuc}}^{Dp_i=Dp_{SMPS}}\frac{dN}{dt}\right]$$

$$\Rightarrow\sum_{Dp_i=Dp_{SMPS}}^{\infty}\frac{dN}{dt}=-\lambda_{outdoor}\sum_{Dp_i=Dp_{SMPS}}^{\infty}N-\sum_{Dp_i=Dp_{SMPS}}^{\infty}\lambda_{d,p}N+J_{nuc,app}$$

$$\Rightarrow J_{nuc,app}=\sum_{Dp_i=Dp_{SMPS}}^{\infty}\frac{dN}{dt}+\lambda_{outdoor}\sum_{Dp_i=Dp_{SMPS}}^{\infty}N+\sum_{Dp_i=Dp_{SMPS}}^{\infty}\lambda_{d,p}N$$

$$\Rightarrow J_{nuc,app}\approx\frac{dN_{total,SMPS}(t)}{dt}+\lambda_{outdoor}N_{total,SMPS}(t)+\sum_{Dp_i=Dp_{SMPS}}^{\infty}\lambda_{d,p}N \quad , \qquad (7.7)$$

where $N_{total,SMPS}(t)$ is the total particle number concentration measured by SMPS at time t, and Dp_{SMPS} is the smallest particle diameter detected by the SMPS (9.65 nm). The terms in the square brackets above were defined as the apparent nucleation rate ($J_{nuc,app}$) because they act together as an effective source term for particles with diameters greater then Dp_{SMPS}. In deriving the above equation, we used the shorthand notation N and $\lambda_{d,p}$ for $N(Dp_i, t)$ and $\lambda_{d,p}(Dp_i)$, respectively. In addition, the derivation assumed that there were a negligible number of particles with sizes larger than the upper detection limit of the SMPS.

Finally, to compute $J_{nuc,app}$, Eq. (7.7) can be solved jointly with Eqs. (7.1) to (7.3) by using $N_{total,SMPS}(t)$ from the measured data. However, we first need to replace Dp_{nuc} with Dp_{SMPS} and J_{nuc} with $J_{nuc,app}$ in Eqs. (7.1) and (7.2) because those particles with diameters below Dp_{SMPS} were eliminated from the model formulation and were accounted for indirectly through the $J_{nuc,app}$ term in Eq. (7.7). Such an approach was extremely useful for studying the evolution of particle sizes after they were detected by the SMPS. It was also useful to compare the model results with measurements of particle size distributions for validating Eqs. (7.1) to (7.3).

The primary limitation of the above approach was that $J_{nuc,app}$ was computed from the measured $N_{total,SMPS}(t)$ in an environmental chamber in which ozone/T-shirt reactions were the only particle source. A similar technique would not be possible in real indoor settings because the measured $N_{total,SMPS}(t)$ would also contain contributions from other particle-generating sources. Therefore, it was necessary to explore a number of theoretical models for nucleation that did not require $N_{total,SMPS}(t)$ as an input. However, the nucleation precursors and mechanism of particle generation from ozone/clothing reactions is itself unknown. Therefore, we chose several popular nucleation models from the literature and compared their performance in order to identify the most suitable model. The models studied were the thermodynamic, kinetic, and activation nucleation models.

The thermodynamic model is based on the classical homogenous nucleation theory, which is derived from the thermodynamic theory of fluctuations. A widely used expression for nucleation rate is the following (Seinfeld and Pandis, 2006):

$$J_{nuc} = \left(\frac{2\omega}{\pi m^5}\right)^{1/2} \frac{vC_{SVOC}^2}{S} \exp\left(\frac{-16\pi}{3k_B^{\,3}} \frac{v^2\omega^3}{T^3(\ln S)^2}\right), \tag{7.8}$$

where ω is the surface tension of the SVOC, m the molecular mass, v the molecular volume, S the super-saturation ratio, k_B the Boltzmann constant, and T the air temperature. The super-saturation ratio of the SVOC is defined as $S=C_{SVOC}/C_{SVOC,sat}$, where $C_{SVOC,sat}$ is the SVOC concentration in a saturated vapor at equilibrium.

Another popular theory of nucleation is the kinetic theory, which assumes that nucleation is determined by the collision rate of molecules rather than by the thermodynamic criterion (Lushnikov, 2010). The nucleation rate is given by:

$$J_{nuc} = k_{kin} C_{SVOC}^2 , \tag{7.9}$$

where k_{kin} is the kinetic nucleation constant.

Recently, the activation nucleation theory was proposed by Kulmala et al. (2006) for explaining atmospheric nucleation events. It was also used by Vartiainen et al. (2006) to compute nucleation of particles from ozone/d-limonene reactions in an indoor environment. Therefore, it was chosen as another possible candidate for computing nucleation. This theory assumes that nucleation occurs through the activation of existing thermodynamically stable clusters by SVOCs, and the nucleation rate is given by:

$$J_{nuc} = k_{act} C_{SVOC} , \tag{7.10}$$

where k_{act} is the activation nucleation constant.

7.1.1.3 Modeling the Condensational Sink (CS) and Deposition Rate Coefficients ($\lambda_{d,SVOC}$ and $\lambda_{d,p}$)

For the condensational growth governed by Eq. (7.3), CS is given by the following expression (Kulmala et al., 2001):

$$CS = 2\pi D_{SVOC} \sum_i \beta_c . Dp_i . N(Dp_i) . \tag{7.11}$$

The SVOC deposition on the chamber walls was computed from Lai and Nazaroff's (2000) deposition model, as suggested by Weschler and Nazaroff (2008). The particle deposition coefficient ($\lambda_{d,p}$) on the chamber walls was taken as 0.25 h^{-1} for all diameters.

7.1.2 Estimating Physical Constants and Model Parameters

The solutions of the model equations (Eqs. (7.1)–(7.11)) require appropriate values for the physical properties of the hypothetical SVOC and particles as well as the various modeling parameters. Table 7.1 shows the values used in this investigation. However, because the ozone/skin-oils reaction byproducts responsible for particle generations are themselves unknown, those physical properties and modeling constants could only be estimated.

Table 7.1. Various physical constants and model parameters used in this investigation.

Variable	Estimated value	Variable	Estimated value
ρ_p	1.2 g cm^{-3}	D_{SVOC}	5×10^{-6} m^2 s^{-1}
$k_{ozone\text{-}ex}$	2×10^{-10} kgm^{-2} h^{-1} ppb^{-1}	$C_{SVOC,sat}$	1×10^{-13} kg m^{-3}
k_{ozone}	1×10^{-3} h^{-1} ppb^{-1}	ω	.025 kg s^{-2}
$C_{0,skin\text{-}oils}$	2×10^{-7} kg m^{-2}	k_{kin}	8.4×10^{25} m^3 kg^{-2} s^{-1}
m	250 g $mole^{-1}$	k_{act}	1.6×10^{16} kg^{-1} s^{-1}

A recent investigation (Wang and Waring, 2014) found SVOCs such as geranyl acetone, 4-methyl-4-octene-1,8-dial (4-MOD), and 4-methyl-8-oxo-4-nonenal (4-MON) responsible for condensational mass transfer to particulate phase from ozone reactions with surface-sorbed squalene (a major component of human skin-oils). The authors also conjectured that SVOCs such as 5,9,13-trimethyltetradeca-4,8,12-trienal (C17-trienal), 4,9,13,17-tetramethyl-octadeca-4,8,12,16-tetraenal (C22-tetraenal), and 4,8,13,17,21-pentamethyl-docosa-4,8,12,16,20-pentaenal (C27-pentaenal) could be responsible for nucleation. Therefore, we considered the hypothetical SVOC as a surrogate for these ozone/squalene generated SVOCs. Its property values for m and D_{SVOC} were estimated by computing the mean property values for the SVOCs mentioned above.

A similar method (i.e., computing the average property values for ozone/squalene-generated SVOCs) was attempted for determining the values of $C_{SVOC,sat}$ and ω used in the thermodynamic nucleation models. However, reasonable results could not be obtained because the nucleation rate expression is extremely sensitive to these parameters. We

therefore fitted the values of $C_{SVOC,sat}$ and ω such that the peak particle number concentration was predicted well for a reference case (a case with intermediate conditions). We chose such a criterion because nucleation primarily influenced the number concentrations. Similarly, we fitted the values of k_{kin} and k_{act} used in the kinetic and activation models, respectively, such that peak number concentrations were best predicted for the same reference case.

Likewise, the values of $\lambda_{d,p}$ and $k_{ozone\text{-}ex}$ in the "excess skin-oils" model were fitted such that the particle size distributions were predicted reasonably well for the reference case. In the case of the "skin-oils depletion" model, we retained the value of $\lambda_{d,p}$ obtained previously and then fitted k_{ozone} and $C_{0,skin\text{-}oils}$ such that the particle mass concentrations for the case with the highest ozone concentration were predicted well. We chose such an approach because the T-shirt in that case was expected to be highly depleted of skin-oils as a result of the high ozone reactions, which means that the "skin-oils depletion" was most suitable. The particle density was taken from Turpin and Lim (2001), who derived their results by using the data of Rogge et al. (1993) for atmospheric organic aerosols.

7.2 Results and Discussions

This section first reports the simulation results for ozone-initiated particle generations from reactions with soiled clothing obtained by using the apparent nucleation formulation (Eq. (7.7)) and their comparison with the measurements described in Chapter 4. These comparisons were useful for evaluating the performance of the various model formulations used in this investigation, except for the nucleation model, because Eq. (7.7) computed the nucleation from the measurements themselves (i.e., the measurements of $N_{total,SMPS}(t)$). However, as discussed previously, it is not practical to use such an approach for computing ozone/clothing-generated particles under realistic indoor conditions, since their individual contributions to particles cannot be isolated from other particle sources. Therefore, we subsequently replaced the apparent nucleation model with different theoretical nucleation models that can compute ozone-initiated particles without the measurement of $N_{total,SMPS}(t)$. We then evaluated the performance of the thermodynamic, kinetic, and activation nucleation models by comparing their predictions

with the corresponding measurements. Finally, we used the thermodynamic model to estimate the ozone-initiated particle generation from human clothing under typical building and airliner cabin conditions, because performance of this model was found to be superior to that of the other two models.

7.2.1 Apparent Nucleation Rate Formulation

Because nucleation modeling was the most difficult aspect of this research, we computed the apparent nucleation rates from Eq. (7.7). To reduce computational expenses, our model assumed that the inlet air contained a negligible number of particles. Therefore, to test the model formulations, we chose those cases from the measurements given in Table 4.1 which had low inlet particle concentrations. The experimental conditions for these cases are summarized in Table 7.2.

Table 7.2 Details of the experimental conditions in the chamber used for simulating particle generation from ozone reactions with human clothing

Case	Corresponding case in Table 4.1	Ozone concentration (ppb)	Hours the T-shirt was worn (h)	Air change rate (h^{-1})
1	12	22	6	0.5
2	3	40	6	0.5
3	7	57	12	0.5
4	4	148	6	0.5
5	10	51	6	2.7
6	11	133	6	2.7

Among these cases, we studied Cases 1–4 with the apparent nucleation formulation. We could not study Cases 5 and 6 with this approach because particle generation was not detected in these cases, which meant that Eq. (7.7) could not be used for computing the nucleation rate ($J_{nuc,app}$). These two cases were used for studying the performance of the various nucleation models, which is discussed in the next subsection.

Figure 7.2 compares the computed and measured ozone-initiated particle number concentrations for Cases 1, 3, and 4. The measurements showed that the ozone-initiated

particle numbers were negligible from t = 0 to t = 2.5 h because the ozone concentration was very low (~ 5 ppb). Particle generation was measured about one hour after ozone injection through a burst of nucleation, and the total number concentrations reached a maximum. The particle numbers then started to decay because of the lack of nucleation and because of particle removal by ventilation and deposition. A secondary burst of nucleation was clearly observed in cases with high ozone concentrations, and the particle numbers showed secondary maxima. The secondary burst was not detected under low ozone conditions, mainly because of the large measurement uncertainties. Finally, the particle numbers decayed further, and the experiments were terminated at t = 12.5 h.

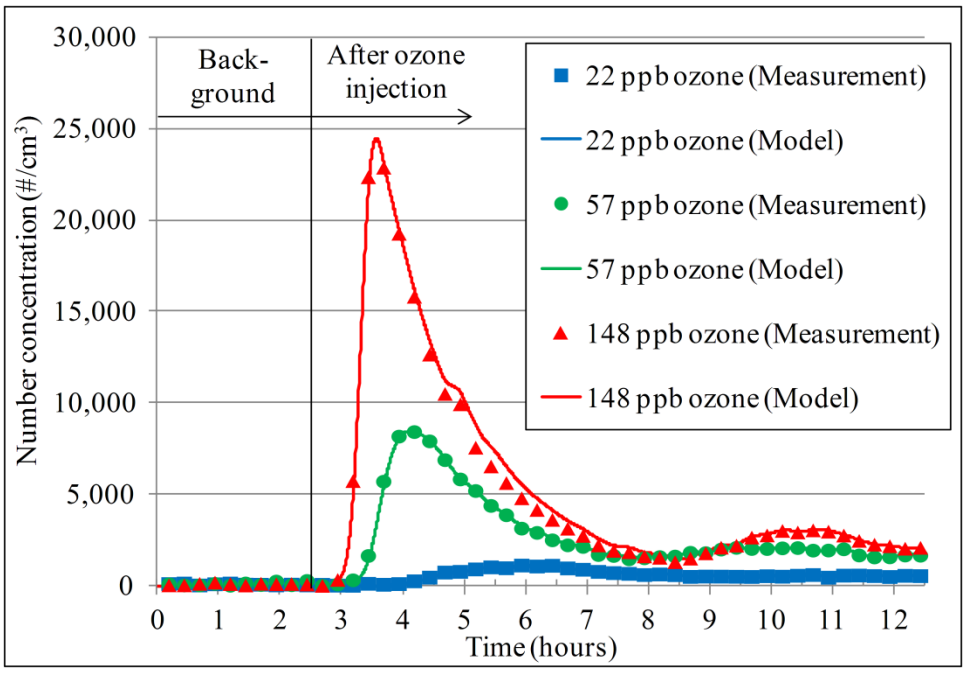

Figure 7.2. Comparison of particle number concentrations computed by the "excess skin-oils" model with the corresponding measurements at different ozone concentrations.

As shown in Figure 7.2 for the "excess skin-oils" model, the computed particle number concentrations were in excellent agreement with the measurements at different ozone levels, primarily because the apparent nucleation rate was estimated from the measurements themselves. Note that in the case of 148 ppb ozone, the model slightly over-predicted the number concentrations at certain times. This case had particle concentrations in excess of 10,000 #/cm^3, meaning that coagulation could be responsible

for a reduction in particle number (Hussein et al., 2009). The fact that coagulation was not included in our model probably led to slight over-prediction. We also obtained excellent agreement in the 40 ppb ozone case (results not shown). The results with the "skin-oils depletion" model were almost identical to the "excess skin-oils" model and therefore are not shown here.

Figure 7.3(a) shows the particle mass concentrations obtained by the two SVOC generation models for the 40 ppb and 148 ppb ozone cases (Cases 2 and 4) and their comparisons with measurements. In both cases, the measured mass concentrations first increased as a result of particle generation after ozone injection, and then decayed toward the end. In the case of 40 ppb ozone, both models predicted the particle mass concentrations reasonably well when compared with the measurements, but the "excess skin-oils" model seemed to provide slightly better predictions than the "skin-oils depletion" model. However, with 148 ppb ozone, the "excess skin-oils" model hugely over-predicted the particle masses, while the "skin-oils depletion" model performed much better, although it still over-predicted the mass concentration by about 30%. Thus, it seems that the soiled T-shirt contained a limited quantity of skin-oils available for ozone reactions. These were consumed faster at the higher ozone concentration, and the T-shirt was significantly depleted of skin-oils, especially at later times.

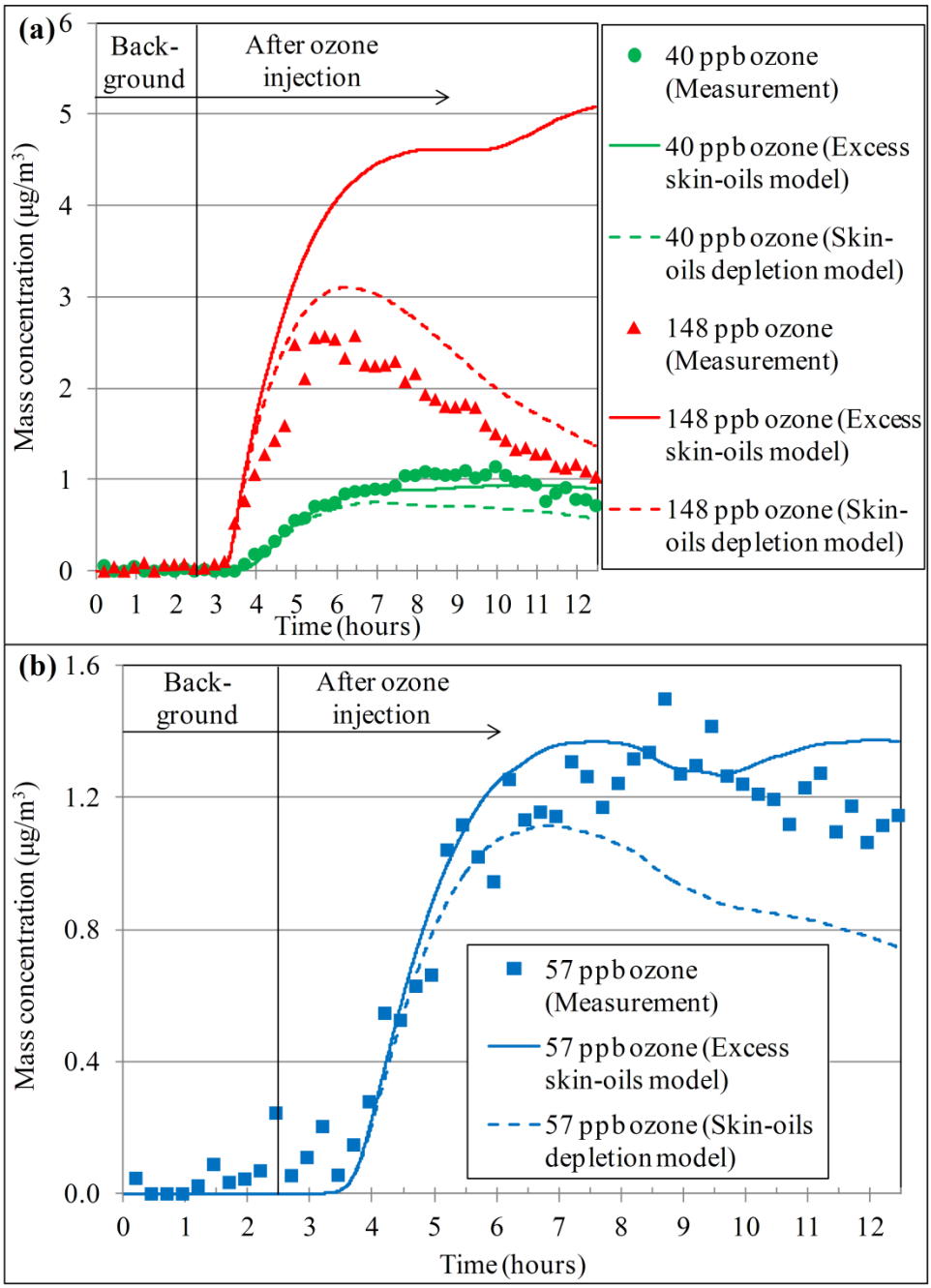

Figure 7.3. Comparisons of particle mass concentrations computed by the "excess skin-oils" and "skin-oils depletion" models with the corresponding measurements at (a) 40 ppb and 148 ppb ozone with 6 hours of T-shirt soiling, and (b) 57 ppb ozone with 12 hours of T-shirt soiling.

In the case of 57 ppb ozone (Case 3), the trends of the results for particle mass concentrations from both models were similar to those in the previous cases, as shown in

Figure 7.3(b). In this case, the T-shirt was soiled for 12 hours, as compared with 6 hours in the previous cases, which means that the quantity of skin-oils in the T-shirt was probably higher. Thus, the performance of the "excess skin-oils model" was somewhat better than that of the skin-oils depletion model, although it still slightly over-predicted the mass concentrations towards the end. We did not make comparisons for mass concentrations in the 22 ppb ozone (Case 1) because there were large uncertainties in the measurements of particle masses at this low ozone level.

Overall, the "skin-oils depletion" model seemed more suitable for simulating ozone-initiated particle generations from the soiled T-shirt over the human simulator because (1) its predictions of particle mass concentration agreed reasonably well with the measurements for all three cases analyzed, and (2) it correctly captured the decreasing trend of particle masses towards the end of the experiments, particularly in the case of 148 ppb ozone. However, it seems that the "excess skin-oils" model would be more appropriate for simulating particle generation with clothing worn by human beings, because the skin-oils would be replenished by human activities. The various discrepancies between the computed and measured values of mass concentration arose because (1) the T-shirt most likely did not contain the same amount of skin-oils in all cases, while the "skin-oils depletion" model assumed otherwise; and (2) the model assumed a first-order reaction between ozone and skin-oils, whereas the actual reaction is very complex.

Figure 7.4 compares the particle size distributions computed by the "skin-oils depletion" model with the corresponding measurements at an ozone concentration of 40 ppb (Case 2). The details of the particle generation, growth, and removal phenomena were provided in Chapter 4, and we briefly describe those results here for the purpose of comparison with model predictions.

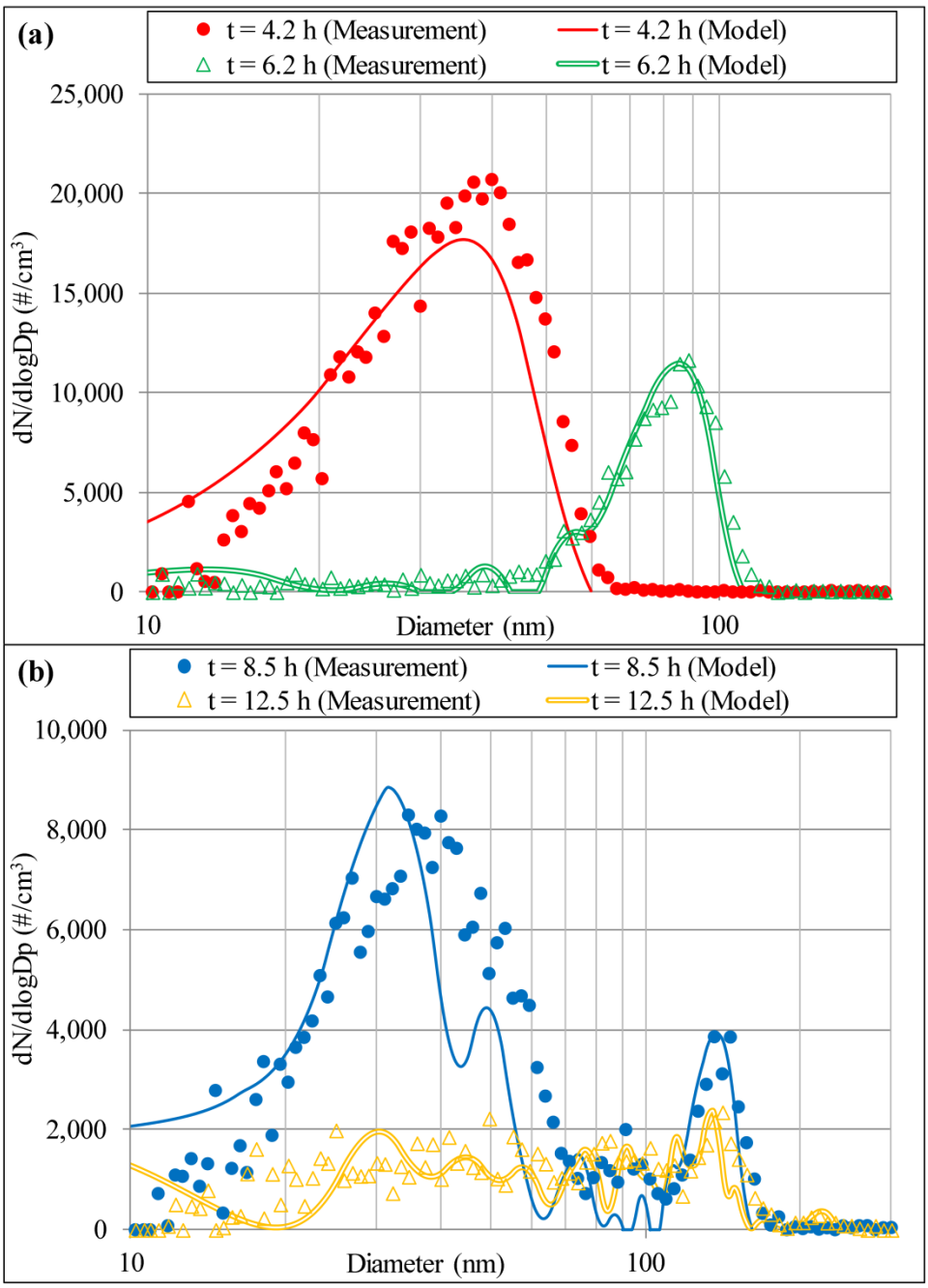

Figure 7.4. Comparisons of particle size distributions computed by the "skin-oils depletion" model with the corresponding measurements at an ozone concentration of 40 ppb for (a) t = 4.2 h and 6.2 h, and (b) t = 8.5 h and 12.5 h.

As shown in Figure 7.4(a), ozone-initiated particles were generated in the ultrafine region with a mode diameter of approximately 40 nm at t = 4.2 h, and this was predicted reasonably well by the model. At t = 6.2 h, the particle mode diameter shifted to 90 nm as

a result of condensational growth, and the number of particles was also depleted by ventilation and deposition losses; these phenomena were also well captured by the model. At t = 8.5 h, the particle size distribution was predominantly bimodal, with modes at 40 nm and 136 nm as shown in Figure 7.4(b). The former mode (40 nm) resulted from a secondary nucleation burst, and the latter (136 nm) was due to condensational growth of the original mode. The model predictions also showed two dominant modes and an overall good match with the measurements. From t = 8.5 h to 12.5 h, the particle concentrations decayed because of ventilation and deposition, and there were no obvious modes in the size distribution at t = 12.5 h. The model prediction also showed decay in particle concentrations, and the overall size distribution was again predicted reasonably well.

Evidently, the model captured the overall trend of particle generation, growth, and removal with good accuracy for the 40 ppb ozone case described above. The model performed slightly worse for the other cases (Cases 1, 3, and 4), but those predictions still compared well with their corresponding measurements. It should be emphasized that the model contained physical formulations for SVOC generation, condensation, and SVOC and particle deposition with few fitting parameters. Hence, these model formulations seemed reasonable, given the good agreement between model predictions and experimental measurements. However, the apparent nucleation rate was computed from the experimental data itself (i.e, the measured $N_{total,SMPS}(t)$), which was a big drawback in applying the model under new indoor conditions. Moreover, even if the $N_{total,SMPS}(t)$ were obtained through measurement, there would be no way to separate the contributions of particles generated from ozone/clothing reactions from those from other indoor sources. Therefore, it was desirable to incorporate a suitable nucleation model for simulating ozone-initiated particles without aid from experimental measurements, as discussed in the next subsection.

7.2.2 Nucleation Models

This section discusses the results obtained by using the different theoretical nucleation models described in Section 7.1.1.2: the activation, kinetic, and thermodynamic

nucleation models. We again used the “skin-oils depletion” model to compute the results for this section because its performance was found to be superior to that of the “excess skin-oils” model.

As discussed in 7.1.2, the modeling constants in the various nucleation models were chosen such that the peak of the particle number concentration (at t = 4.2 h) in the reference case (40 ppb ozone) was captured reasonably well. Thus, all the nucleation models provided a good prediction of the maximum particle concentration in the case of 40 ppb ozone, as shown in Figure 7.5(a). However, none of the nucleation models could effectively capture the steep decline in particle number from t = 4.2 h to t = 7.0 h and the subsequent secondary nucleation burst. In the case of 148 ppb ozone, the thermodynamic model over-predicted the peak particle concentration by about 30%, whereas the kinetic and activation models under-predicted it by about 10% and 40%, respectively, as shown Figure 7.5(b). Subsequently, all the models over-predicted the number concentrations, but the overall trend was better captured by the thermodynamic model than by the other two models.

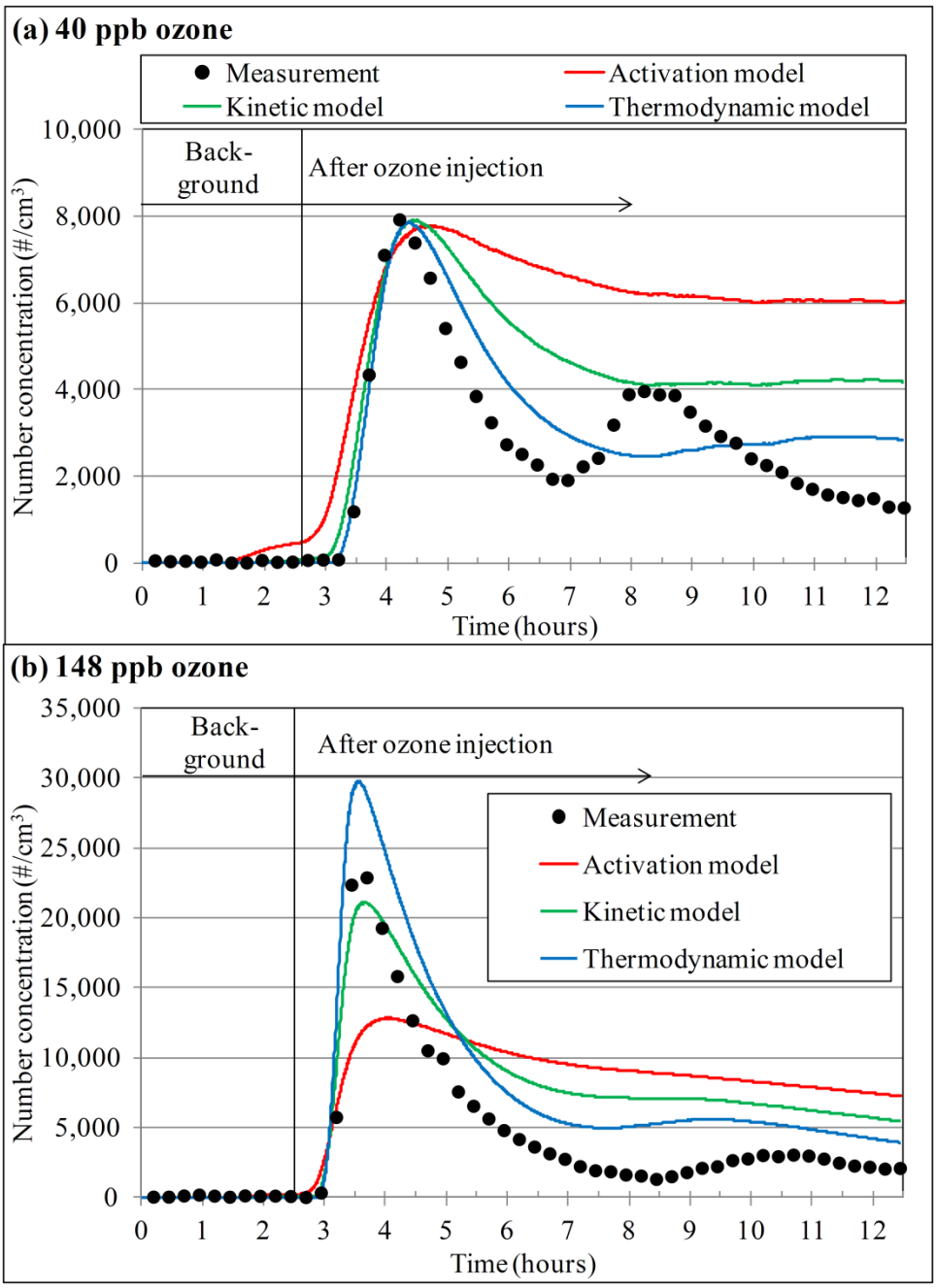

Figure 7.5. Comparisons of particle number concentrations computed by the different nucleation models with the corresponding measurements at an air change rate of 0.5 h^{-1} with (a) 40 ppb ozone and (b) 148 ppb ozone.

Figure 7.6 compares the particle number concentrations obtained by different nucleation models with their corresponding measurements for Cases 5 and 6 conducted at high air change rates with different ozone concentrations. In both cases, particle generation was

not measured. However, the different nucleation models generally predicted particle generation, as shown in Figures 7.6(a) and (b). In the case of 51 ppb ozone, the predictions of the thermodynamic model were the best, and those of the activation model were the worst. However, the opposite was true in the case of 133 ppb ozone. All the nucleation models failed overall in these cases, especially at the higher ozone concentration.

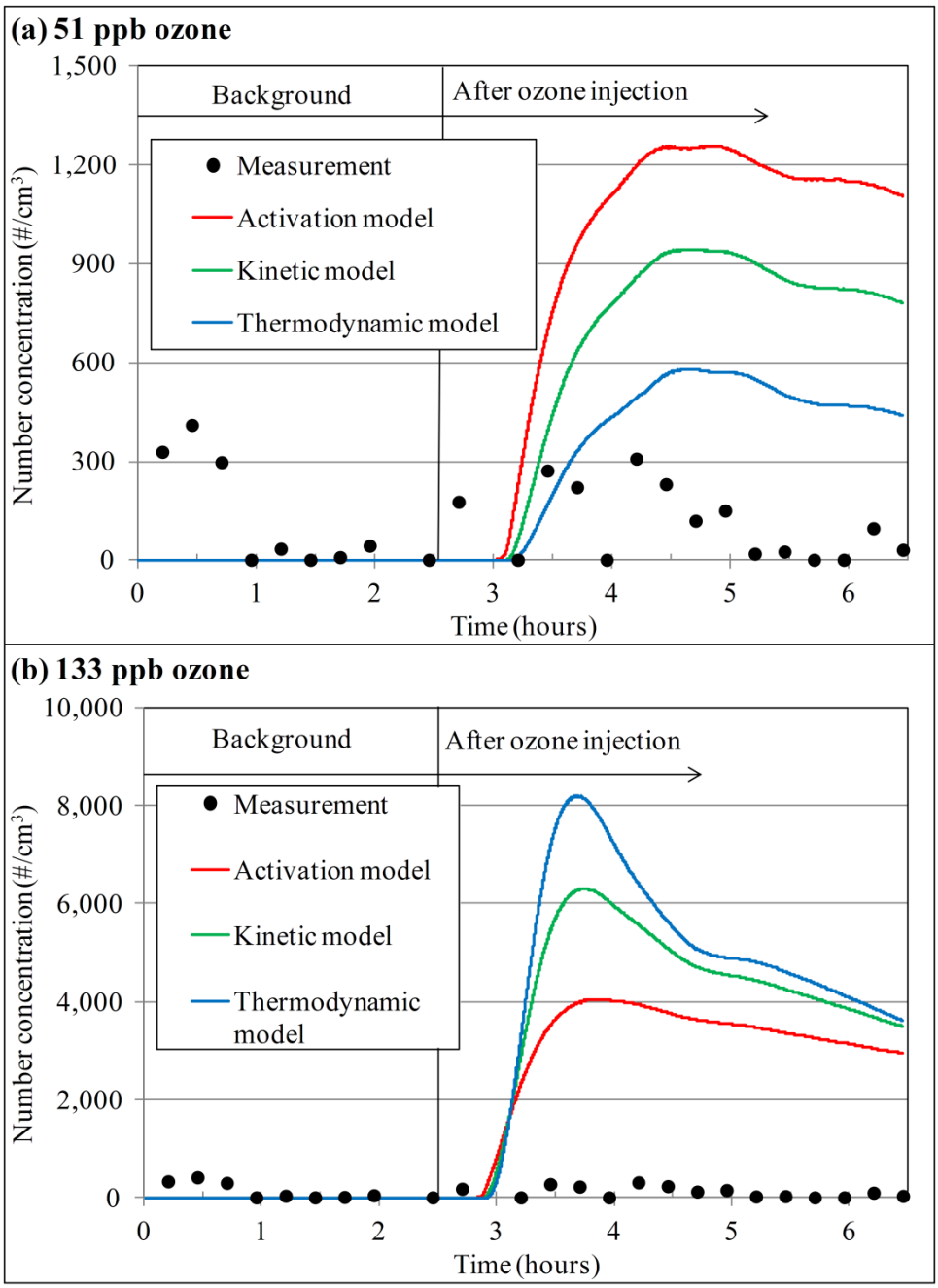

Figure 7.6. Comparisons of particle number concentrations computed by the different nucleation models with the corresponding measurements at an air change rate of 2.7 h^{-1} with (a) 51 ppb ozone and (b) 133 ppb ozone.

For Cases 1 and 3, all the nucleation models generally over-predicted the particle number concentrations. For example, the activation, kinetic, and thermodynamic models over-predicted the peak particle concentrations by about 400%, 260%, and 60%, respectively,

in Case 1; and by about 10%, 30%, and 40% in Case 3. By and large, the thermodynamic model performed the best, and the activation model performed the worst in these cases.

In contrast to the significantly different predictions obtained for number concentrations by the various nucleation models, the predicted mass concentrations were similar among the three models, as shown in Figure 7.7 for the 40 ppb and 148 ppb ozone cases. In all the other cases that were analyzed, the particle mass concentrations generally were not very sensitive to the choice of nucleation model. This result was reasonable because mass transfer from vapor to liquid particles is determined primarily by condensation, and nucleation plays a secondary role. The reasons for the discrepancies between the model predictions and measurements (as seen in Figure 7.7) were discussed previously and can be attributed to the assumptions used in the “skin-oils depletion” model.

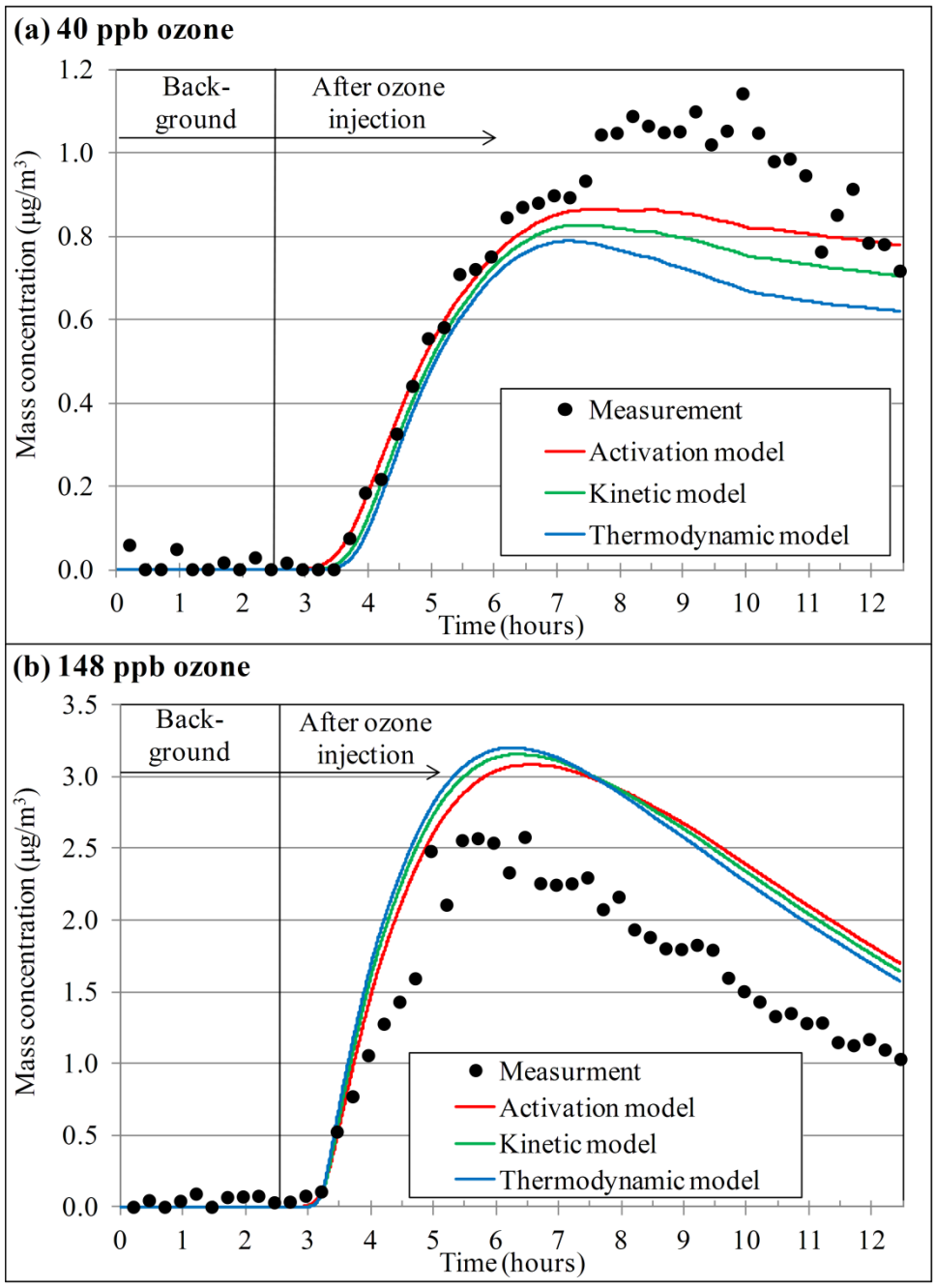

Figure 7.7. Comparisons of particle mass concentrations computed by the different nucleation models with the corresponding measurements at (a) 40 ppb ozone and (b) 148 ppb ozone.

Figure 7.8 compares the particle size distributions calculated by the different nucleation models with their corresponding measurements at several instants of time in the case of 40 ppb ozone. At t = 4.2 h, all the models predicted the particle size distributions

reasonably well, as shown in Figure 7.8(a). At t = 6.2 h, the predictions by the thermodynamic and kinetic model seem reasonable, but those by the activation model are quite poor when compared with the measurements. The model predictions become much worse at t = 8.5 h and 12.5 h, as shown in Figures 7.8(c) and (d), respectively, and none of the models could reasonably capture the secondary nucleation burst.

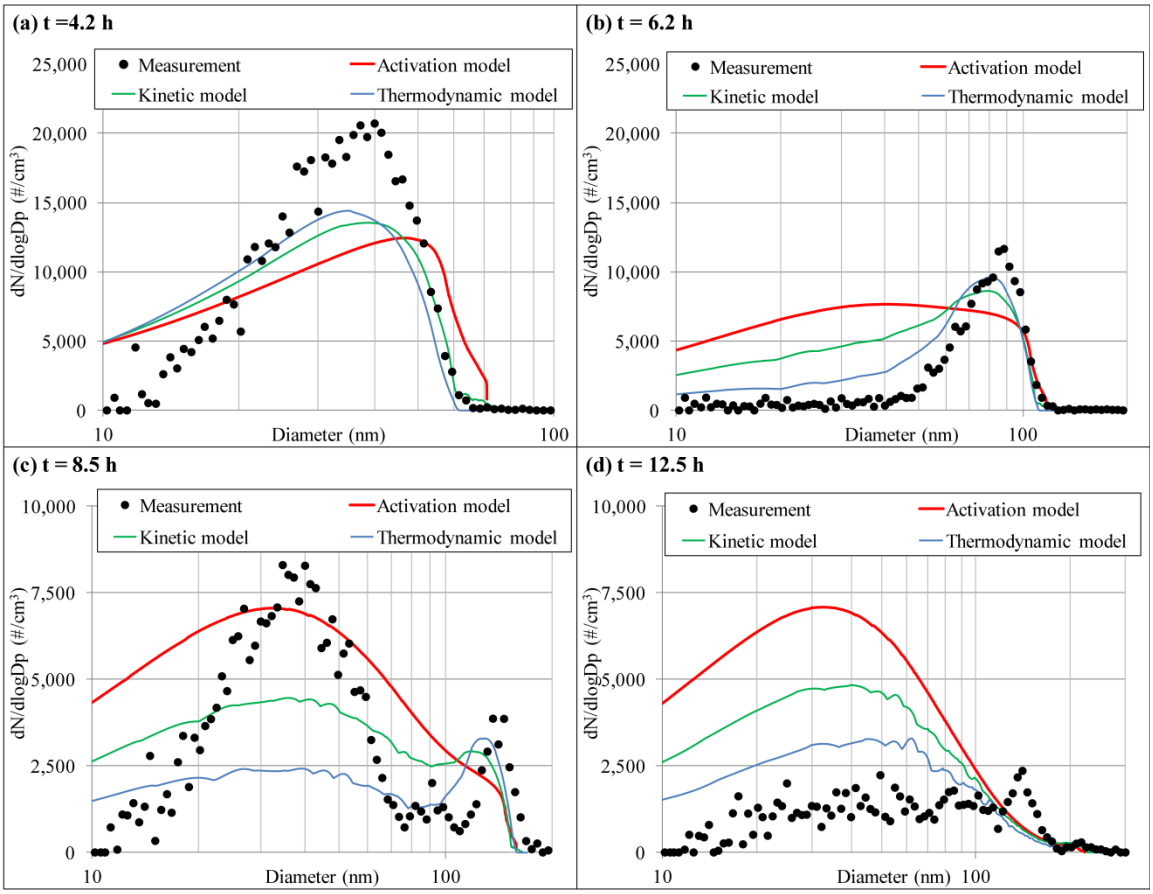

Figure 7.8. Comparisons of particle size distributions computed by the different nucleation models with the corresponding measurements at 40 ppb concentration for (a) t = 4.2 h, (b) t = 6.2 h, (c) t = 8.5 h, and (d) t = 12.5 h.

It was also illustrative to compare Figures 7.4 and 7.8 for identifying the differences between the results obtained from the apparent nucleation formulation and the various theoretical nucleation models. After the theoretical nucleation models were introduced in place of the apparent nucleation approach, the computed results showed significant deterioration when compared to the measurements. Therefore, an accurate nucleation

model is vital for correctly computing the size-resolved particle concentrations generated from ozone reactions with human-worn clothing.

In Cases 1, 3, and 4, the comparisons between particle size distributions predicted by the different nucleation models and their corresponding measurements were similar to the comparisons obtained in Case 2 (40 ppb ozone). In Cases 5 and 6, all the models predicted particle generation, but no generation was observed in the experiments. Hence, all the nucleation models failed in these two cases. The discrepancies can be attributed primarily to the unknown nucleation precursors and mechanism as well as the limitations of the different nucleation theories (Anisimov, 2003; Seinfeld and Pandis, 2006).

7.2.3 Ozone-initiated Particles under Different Indoor Environments

In spite of the disagreement between the model predictions and measurements, it was seen that the thermodynamic nucleation model worked reasonably well in five out of six cases. Hence, we used this model to simulate particle generation from ozone reactions with occupant's clothing in the following indoor settings: a classroom, office, and home as building environments, and Boeing 737-700 and Boeing 777 airliner cabins as airplane environments.

To compute ozone-initiated particle generation due to reactions with human clothing, we first studied a typical classroom with a volume of 182 m^3 occupied by 25 pupils and one teacher, as described in Fischer et al. (2013), under different air change rates. We assumed outdoor ozone concentrations of 50 ppb and 100 ppb, which represent clean and polluted environments, respectively. The outdoor-to-indoor ozone transport was calculated according to the mass balance model from Weschler (2000). We also analyzed the influence of background particles on the generation of new ozone-initiated particles by simulating conditions with and without background particles. It should be noted that background particles can significantly decrease the generation of new particles because the condensation of SVOC on background particles is more favorable than its nucleation. To generate a typical background particle profile, we utilized the study of Franck et al. (2003), which computed the average size distribution for indoor particles of outdoor

origin. That distribution was approximately lognormal with a total concentration of around 1450 #/cm^3 and mode diameter of about 100 nm. We utilized this representative distribution to compute an additional condensational sink for the SVOC vapor from Eq. (7.11) of 6.4 h^{-1} by assuming that the background particles remained unchanged.

Figure 7.9 shows the four-hour averaged UFP number concentrations computed for the classroom under two different outdoor ozone levels with and without background particles. Under all the conditions, the particle concentrations were quite low at the low air change rates because there was insufficient outdoor-to-indoor ozone transport to generate particles. The particle concentrations then increased with increasing ventilation rates due to higher indoor ozone concentrations, which led to higher particle generations. A further increase in ventilation rate led to a decrease in particle concentrations because the particle-forming precursors were quickly removed from the classroom.

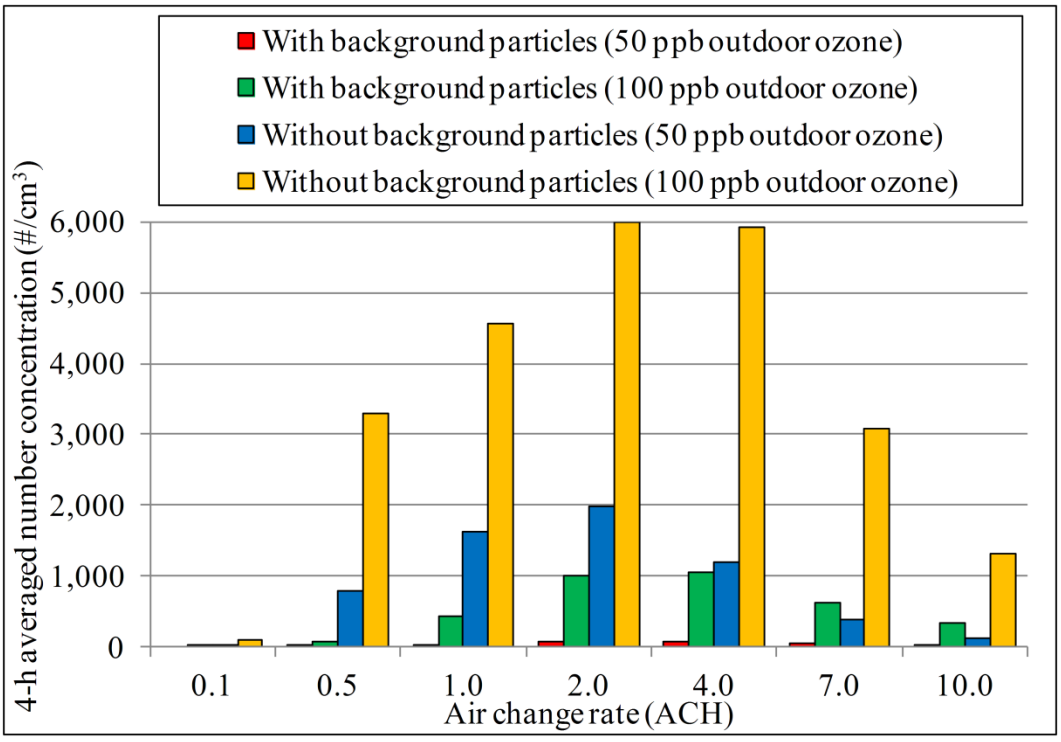

Figure 7.9. Four-hour averaged ultrafine particle number concentrations computed for a typical classroom under various air change rates for 50 and 100 ppb outdoor ozone conditions with and without background particles.

Figure 7.9 also shows that the particle concentrations were lowest in the presence of background particles at the 50 ppb outdoor ozone concentration under different air change rates. Under the same level of background particles, the concentrations of ozone-initiated particles increased as the outdoor ozone was increased from 50 to 100 ppb, as a result of the higher reaction rate. The ozone-initiated particle concentrations were much higher in the cases without background particles than in those with background particles under the same outdoor ozone conditions. Again, in those cases (without background particles) the particle concentrations increased with increasing ozone levels. Overall, the maximum particle generation was computed under high ozone concentrations and without pre-existing background particles.

In addition to classroom conditions, we also studied particle generation for typical office and home environments. These cases assumed the same conditions as in the classroom, except that there were four occupants in the office and two in the home. UFP generation in the office and home was much lower because the reduced occupancy resulted in lower ozone reactions, as shown in Figure 7.10 for 100 ppb outdoor ozone without background particles. Even under conditions that were favorable for new particle generation, the maximum UFP concentration was only 400 #/cm^3 for the office and 40 #/cm^3 for the home, obtained at an air change rate of 1 h^{-1}. Hence, it seems that such ozone-initiated particles would not be significant under low occupancy conditions.

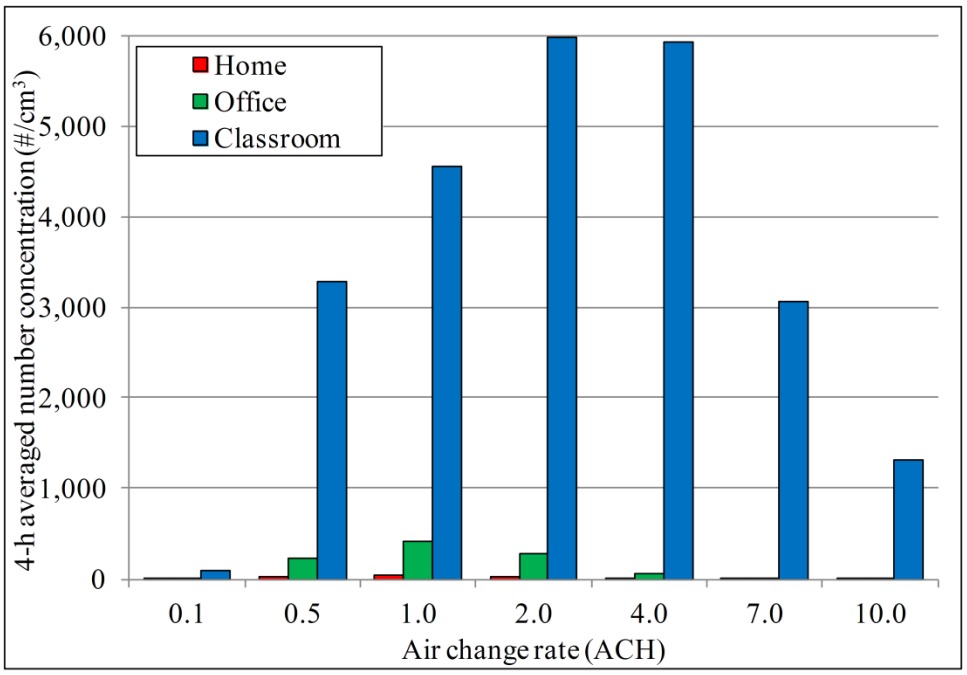

Figure 7.10. Four-hour averaged ultrafine particle number concentrations computed for different buildings under various air change rates for 100 ppb without background particles.

Since the ozone/clothing generated UFPs were found to be significant under high ozone and occupancy conditions without background particles, we also studied those particle generations in airliner cabins that usually have such conditions. This investigation simulated UFP generation from ozone/clothing reactions in a fully occupied Boeing-777 flight for a duration of 10 hours without background particles. The flight is typically trans-continental. The cabin ozone concentration was taken to be 50 ppb. It was predicted that the flight would have significant UFP generation, and the time-averaged particle concentration was computed as 6800 #/cm^3.

Next, we conducted a case study for a typical domestic flight of 1.5 hours. The flight was made by a partially occupied B737-700 airliner for which ozone-initiated UFP generation was recently measured by Spengler et al. (2012). The measured ozone and particle concentrations very quite low initially, as shown in Figure 7.11. After 15 minutes, the ozone concentration started to increase, and after another five minutes the particle concentrations also rose steeply. The particle concentration then remained steady

throughout the cruising portion of the flight. Finally, the ozone and particles decayed sharply during the descent. Figure 7.11 also shows the contributions of UFPs generated from ozone reactions with the passengers' clothing as computed by our model. These reactions can account for about 40% of the total UFPs measured. Obviously, other ozone-initiated mechanisms of particle generation must have prevailed, such as the reaction of ozone with various terpene-containing consumer products, but taking these reactions into account was beyond the scope of this investigation. Nevertheless, the model results indicate that ozone reaction with passengers' clothing could be a significant contributor of UFPs under typical airliner cabin conditions.

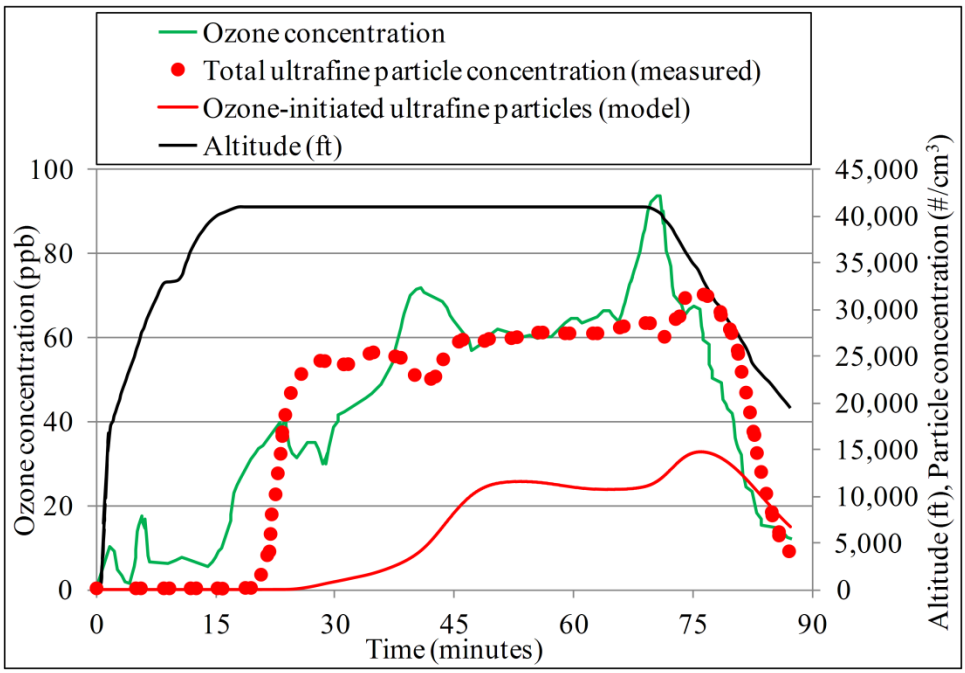

Figure 7.11. Measurements of the ozone-initiated UFPs in a Boeing 737-700 flight and the corresponding contributions by ozone reactions with passengers' clothing as computed by the model.

7.3 Conclusions

This chapter described numerical models to study particle generation from the reaction of ozone with human-worn clothing. The models were developed with the use of experimental measurements of particle generation in an environmental chamber and physical formulations for particle nucleation, growth, and removal mechanisms. The

models can predict size-resolved particle number concentrations, and they have provided insights into the overall particle-generation mechanism.

The particle size distributions predicted with the apparent nucleation formulation were in good agreement with the experimental data, in which the “nucleation rate” was directly estimated from the measured value of the total particle number concentration. However, the numerical models in combination with different theoretical nucleation models displayed significant discrepancies in predicting the particle size distributions because of some fundamental limitations of the nucleation models. Overall, the thermodynamic model based on the classical homogeneous nucleation theory provided the most reasonable predictions for five out of the six experimental cases.

Finally, the thermodynamic model was used to compute particle generation from ozone reactions with human-worn clothing in different building and airplane environments. The results show that ozone reactions could significantly contribute to UFP generation in high-occupancy spaces such as classrooms and airliner cabins. Ozone/clothing reactions may have accounted for about 40% of the UFPs measured in a Boeing 737-700 flight. However, their contributions to UFPs in office and home environments did not seem to be important because of the low occupant density.

CHAPTER 8. CONCLUSIONS AND FUTURE WORK

8.1 Conclusions

This research developed numerical models for computing the concentrations of ozone and its reaction byproducts (VOCs and particles) in the indoor environment and estimating the resulting exposure of occupants.

To develop these models, we first measured ozone consumption and ozone-initiated VOC emissions from ozone reactions with a T-shirt soiled with human skin oils in an environmental chamber. It was found that these ozone/T-shirt reactions consumed ozone and generated VOCs such as C6–C10 straight-chain saturated aldehydes, acetone, and 4-oxopentanal. The ozone reactions were significantly affected by the different factors that were studied (such as ozone concentration, humidity, soiling degree of the T-shirt, and air change rate). The total molar yield for most cases was 0.5, which means that for every two moles of ozone removed by the T-shirt surface, one mole of VOCs was produced.

We also examined the possibility of particle generation from the ozone/T-shirt reactions through the same chamber experiments. Particle generation was indeed observed from these reactions, and it was enhanced by the soiling of the T-shirt with human skin oils. Initially, the ozone reactions generated a burst of ultrafine particles (UFPs), and then the particles grew to larger sizes. Particle generation was also affected by the various factors that were studied, and ozone reactions with human clothing were identified as another potential source of indoor UFPs.

Next, this research developed modeling techniques for extending the experimental data to realistic indoor conditions. We first developed a CFD model for simulating the ozone distribution in an airliner cabin. The CFD model provided a reasonably good prediction

of the rate of ozone removal by the different reaction surfaces in the airliner cabin when compared with their corresponding measurements. The CFD results also indicated that the ozone is depleted by about 10% in the breathing zone of passengers as compared to its concentration in the bulk cabin air because of its reactions with human skin and clothing. Hence, the ozone concentration in the breathing zone should be used for assessing the exposure of airliner passengers.

We subsequently developed models for computing the ozone-initiated secondary emissions of acetone, 4-oxopentanal (4-OPA), nonanal, and decanal from reactions with human-worn clothing in an aircraft cabin. We developed empirical equations to compute secondary VOC emissions from the prevailing environmental conditions (such as ozone concentration, humidity, and air change rate) on the basis of our chamber measurements. These models were then used in a mass balance analysis to compute the contributions of human surfaces (skin, hair, and clothing) to ozone-initiated VOCs in an aircraft cabin mockup for three different cases. The model predictions showed some discrepancies when compared with the corresponding measurements because of the limited dataset used to develop the model as well as the many complexities of the cabin mockup. Nevertheless, the models were useful for computing rough estimates of ozone-initiated VOCs from the given indoor conditions. The VOC emission models were also integrated into a CFD model, and the breathing zone concentrations of different VOCs were computed for passengers seated in various locations in an occupied cabin mockup. It was found that the various VOCs were enriched in the breathing zone by about 10%–50% when compared with their corresponding exhaust concentrations. Therefore, it was recommended that the concentrations of ozone-initiated VOCs in the breathing zone be used for assessing the exposure of airliner passengers.

This investigation also developed a numerical model to study particle generation from ozone reactions with human-worn clothing. The model was developed on the basis of our chamber measurements of particle generation and contained physical formulations for particle nucleation, growth, and removal mechanisms. The model was capable of predicting size-resolved particle number concentrations and provided insights into the

overall particle generation mechanism. Finally, the model was used to compute particle generation from ozone reactions with human-worn clothing in different indoor environments, keeping in mind that these results need to be further validated because of the limitations of the nucleation model that was used. It was predicted that such ozone reactions could significantly contribute to UFP generation in high-occupancy settings such as classrooms and airliner cabins. It was also shown that ozone/clothing reactions may have accounted for about 40% of the UFPs measured in a Boeing 737-700 flight. However, their contributions to UFPs in office and home environments did not seem to be significant because of the lower occupant densities of these environments.

8.2 Future Work

This investigation provided a number of insights into ozone reactions with human-worn clothing occurring in the indoor environment. However, many research questions remain unanswered and should be explored in future work.

We conducted chamber experiments to quantify the ozone consumption and ozone-initiated VOC emissions from reactions with a cotton T-shirt under various conditions. However, we did not characterize the influence of clothing fabric (e.g. wool, polyester, etc.), garment type (e.g. trousers, outerwear, etc.), or the human subjects themselves on the ozone reactions. It is hypothesized that these factors would significantly alter the ozone-initiated VOC and particle generation, which should be further explored though additional chamber experiments. Such experiments would also generate more data for improving the empirical models developed for computing ozone-initiated VOC emissions.

Our chamber experiments measured particle generation from ozone/clothing reactions, and we also developed numerical models to compute the concentrations ozone-initiated particles under realistic indoor conditions. The results of our model indicated that these ozone reactions are potential sources of UFPs in densely occupied indoor environments such as classrooms and aircraft cabins. However, our results need to be substantiated by measuring UFPs in real or simulated indoor settings with and without occupants.

A fundamental difficulty in modeling particle generation from ozone/clothing reactions was that the nucleation mechanism was unknown, and none of the tested nucleation models could predict the nucleation rates with reasonably good accuracy. Future research into the nucleation mechanism may help to better understand and predict particle generation in the indoor environment.

LIST OF REFERENCES

LIST OF REFERENCES

Anderson, S.E., Franko, J., Jackson, L.G., Wells, J.R., Ham, J.E., Meade, B.J., 2012. Irritancy and allergic responses induced by exposure to the indoor air chemical 4-oxopentanal. Toxicol. Sci. 127, 371–381.

Anisimov, M.P., 2003. Nucleation: theory and experiment. Russ. Chem. Rev. 72, 591–628.

ASHRAE (American Society of Heating, Refrigerating and Air-Conditioning Engineers, Inc.), 2009a. ASHRAE handbook fundamentals.

ASHRAE (American Society of Heating, Refrigerating and Air-Conditioning Engineers, Inc.), 2009b. Practice for selection of sorbents, sampling, and thermal desorption analysis procedures for volatile organic compounds in air.

ASHRAE (American Society of Heating, Refrigerating and Air-Conditioning Engineers, Inc.), 2009c. Test method for determination of formaldehyde and other carbonyl compounds in air (active sampler methodology).

Bell, M.L., Dominici, F., Samet, J.M., 2005. A meta-analysis of time-series studies of ozone and mortality with comparison to the national morbidity, mortality, and air pollution study. Epidemiology 16, 436–445.

Bell, M.L., McDermott, A., Zeger, S.L., Samet, J.M., Dominici, F., 2004. Ozone and short-term mortality in 95 US urban communities, 1987-2000. JAMA-J. Am. Med. Assoc. 292, 2372–2378.

Bell, M.L., Peng, R.D., Dominici, F., 2006. The exposure–response curve for ozone and risk of mortality and the adequacy of current ozone regulations. Environ. Health Perspect. 114, 532–536.

Bhangar, S., Cowlin, S.C., Singer, B.C., Sextro, R.G., Nazaroff, W.W., 2008. Ozone levels in passenger cabins of commercial aircraft on North American and transoceanic routes. Environ. Sci. Technol. 42, 3938–3943.

Brown, S.K., Sim, M.R., Abramson, M.J., Gray, C.N., 1994. Concentrations of volatile organic compounds in indoor air – a review. Indoor Air 4, 123–134.

Cano-Ruiz, J.A., Kong, D., Balas, R.B., Nazaroff, W.W., 1993. Removal of reactive gases at indoor surfaces: combining mass transport and surface kinetics. Atmos. Environ. A-Gen. 27A, 2039–2050.

Carslaw, N., Langer, S., Wolkoff, P., 2009. New directions: where is the link between reactive indoor air chemistry and health effects? Atmos. Environ. 43, 3808–3809.

Cogliano, V.J., Grosse, Y., Baan, R.A., Straif, K., Secretan, M.B., Ghissassi, F.E., the working group for volume 88, 2005. Meeting report: summary of IARC monographs on formaldehyde, 2-butoxyethanol, and 1-tert-butoxy-2-propanol. Environ. Health Perspect. 113, 1205–1208.

Coleman, B.K., Destaillats, H., Hodgson, A.T., Nazaroff, W.W., 2008a. Ozone consumption and volatile byproduct formation from surface reactions with aircraft cabin materials and clothing fabrics. Atmos. Environ. 42, 642–654.

Coleman, B.K., Lunden, M.M., Destaillats, H., Nazaroff, W.W., 2008b. Secondary organic aerosol from ozone-initiated reactions with terpene-rich household products. Atmos. Environ. 42, 8234–8245.

Destaillats, H., Lunden, M.M., Singer, B.C., Coleman, B.K., Hodgson, A.T., Weschler, C.J., Nazaroff, W.W., 2006. Indoor secondary pollutants from household product emissions in the presence of ozone: a bench-scale chamber study. Environ. Sci. Technol. 40, 4421–4428.

Dominici, F., Peng, R.D., Bell, M.L., Pham, L., McDermott, A., Zeger, S.L., Samet, J.M., 2006. Fine particulate air pollution and hospital admission for cardiovascular and respiratory diseases. JAMA-J. Am. Med. Assoc. 295, 1127–1134.

Donaldson, K., Li, X.Y., MacNee, W., 1998. Ultrafine (nanometre) particle mediated lung injury. J. Aerosol Sc. 29, 553–560.

Donaldson, K., Stone, V., Clouter, A., Renwick, L., MacNee, W., 2001. Ultrafine particles. Occup. Environ. Med. 58, 211–216.

Dua, S.K., Hopke, P.K., 1996. Hygroscopic growth of assorted indoor aerosols. Aerosol Sci. Tech. 24, 151–160.

EPA (U.S. Environmental Protection Agency), 2006. Air quality criteria for ozone and related photochemical oxidants (final).

EPA (U.S. Environmental Protection Agency), 2008. Final ozone NAAQS regulatory impact analysis.

EPA (U.S. Environmental Protection Agency), 2012. Ozone and your patients' health training for health care providers.

FAA (Federal Aviation Administration), 2013. FAA aerospace forecast fiscal years 2013-2033.

Fadeyi, M.O., Weschler, C.J., Tham, K.W., Wu, W.Y., Sultan, Z.M., 2013. Impact of human presence on secondary organic aerosols derived from ozone-initiated chemistry in a simulated office environment. Environ. Sci. Technol. 47, 3933–3941.

Fenske, J.D., Paulson, S.E., 1999. Human breath emissions of VOCs. J. Air Waste Manag. Assoc. 49, 594–598.

Fischer, A., Ljungström, E., Langer, S., 2013. Ozone removal by occupants in a classroom. Atmos. Environ. 81, 11–17.

FLUENT, 2009. ANSYS FLUENT 12.0 Theory Guide.

Franck, U., Herbarth, O., Wehner, B., Wiedensohler, A., Manjarrez, M., 2003. How do the indoor size distributions of airborne submicron and ultrafine particles in the absence of significant indoor sources depend on outdoor distributions? Indoor Air 13, 174–181.

Fuchs, N.A., Sutugin, A.G., 1971. Topics in current aerosol research. Pergamon, New York.

Hubbell, B.J., Hallberg, A., McCubbin, D.R., Post, E., 2005. Health-related benefits of attaining the 8-hr ozone standard. Environ. Health Perspect. 113, 73–82.

Hussein, T., Hruška, A., Dohányosová, P., Džumbová, L., Hemerka, J., Kulmala, M., Smolík, J., 2009. Deposition rates on smooth surfaces and coagulation of aerosol particles inside a test chamber. Atmos. Environ. 43, 905–914.

Ito, K., De Leon, S.F., Lippmann, M., 2005. Associations between ozone and daily mortality. Epidemiology 16, 446–457.

Ito, K., Harashima, H., 2008. Fundamental chamber experiment on indoor secondary aerosol derived from ozone/VOC reactions. Journal of Asian Architecture and Building Engineering 7, 419–425.

Ito, K., Harashima, H., 2011. Coupled CFD analysis of size distributions on indoor secondary organic aerosol derived from ozone/limonene reactions. Build. Environ. 46, 711–718.

Jones, A.P., 1999. Indoor air quality and health. Atmos. Environ. 33, 4535–4564.

Kagi, N., Fujii, S., Tamura, H., Namiki, N., 2009. Secondary VOC emissions from flooring material surfaces exposed to ozone or UV irradiation. Build. Environ. 44, 1199–1205.

Kerminen, V.-M., Kulmala, M., 2002. Analytical formulae connecting the “real” and the “apparent” nucleation rate and the nuclei number concentration for atmospheric nucleation events. J. Aerosol Sc. 33, 609–622.

Klepeis, N.E., Nelson, W.C., Ott, W.R., Robinson, J.P., Tsang, A.M., Switzer, P., Behar, J.V., Hern, S.C., Engelmann, W.H., 2001. The national human activity pattern survey (NHAPS): a resource for assessing exposure to environmental pollutants. J. Expo. Anal. Env. Epid. 11, 231.

Kostiainen, R., 1995. Volatile organic compounds in the indoor air of normal and sick houses. Atmos. Environ. 29, 693–702.

Kulmala, M., 1988. Nucleation as an aerosol physical problem (Ph.D. thesis). University of Helsinki, Helsinki, Finland.

Kulmala, M., Lehtinen, K.E.J., Laaksonen, A., 2006. Cluster activation theory as an explanation of the linear dependence between formation rate of 3nm particles and sulphuric acid concentration. Atmos. Chem. Phys. 6, 787–793.

Kulmala, M., Maso, M.D., Mäkelä, J.M., Pirjola, L., Väkevä, M., Aalto, P., Miikkulainen, P., Hämeri, K., O'dowd, C.D., 2001. On the formation, growth and composition of nucleation mode particles. Tellus B 53, 479–490.

Kumar, S., Ramkrishna, D., 1997. On the solution of population balance equations by discretization—III. Nucleation, growth and aggregation of particles. Chem. Eng. Sci. 52, 4659–4679.

Lai, A.C.K., Nazaroff, W.W., 2000. Modeling indoor particle deposition from turbulent flow onto smooth surfaces. J. Aerosol Sc. 31, 463–476.

Lee, K., Vallarino, J., Dumyahn, T., Ozkaynak, H., Spengler, J.D., 1999. Ozone decay rates in residences. J. Air Waste Manag. Assoc. 49, 1238–1244.

Leungsakul, S., Jaoui, M., Kamens, R.M., 2005. Kinetic mechanism for predicting secondary organic aerosol formation from the reaction of d-limonene with ozone. Environ. Sci. Technol. 39, 9583–9594.

Levy, J.I., Chemerynski, S.M., Sarnat, J.A., 2005. Ozone exposure and mortality. Epidemiology 16, 458–468.

Liu, L.-J.S., Olson, M.P., Allen, G.A., Koutrakis, P., McDonnell, W.F., Gerrity, T.R., 1994. Evaluation of the harvard ozone passive sampler on human subjects indoors. Environ. Sci. Technol. 28, 915–923.

Long, C.M., Suh, H.H., Koutrakis, P., 2000. Characterization of indoor particle sources using continuous mass and size monitors. J. Air Waste Manag. Assoc. 50, 1236–1250.

Lushnikov, A.A., 2010. Condensation, evaporation, nucleation. In: Agranovski, I. (Ed.), Aerosols - Science and Technology. Wiley-VCH Verlag GmbH & Co. KGaA, pp. 91–126.

Morawska, L., He, C., Johnson, G., Guo, H., Uhde, E., Ayoko, G., 2009. Ultrafine particles in indoor air of a school: possible role of secondary organic aerosols. Environ. Sci. Technol. 43, 9103–9109.

Morrison, G., 2008. Interfacial chemistry in indoor environments. Environ. Sci. Technol. 42, 3495–3499.

Morrison, G.C., Nazaroff, W.W., 2000. The rate of ozone uptake on carpets: experimental studies. Environ. Sci. Technol. 34, 4963–4968.

Morrison, G.C., Nazaroff, W.W., 2002. Ozone interactions with carpet: secondary emissions of aldehydes. Environ. Sci. Technol. 36, 2185–2192.

Nazaroff, W.W., Weschler, C.J., 2010. Ozone in passenger cabins: concentrations and chemistry (Final Report).

NRC, 2002. The airliner cabin environment and the health of passengers and crew. National Academies Press.

Pandrangi, L.S., Morrison, G.C., 2008. Ozone interactions with human hair: ozone uptake rates and product formation. Atmos. Environ. 42, 5079–5089.

Patankar, S.V., 1980. Numerical heat transfer and fluid flow. Taylor & Francis.

Peters, A., Wichmann, H.E., Tuch, T., Heinrich, J., Heyder, J., 1997. Respiratory effects are associated with the number of ultrafine particles. Am. J. Respir. Crit. Care Med. 155, 1376–1383.

Pope, C.A., 2000. Review: epidemiological basis for particulate air pollution health standards. Aerosol Sc. & Tech. 32, 4–14.

Pope, C.A., Dockery, D.W., 2006. Health effects of fine particulate air pollution: lines that connect. J. Air Waste Manag. Assoc. 56, 709–742.

Reiss, R., Ryan, P.B., Koutrakis, P., Tibbetts, S.J., 1995. Ozone reactive chemistry on interior latex paint. Environ. Sci. Technol. 29, 1906–1912.

Rim, D., Novoselec, A., Morrison, G., 2009. The influence of chemical interactions at the human surface on breathing zone levels of reactants and products. Indoor Air 19, 324–334.

Rogge, W.F., Mazurek, M.A., Hildemann, L.M., Cass, G.R., Simoneit, B.R.T., 1993. Quantification of urban organic aerosols at a molecular level: identification, abundance and seasonal variation. Atmos. Environ. A-Gen. 27, 1309–1330.

Russo, J., Khalifa, H.E., 2010. CFD analysis of personal ventilation with volumetric chemical reactions. HVAC&R Res. 16, 799–812.

Russo, J., Khalifa, H.E., 2011. Surface reactions on the human body: using personal ventilation to remove squalene oxidation products from the breathing zone with CFD. Presented at the 12th International Conference on Indoor Air Quality and Climate, Indoor Air Austin, TX, USA.

Sarwar, G., Corsi, R., 2007. The effects of ozone/limonene reactions on indoor secondary organic aerosols. Atmos. Environ. 41, 959–973.

Sarwar, G., Corsi, R., Allen, D., Weschler, C., 2003. The significance of secondary organic aerosol formation and growth in buildings: experimental and computational evidence. Atmos. Environ. 37, 1365–1381.

Sarwar, G., Olson, D.A., Corsi, R.L., Weschler, C.J., 2004. Indoor fine particles: the role of terpene emissions from consumer products. J. Air Waste Manag. Assoc. 54, 367–377.

Seaton, A., Godden, D., MacNee, W., Donaldson, K., 1995. Particulate air pollution and acute health effects. The Lancet 345, 176–178.

Seinfeld, J.H., Pandis, S.N., 2006. Atmospheric chemistry and physics: from air pollution to climate change. John Wiley & Sons.

Singer, B.C., Coleman, B.K., Destaillats, H., Hodgson, A.T., Lunden, M.M., Weschler, C.J., Nazaroff, W.W., 2006. Indoor secondary pollutants from cleaning product and air freshener use in the presence of ozone. Atmos. Environ. 40, 6696–6710.

Sioutas, C., Delfino, R.J., Singh, M., 2005. Exposure assessment for atmospheric ultrafine particles (UFPs) and implications in epidemiologic research. Environ. Health Perspect. 113, 947–955.

Sørensen, D.N., Weschler, C.J., 2002. Modeling-gas phase reactions in indoor environments using computational fluid dynamics. Atmos. Environ. 36, 9–18.

Spengler, J.D., Ludwig, S., Weker, R.A., 2004. Ozone exposures during trans-continental and trans-pacific flights. Indoor Air 14, 67–73.

Spengler, J.D., Vallarino, J., McNeely, E., Estephan, H., 2012. In-flight/onboard monitoring: ACER's component for ASHRAE 1262, Part 2.

Strøm-Tejsen, P., Weschler, C.J., Wargocki, P., Myśków, D., Zarzycka, J., 2008. The influence of ozone on self-evaluation of symptoms in a simulated aircraft cabin. J. Expo. Sci. Env. Epid. 18, 272–281.

Tamás, G., Weschler, C.J., Bako-Biro, Z., Wyon, D.P., Strøm-Tejsen, P., 2006. Factors affecting ozone removal rates in a simulated aircraft cabin environment. Atmos. Environ. 40, 6122–6133.

Turpin, B.J., Lim, H.-J., 2001. Species contributions to PM2.5 mass concentrations: revisiting common assumptions for estimating organic mass. Aerosol Sci. Tech. 35, 602–610.

Vartiainen, E., Kulmala, M., Ruuskanen, T.M., Taipale, R., Rinne, J., Vehkamäki, H., 2006. Formation and growth of indoor air aerosol particles as a result of d-limonene oxidation. Atmos. Environ. 40, 7882–7892.

Wallace, L., Ott, W., 2011. Personal exposure to ultrafine particles. J. Expo. Sci. Env. Epid. 21, 20–30.

Wang, C., Waring, M.S., 2014. Secondary organic aerosol formation initiated from reactions between ozone and surface-sorbed squalene. Atmos. Environ. 84, 222–229.

Wang, H., Morrison, G., 2010. Ozone-surface reactions in five homes: surface reaction probabilities, aldehyde yields, and trends. Indoor Air 20, 224–234.

Wang, H., Morrison, G.C., 2006. Ozone-initiated secondary emission rates of aldehydes from indoor surfaces in four homes. Environ. Sci. Technol. 40, 5263–5268.

Waring, M.S., Siegel, J.A., 2013. Indoor secondary organic aerosol formation initiated from reactions between ozone and surface-sorbed d-Limonene. Environ. Sci. Technol. 47, 6341–6348.

Weisel, C.P., Weschler, C.J., Mohan, K.R., Vallarino, J., Spengler, J.D., 2013. Ozone and ozone by-products in the cabins of commercial aircraft. Environ. Sci. Technol.

Weschler, C.J., 2000. Ozone in indoor environments: concentration and chemistry. Indoor Air 10, 269–288.

Weschler, C.J., 2004. New directions: ozone-initiated reaction products indoors may be more harmful than ozone itself. Atmos. Environ. 38, 5715–5716.

Weschler, C.J., 2006. Ozone's impact on public health: contributions from indoor exposures to ozone and products of ozone-initiated chemistry. Environ. Health Perspect. 114, 1489–1496.

Weschler, C.J., 2011. Chemistry in indoor environments: 20 years of research. Indoor Air 21, 205–218.

Weschler, C.J., Nazaroff, W.W., 2008. Semivolatile organic compounds in indoor environments. Atmos. Environ. 42, 9018–9040.

Weschler, C.J., Shields, H.C., 1997. Potential reactions among indoor pollutants. Atmos. Environ. 31, 3487–3495.

Weschler, C.J., Shields, H.C., 1999. Indoor ozone/terpene reactions as a source of indoor particles. Atmos. Environ. 33, 2301–2312.

Weschler, C.J., Shields, H.C., 2000. The influence of ventilation on reactions among indoor pollutants: modeling and experimental observations. Indoor Air 10, 92–100.

Weschler, C.J., Shields, H.C., 2003. Experiments probing the influence of air exchange rates on secondary organic aerosols derived from indoor chemistry. Atmos. Environ. 37, 5621–5631.

Weschler, C.J., Wisthaler, A., Cowlin, S., Tamás, G., Strøm-Tejsen, P., Hodgson, A.T., Destaillats, H., Herrington, J., Zhang, J., Nazaroff, W.W., 2007. Ozone-initiated chemistry in an occupied simulated aircraft cabin. Environ. Sci. Technol. 41, 6177–6184.

Wisthaler, A., Tamás, G., Wyon, D.P., Strøm-Tejsen, P., Space, D., Beauchamp, J., Hansel, A., Märk, T.D., Weschler, C.J., 2005. Products of ozone-initiated chemistry in a simulated aircraft environment. Environ. Sci. Technol. 39, 4823–4832.

Wisthaler, A., Weschler, C.J., 2010. Reactions of ozone with human skin lipids: sources of carbonyls, dicarbonyls, and hydroxycarbonyls in indoor air. P. Natl. Acad. Sci. USA 107, 6568–6575.

Yakhot, V., Orszag, S.A., 1986. Renormalization group analysis of turbulence. J. Sci. Comput. 1, 3–51.

Zhang, Z., Chen, X., Mazumdar, S., Zhang, T., Chen, Q., 2009. Experimental and numerical investigation of airflow and contaminant transport in an airliner cabin mockup. Build. Environ. 44, 85–94.

APPENDICES

Appendix A. Experimental Data for the VOC measurements

Table A.1. VOC concentrations measured during the ozone reactions with clothing in Chapter 3.

Case	Chamber condition	Formal-dehyde (ppb)	Acetal-dehyde (ppb)	C6–C8 aldehydes (ppb)	Nonanal (ppb)	Decanal (ppb)	Acetone (ppb)	4-OPA (ppb)
1	background	0.0	0.7	0.6	1.1	2.3	4.9	0.1
	with ozone	2.7	2.1	0.9	1.9	2.8	2.4	0.3
2	background	2.5	2.7	0.3	1.1	2.0	9.2	0.0
	with ozone	4.5	2.1	2.6	6.8	15.7	6.8	1.5
3	background	1.1	0.4	0.4	1.3	1.5	4.0	0.0
	with ozone	4.8	2.5	2.8	9.0	9.6	15.2	7.2
4	background	1.7	1.7	0.4	0.9	1.5	7.7	0.1
	with ozone	15.9	3.1	11.6	19.9	38.4	20.9	19.3
5	background	2.6	0.9	1.3	2.4	4.0	3.2	0.3
	with ozone	4.6	2.3	14.4	25.6	54.1	19.2	19.6
6	background	3.0	1.3	0.9	2.1	4.6	5.0	0.0
	with ozone	8.2	3.5	12.0	19.9	37.5	13.5	14.7
7	background	0.8	4.0	1.6	3.2	7.9	6.5	0.6
	with ozone	6.1	2.5	11.7	18.3	38.1	17.4	21.1
8	background	1.8	2.0	1.6	2.6	5.7	6.3	0.4
	with ozone	4.4	4.6	13.0	21.7	40.3	19.8	20.6
9	background	0.7	0.2	1.0	1.2	2.0	6.6	0.0
	with ozone	1.2	1.1	1.0	2.7	3.7	5.4	0.8
10	background	0.0	1.0	0.1	0.3	0.4	5.5	0.0
	with ozone	2.4	2.0	1.2	2.2	3.2	13.0	3.0
11	background	0.7	2.1	0.5	0.9	1.8	2.9	0.1
	with ozone	3.5	3.0	3.7	7.9	12.1	13.9	5.6
12	background	2.2	1.8	0.6	2.0	4.5	4.6	0.0
	with ozone	2.5	2.8	3.9	6.6	14.3	12.7	9.6
13	background	4.4	1.6	2.1	3.5	7.6	4.2	0.4
	with ozone	6.2	2.4	6.8	12.0	18.2	12.8	9.3
3D	background	2.5	2.3	0.6	1.8	2.5	3.3	0.0
	with ozone	4.7	1.9	2.7	7.4	10.6	13.1	6.1
10D	background	0.0	1.3	0.5	1.0	2.2	3.0	1.3
	with ozone	2.3	1.8	1.4	2.5	4.0	9.8	1.8

Appendix B. Particle Generation and Growth

As discussed in Chapter 4, the generation of new particles by nucleation versus particle growth by condensation depends on the surface area of existing particles. A low particle surface area concentration in the chamber favored generation of new particles (by nucleation), whereas a high surface area concentration favored particle growth (by condensation). To illustrate this, the variations of particle number and surface area concentrations with time are shown in Figure B.1 for Case 3. As shown in the figure, initially the particle surface area concentration was very low and facilitated a huge primary burst (t = 3.4 h) of ultrafine particles from the ozone reactions. The surface area concentration then increased until about t = 6.0 h due to particle generation and growth. Then, from t = 6.0 h to t = 7.5 h, the surface area concentration decreased, which probably led to the secondary burst of particles by nucleation at t = 7.2 h since insufficient surface area was available for particle growth by condensation. Finally the particle number and area concentrations decayed till the end of the experiment, probably due to a reduction in ozone-initiated particle generations because of depletion of skin-oils from the T-shirt.

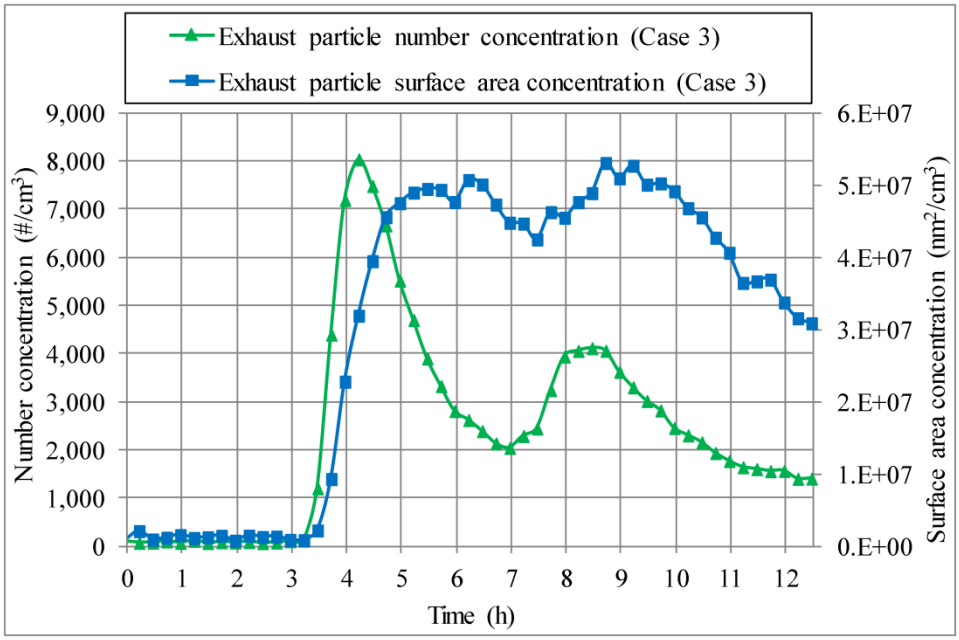

Figure B.1. Particle number and surface area concentrations in Case 3.

Figure B.2 compares the surface area concentrations in Cases 3 (12% RH) with that in Case 5 (44% RH). The particle surface areas were much higher in Case 5 probably due to hygroscopic growth of particles at high humidity conditions. The high surface areas in Case 5 favored condensation over nucleation and reduced the secondary burst of particles in Case 5 compared to that in Case 3 as shown in Figure 4.5.

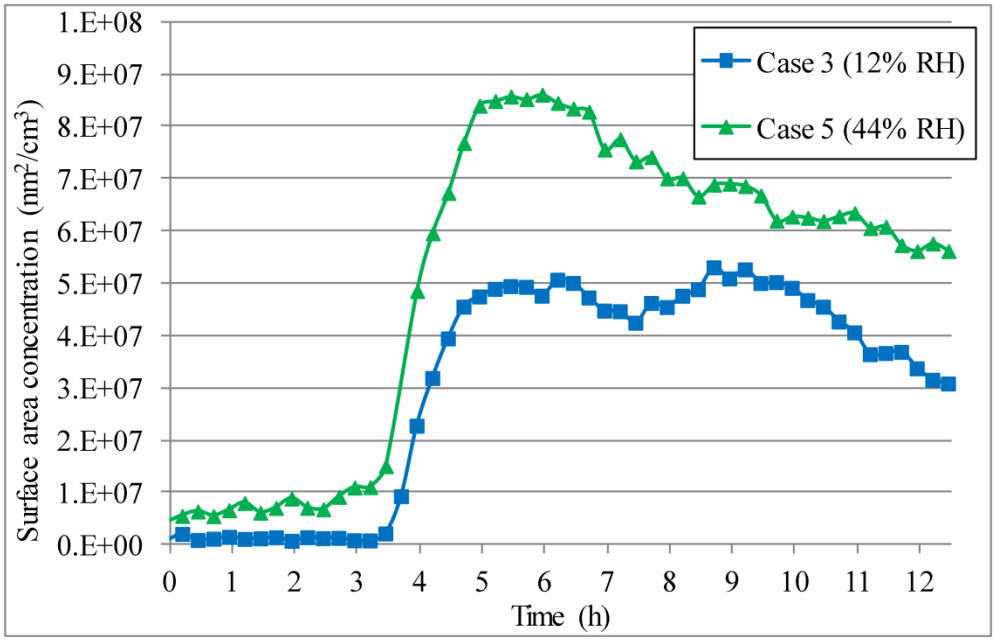

Figure B.2. Effect of relative humidity on the particle surface area concentration.

Exposure to Ozone-initiated Ultrafine Particles under Building Conditions

We analyzed the contributions of ozone-initiated particle generation in realistic indoor conditions. It was assumed that the particle number concentration reaches steady state (as seen in Figure 4.8), the chamber air was well mixed, and deposition was negligible, then:

$$S_p \times A_{T-shirt} = Q_{outdoor} \times \left(N_{exhaust} - N_{inlet} \right), \quad \text{(B.1)}$$

where S_p is the particle number generation per unit time per unit area of the human surface; $A_{T\text{-}shirt}$ the area of the T-shirt; $Q_{outdoor}$ the outdoor airflow rate to the chamber; and N_{inlet} and $N_{exhaust}$ the particle number concentrations at inlet and exhaust, respectively.

For Case 12 (in Table 4.1) that corresponded to a typical building condition on a poor air quality day (22 ppb ozone and 0.5 h^{-1} outdoor air change rate):

$A_{T\text{-}shirt} = 0.9\ m^2$, $Q_{outdoor} = 2.55\ m^3/h$, $N_{inlet} \approx 0$, and $N_{exhaust} \approx 600\ \#/cm^3$

$\Rightarrow S_p = 472222\ \#/m^2\text{-}s$ (from Eq. (B.1))

Next, we estimated the particle generation from the ozone reaction with human surfaces for a full-scale building environment by assuming that conditions for Case 12 were applicable. It was further assumed that the building is occupied by P_{num} occupants and each occupant contributes an area of 1.7 m^2 (total area = $1.7 \times P_{num}$ m^2) for the ozone reactions. From Eq. (B.1):

$$\begin{aligned} & S_p \times A_{T-shirt} = Q_{outdoor} \times \left(N_{exhaust} - N_{inlet} \right) \\ & \Rightarrow S_p \times 1.7 \times P_{num} = P_{num} \times R_p \times \left(N_{exhaust} - N_{inlet} \right) \\ & \Rightarrow \left(N_{exhaust} - N_{inlet} \right) = \Delta N = \left(S_p \times 1.7 \right) / R_p , \end{aligned} \tag{B.2}$$

where ΔN is the increase in particle number concentrations due to the ozone reactions and R_p is the outdoor airflow rate per person. We used the above equation to calculate ΔN = 80–160 $\#/cm^3$ for R_p between 5–10 L/s.